

## ABSTRACT

Title of Document: THE DESIGN, CONSTRUCTION AND TESTING OF A SCOUR MONITORING SYSTEM USING MAGNETOSTRICTIVE MATERIALS

Steven Richard Day, M.S., 2014

Directed By: Professor Alison Flatau, Aerospace Engineering

A system for the continuous monitoring of scour has been designed, constructed and implemented. The system detects the level of scour by attaching flow to a buried post at known depths, and detecting when individual sensors become unearthed. Two bio-inspired flow sensors were designed and constructed for use on the post. The first, resembling a seal whisker, utilized the magnetostrictive materials Alfenol and Galfenol and was optimized for  $>0.15\text{m/s}$  flow. The second, resembling seaweed, used a conventional permanent magnet and was optimized for  $<0.15\text{m/s}$  flow. A small, low powered data acquisition system was designed and constructed to monitor and record the data from the sensors. A total of four scour posts were installed at two different sites; two vertically to monitor conventional scour and two horizontally to monitor lateral riverbed migration. Data from the posts was analyzed and presented and lessons learned were documented.

THE DESIGN, CONSTRUCTION AND TESTING OF A SCOUR  
MONITORING SYSTEM USING MAGNETOSTRICTIVE MATERIALS

By

Steven Richard Day

Thesis submitted to the Faculty of the Graduate School of the  
University of Maryland, College Park, in partial fulfillment  
of the requirements for the degree of  
Master of Science  
2014

Advisory Committee:  
Professor Alison Flatau, Chair  
Professor Norman Wereley  
Professor Mary Bowden

© Copyright by  
Steven R. Day  
2014

## Acknowledgements

The scope and size of this project required a very large group effort, and I could not have asked for a better team to help me through it.

I would first and foremost like to thank Dr. Flatau for accepting me as one of her Master's students and providing me with a research assistantship on such a fun and interesting project. While getting to know Dr. Flatau, it becomes quickly apparent how highly she regards her students and how passionate she is about engineering. Like most projects, there were times when the work carried on late into the night. As a true proponent of the philosophy "lead by example," Dr. Flatau was always working next to us in the early hours of the morning, continually volunteering to undertake the least desirable tasks. These qualities in combination with her patience in teaching and faith in the abilities of her students make me appreciative and proud to have Dr. Flatau as a mentor.

I would also like to thank all the members of Dr. Flatau's team that helped me complete the project: Dr. Souk Min Na, the Material's Engineering Post Doc of our group, who spent countless hours crafting and refining the many, many magnetostrictive whiskers required for the project; My fellow graduate student Ganesh Raghunath for aiding me with all aspects of the project, particularly with the characterization of the magnetostrictive whiskers; Dr. Zohaib Husnain for always lending his consultation when I became stuck on a problem; Koji Yanaga, our exchange student from Japan, for his immense help with testing and installations;

And to the many undergrads who greatly contributed along the way: Vera Klimchenko, Spencer Stebins, Oluseye Soyombo, Bayo Sule, Kyle Meyers, and Abel Kebekabe.

The success of this project could not have been achieved without the help of several professors as well as their teams. I would like to thank our collaborators on the project from Michigan Tech led by Dr. Andrew Swartz; Dr. Kaye Brubaker for providing us guidance on all things Civil Engineering; and Dr. Mary Bowden for providing the use of her much needed lab space.

I would like to thank the members of Taurus Engineering: Tyler Flatau for devising and executing solutions for many of the complicated installation issues; Adrian Ross for keeping a lookout for potential opportunities to commercialize of the project; Our bridge experts Tom Hughes, John Cote, Antonio Iada and Paul Deleo for their extensive experience and expertise in bridge construction and maintenance, without which we would have been completely lost.

The project could never have been completed without the generous funding and advisement from RITA/USDOT, MDOT, and MDSHA. From the MDSHA, Andy Kosicki, Stan Davis and Jeffrey Knaub were instrumental in their help with install site selection and permitting.

I could never be where I am or who I am today without my amazing family. To my parents, Brenda and Eric Day, who inspire me to strive for every ambition and are always there to provide me with the support and encouragement to succeed. To my older siblings, Mike and Erica, who have always taken their job as my role

models seriously and constantly steer me in the right direction. And of course, to my beautiful wife Jamie, who is patient when I need to work late, distracts me when she knows I need a break, and uplifts me when things become overwhelming. I love you all.

I would like to specially thank David Flatau who we tragically lost along the way. He was the first person to even consider using our magnetostrictive flow sensors for scour detection and the project would not have been possible without him. As a man with an unparalleled love for bridges, he always showed tremendous enthusiasm for the project and made everyone feel excited just to be involved. His genuine and uplifting character still effects the project today. We will miss you and your infectious smile David. Rest in peace.



# Table of Contents

Acknowledgements.....	ii
Table of Contents .....	v
List of Tables .....	xi
List of Figures .....	xii
Chapter 1: Introduction.....	1
1.1 Scour Basics.....	1
1.1.1 Definition of Bridge Scour.....	1
1.1.2 Difficulties Detecting Scour .....	1
1.1.3 Common Scour Detection Methods.....	2
1.1.4 Current High Tech Scour Monitoring Solutions.....	3
1.2 Proposed Solution.....	4
1.3 Magnetostriction .....	6
1.3.1 Joule Effect .....	6
1.3.2 Villari Effect .....	7
1.3.3 Magnetostrictive Material Selection .....	8
1.4 Design Requirements .....	10
1.4.1 Sensor Sensitivity to water.....	10
1.4.2 Ten Year Lifespan.....	10

1.4.3 Simple Design .....	11
1.4.4 Low Power consumption .....	11
1.4.5 Wireless Communication.....	12
1.4.6 Easily Installable .....	13
1.4.7 Cost Effective.....	13
Chapter 2: Sensor Design.....	14
2.1 Whisker Sensor .....	14
2.1.1 Bio Inspiration .....	14
2.1.2 Magnetostriction within a Galfenol or Alfenol Whisker .....	15
2.1.3 Basic Sensor Setup.....	16
2.2 Seaweed Sensor .....	19
2.2.1 Motivation and Bio-Inspiration.....	19
2.2.2 Basic Design .....	20
2.3 Flume Testing .....	21
2.3.1 Whisker Sensor Flume Results .....	21
2.3.2 Seaweed Flume Results .....	24
Chapter 3: Data Acquisition System (DAQ) Development .....	26
3.1 DAQ Requirements.....	26
3.1.1 ADC Resolution and Sampling Rate .....	26
3.1.2 Sleep Mode and Sensor Power Control .....	28
3.2 Basic Arduino Setup .....	29
3.2.1 Arduino Platform .....	29



3.2.2 DAQ Components.....	30
3.2.3 Basic DAQ procedure and SD Card Bottleneck .....	32
3.2.4 Utilization of NilRTOS and a FIFO buffer.....	34
3.3 First Full Function DAQ.....	37
3.3.1 First Prototype Sleep Cycle .....	37
3.3.2 Lesson Learned: Continuous Reset.....	39
3.4 Hand Built DAQ .....	40
3.4.1 Hand Build DAQ Motivation.....	40
3.4.2 Hand Built DAQ Components and Construction.....	41
3.4.3 Problems Encountered .....	44
3.5 PCB CAD DAQ.....	45
3.5.1 PCB DAQ Description.....	45
3.5.2 Additional Features .....	47
3.6 Temporary Development Board DAQ.....	48
3.7 Batteries and Overheating.....	49
Chapter 4: First Installation – Bacon Ridge.....	52
4.1 Install Site Description.....	52
4.1.1 Site Selection .....	52
4.1.2 Flow Speeds.....	52
4.2 Scour Posts.....	54
4.2.1 Structural Characteristics .....	54
4.2.2 Sensors and Wiring .....	55

4.3 Installation.....	58
4.4 Lessons Learned.....	61
4.4.1 Simplification of Initial Prototype .....	61
4.4.2 Whisker Pre-stress .....	63
4.4.3 Wiring Lessons Learned .....	65
4.4.4 Other Lessons Learned .....	67
4.5 Results.....	68
Chapter 5: Second Installation – Bennett Creek.....	71
5.1 Install Site Description.....	71
5.2 Scour Posts.....	72
5.2.1 Method for Measuring Lateral Riverbed Migration .....	72
5.2.2 Structural Characteristics .....	74
5.2.3 New Seaweed Sensor Design.....	74
5.2.4 Wiring .....	75
5.3 Installation.....	79
5.4 Lessons Learned.....	81
5.4.1 Erosion Due to Drilling.....	81
5.4.2 Ice Formation around the Post .....	82
5.4.3 Ferromagnetic Particle Clumping .....	83
5.4.4 Underwater Post Specific DAQ Problems .....	83
5.5 Second Prototype Results .....	85
5.5.1 System Verification .....	85

5.5.2 DAQ readings .....	87
5.6 Whisker Post Cap Addition .....	89
5.6.1 Post Cap Description and Attachment .....	89
5.6.2 Whisker Cap Results.....	91
Chapter 6: Conclusions .....	93
6.1 Summary .....	93
6.2 Future Work .....	95
Appendices.....	97
Appendix A: Airfoil Study.....	97
A.1 Introduction of Airfoil Study .....	97
A.2 Necessity of Oscillatory Response.....	97
A.3 Unstable Airfoil Concept .....	98
A.3.1 Static Margin.....	98
A.3.2 Experimental Setup.....	98
A.4 Plastic Molded Airfoils .....	101
A.5 Results .....	101
A.5.1 Data Format.....	101
A.5.2 Results for No Airfoil Configuration .....	102
A.5.3 Results for Airfoil Configuration.....	103
A.6 Airfoil Study Conclusions.....	104
Appendix B: Sensor Protection Using Rock Salt .....	105
Appendix C: DAQ Code.....	108

C.1 DAQ Code.....	108
C.2 ATtiny Code.....	121
Appendix D: PCB DAQ Schematic and BOM.....	123
Appendix E: Custom Submersible Wire Specifications .....	126
Bibliography .....	128

## List of Tables

Table 1. Properties of common magnetostrictive materials.....	9
Table 2: Properties of the whiskers used on the scour post whisker caps .....	90
Table 3. Bill of Materials for PCB DAQ.....	123

## List of Figures

Figure 1. Most common methods used for scour detection: Scuba Divers (left), Sounding Rods (right).....	3
Figure 2. Current high tech solutions available for scour monitoring: Sonar (left), Sliding Collars (middle), transmission beacons (right). .....	4
Figure 3. Proposed scour monitoring system composed flow sensors to detect the presence or absence of water flow .....	5
Figure 4. Illustration of the Joule Effect: (a) Pre-stressed material, (b) Dipoles beginning to rotate due to external magnet, causing the material to elongate (c) Dipoles fully rotated achieving maximum elongation.....	6
Figure 5. Illustration of the Villari Effect: (a) Magnetic dipoles aligned by biasing magnet (b) Stress from the applied force causes dipoles to rotate and create magnetic inductance in the x-direction (c) Magnetic Dipoles are fully rotated achieving maximum change in magnetic induction in the x direction.....	8
Figure 6. Harbor Seal with highly sensitive flow detecting whiskers (Brenner, 2002) .....	14
Figure 7. Arrangement of magnetic dipoles in an (a) undeflected, stress free whisker and (b) deflected whisker experiencing compressive ( $-\sigma$ ) and tensile ( $+\sigma$ ) stresses ..	16
Figure 8. Whisker Dimension Definitions .....	17
Figure 9. Illustration of basic whisker sensor concept.....	19

Figure 10. Photograph of basic whisker sensor setup.....	19
Figure 11. Photographs of a seaweed sensor with a holder for a vertical post .....	20
Figure 12. Setup for testing whisker performance in a flume.....	21
Figure 13. Comparison between a whisker being continuously deflected in steady state flow and an undeflected whisker in air.....	22
Figure 14. Transient response of the whisker as experienced during the flume startup (left) compared to a no flow condition (left) .....	23
Figure 15. Unique whisker geometries used in an attempt to induce oscillations .....	24
Figure 16. Seaweed sensor flume results at 0.01 m/s, 0.03 m/s, 0.09 m/s and 0.15m/s .....	25
Figure 17. A pre-constructed Arduino development board, the Arduino Mega 2560 (Arduino, n.d.).....	30
Figure 18. DS3234 RTC with SparkFun Electronics™ breakout board (a) DS3234 RTC (b) 12mm coin cell battery holder (SparkFun Electronics, n.d.).....	31
Figure 19. Sparkfun Electronics™ microSD Shield with Hex Converter and microSD Socket (SparkFun Electronics, n.d.) .....	32
Figure 20. Visualization the data logging process for a simple DAQ .....	33
Figure 21. Visualization of niRTOS modified data logging process.....	37
Figure 22. Photograph of the initial DAQ prototype with labeled components .....	39
Figure 23. Photograph of one of the hand built DAQs from the front (top) and back (bottom).....	44

Figure 24. CAD drawings of the PCB DAQ board, including individual representations of each copper layer. The three segregated power planes have been labeled for the reader's convenience.....	48
Figure 25. Temporary DAQ created using SparkFun Electric's™ Arduino Mega Pro .....	49
Figure 26. Heat sink used to prevent overheating of the 5V regulators .....	50
Figure 27. Typical batteries used to power the DAQs in this study. 12V-35amp-hr (left) 6V-13amp-hr (right).....	50
Figure 28. First install site at Bacon Ridge Branch tidal bridge. (a) North face of the Bridge (b) South side of the bridge (c) View of the bridge from the north looking south.....	53
Figure 29. Illustration of the first install site at Bacon Ridge depicting the general placement of each component.....	54
Figure 30. Structural components of the first prototype scour post. (a) Clevis used to hoist the post (b) Bare scour post encased with concrete (c) Process of encasing the scour post in concrete by vertically standing it inside a Sano tube and pouring in concrete.....	55
Figure 31. Illustration and photograph of seaweed sensor placement for the first post installation.....	56
Figure 32. Example of the seaweed sensor holders used on the first post installation	57
Figure 33. 22 gauge wire inserted and soldered into 18 gauge wire to allow for connection to hall sensors and DAQ.....	57



Figure 34. Hollow stem auger section with labeled shaft connector and cutter ..... 59

Figure 35. Photos of full-scale installation at Bridge No. 02072 on MD450 over Bacon Ridge Branch. a) students building installation working platform; b) installation of electronics housing on bridge structure; c) contact Miss Utility well in advance as fiber optic cable had to be avoided on the south side of the bridge; d) deploy hardware to installation site; e) assemble auger on bridge deck; f) once hollow stem auger is to appropriate depth, knock loose plug at base of auger and with excavator, place sensor post into position; g) after removing auger, run wiring to data acquisition system on bridge wall; h) install battery; retrieve data card periodically to download data recorded from flow sensors for one minute every hour until such time that a wireless data logger is added to allow for interrogation of sensors from a remote location..... 60

Figure 36. Whisker sensor used for the first installation prototype. The whiskers were angled at 45 degrees to allow them to fit into the auger ..... 64

Figure 37. Broken seaweed sensor with disconnected wire from first installation .... 67

Figure 38. Preliminary results from the sensor post on the north side of the Bacon Ridge Branch Bridge. All seven data sets from the sensor 7.5 cm (3 inches) below the top of the sensor post show the sensor is in water because the response exhibits flow induced motion. The sensor at 22.9 cm (9 inches) below the top of the post is just barely buried and only shows motion at the time of highest flow velocity, between low and high tide. The sensor that is 38 cm (15 inches) below the top of the post is fully buried and shows no motion..... 69

Figure 39. South post sensors reading constant static signal .....	70
Figure 40. Photographs of the second installation site before installation. (a) Exposed guard rail due to lateral riverbed migration before the addition of rip rap protection. (b) Installation site as viewed from up stream. (c) View of upstream conditions as viewed from the installation site. (d) Bridge No. 1008600 viewed at a distance .....	72
Figure 41. Illustration of horizontal post installation for detection of lateral riverbed migration .....	73
Figure 42. Installation locations of the lateral riverbed migration posts .....	73
Figure 43. Seaweed sensors specially designed for the horizontal posts.....	75
Figure 44. Submersible wire used in the second installation, consisting of a 3 conductor wire (left) and 13-conductor wire (right) .....	76
Figure 45. Second post wiring process (a) Seaweed sensors are fed through the post (b) three-conductor and 13-conductor cables are soldered together (c) Shrink tube on individual conductors heated (d) Large shrink tube placed around connection bundle before being filled with epoxy (e) Completed junction with cured epoxy .....	78
Figure 46. Photos of full-scale installation at Bridge No. 1008600 on MD355 over Bennett Creek. a) Jeff Knaub of MDSHA showing UMD students target location for sensors; Rip rap protecting bank from prior scour event at top left of photo; b) installation of turbidity curtain on morning of installation; c) BelAir drill rig ~9.2m (30 ft) from where sensor will protrude from bank; d) sensor used to track depth and lateral position of drill tip; e) feeding wiring and sensor post into bank ~60 cm (2 ft) above nominal water level as drill bit is retracted; f) admiring successful installation	

of the in-air sensor post; g) feeding wiring and sensor post into bank at depth of ~15.25cm (6 inches) below nominal water level for this site. ....	80
Figure 47. Electrical box for storing DAQ and electrical components for the second installation.....	81
Figure 48. Residual cove formed from drilling .....	82
Figure 49. State of the lateral riverbed migration scour posts upon taking of data ....	85
Figure 50. Data from the riverbed migration in air post recorded using a high powered DAQ.....	86
Figure 51. Data from the riverbed migration underwater post recorded using a high powered DAQ .....	87
Figure 52. Data from the riverbed migration in air post recorded using the temporary DAQ.....	88
Figure 53. Data from the riverbed migration underwater post recorded using the temporary DAQ .....	88
Figure 54. Whisker Cap components (a) Cap design with place holders for whisker sensors (b) Insertable whisker sensor (c) Complete whisker cap assembly .....	89
Figure 55. Whisker post caps attached to both the in-air and unwater posts via zip ties .....	90
Figure 56. Time response data for the whiskers attached to the whisker post cap .....	91
Figure 57. Time response data for the whiskers attached to the whisker post cap .....	92
Figure 58. Whisker holder used in the experimental setup: side view (left), front view (Middle), top view (Right).....	99

Figure 59. Assembled experimental setup: close up of mounting plate configuration (left), Flume Setup (right).....	100
Figure 60. Galfenol Whisker with attached airfoil. ....	101
Figure 61. Comparison between stationary whisker (left) and oscillating whisker (right) .....	102
Figure 62. Frequency responses of a whisker without an airfoil for flow rates from 0 ft/s to 0.82 ft/s .....	103
Figure 63. Frequency responses of a whisker with an airfoil for flow rates from 0 ft/s to 0.82A ft/s .....	104
Figure 64. Rock salt encasement procedure (a) Hot aqueous sodium acetate is poured over dirt and rocks contained in a Sano tube (b) Sano tube is removed after rock salt mix cools (c) Rock salt remains attached when lifting by the PVC pipe (d) Rock salt dissolving in low flow velocity water .....	107
Figure 65. PCB DAQ Schematic .....	125
Figure 66. Spec. sheet for the three-conductor submersible wire.....	126
Figure 67. Spec. sheet for 13-conductor submersible wire.....	127

# Chapter 1: Introduction

## 1.1 Scour Basics

### **1.1.1 Definition of Bridge Scour**

Bridge Scour is defined as “the erosion or removal of streambed or bank material from bridge foundations due to flowing water” (Waren, 2013). Over time, this erosion can become deep enough to compromise the stability of the foundation of the bridge and cause it to fail. Historically, bridge scour has been the most common cause of bridge failure. One event in particular, the collapse of an Interstate Highway bridge over Schoharie Creek in New York State in 1987, was responsible for the introduction of major revisions to federally mandated regulation pertaining to bridge scour. As a result of these revisions, states are now required to classify all bridges over water based on their potential for scour complications. (Kattell & Merv, 1998)

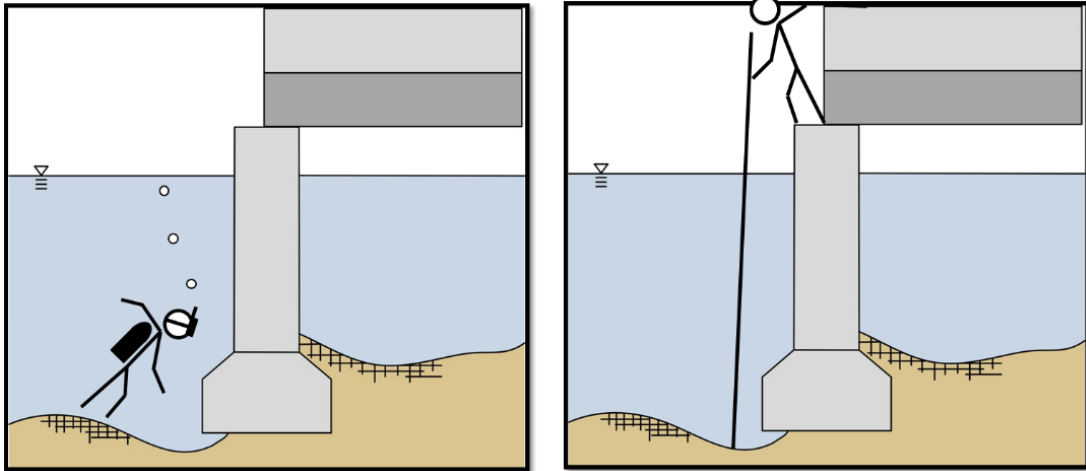
### **1.1.2 Difficulties Detecting Scour**

There are several issues that make the detection of scour difficult. As it occurs beneath the surface of the water, sediment or debris can cause scour not to be visible. Furthermore, scour is in constant flux, meaning a large scour event may occur during a storm, only to be filled back in before being detected; never allowing bridge maintainers to know the bridge was in danger of collapsing. Finally, large

debris such as logs or rocks are constantly floating or rolling down the river and have the potential to cause damage to any installed monitoring system.

### **1.1.3 Common Scour Detection Methods**

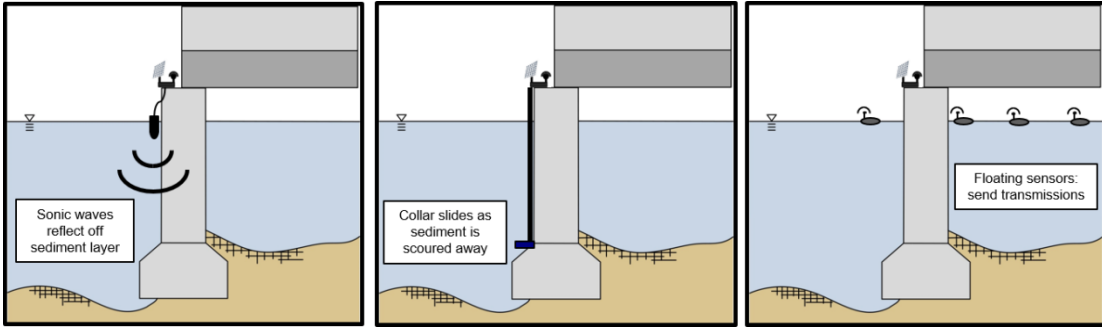
The most common methods used to monitor scour involve human inspection as depicted in Figure 1. For deeper bridges this involves sending specially trained scuba divers to investigate the foundation around piers after large storms or flooding events. The process is both expensive and inefficient, as typically the bridge must remain closed until the divers have completed the inspection and insured its safety. For smaller bridges, which includes the majority of the bridges in the United States, scour inspection consists of using a sounding rod to measure the depth of the foundation in scour sensitive locations. While this method is inexpensive and can produce accurate results, the task is typically only left to a few individuals, causing long lapses between inspections for a single bridge. Furthermore, human dependent methods are susceptible to the fluctuations of scour as they are unable to be performed during harsh weather, when the riverbed is most susceptible to erosion, and the scour holes are likely to refill as the weather settles.



**Figure 1.** Most common methods used for scour detection: Scuba Divers (left), Sounding Rods (right)

### **1.1.4 Current High Tech Scour Monitoring Solutions**

There are currently several high tech solutions available but none have been widely adopted. Some of these solutions are illustrated in Figure 2. Solutions such as sonar detection prove to be too costly to implement on the vast number of bridges requiring monitoring. Other solutions such as using a sliding collar that sinks with the eroding riverbed, or floating beacons that rise to the surface and begin transmitting as they are unearthed by displaced sediment are only good for detecting a single scour event. As mentioned above, the tendency for scour to constantly fluctuate does not allow for such single use applications to provide a practical solution. For this reason, it is desirable to have a robust, automated scour monitoring system, capable of monitoring numerous, separate scour events under unfavorable weather conditions.

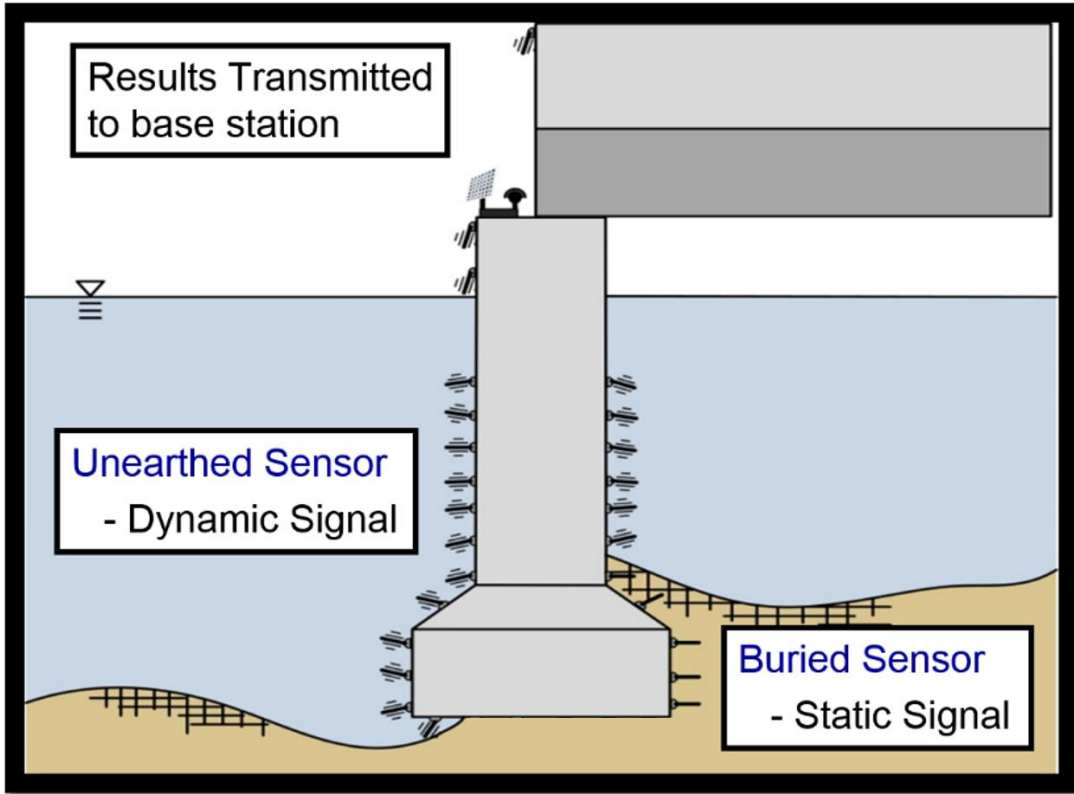


**Figure 2.** Current high tech solutions available for scour monitoring: Sonar (left), Sliding Collars (middle), transmission beacons (right).

1.2 Proposed Solution

The solution investigated in this thesis is depicted in Figure 3. The design consists of a series of sensors capable of detecting the presence of flowing water. The underlying concept being that sensors buried underneath the river bed sediment will not be deflected by the flow of the water and will therefore transmit a static signal. Conversely, an unearthed sensor will be continually deflected by the water, transmitting a dynamic signal. With knowledge of the depth of each sensor, the erosion state of the riverbed can be inferred. The results of these readings are then transmitted to a base station as part of a network, where the scour health of several bridges can be monitored simultaneously.





**Figure 3.** Proposed scour monitoring system composed flow sensors to detect the presence or absence of water flow

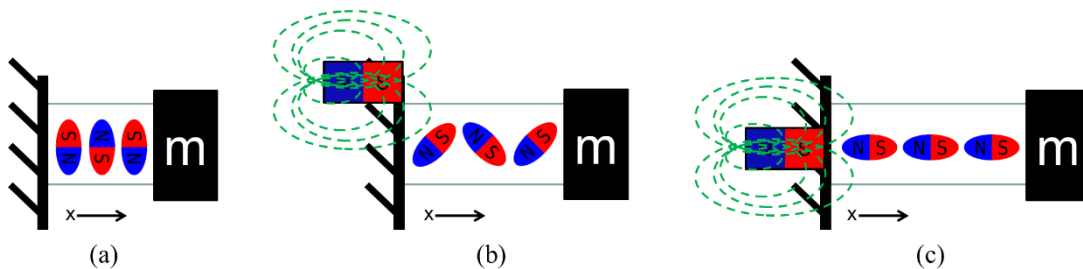
As mentioned above, the system needs to be able to withstand impact from large debris without sustaining appreciable damage. For this reason, magnetostrictive materials that can be made out of flexible metal alloys have been selected as the material used to construct the flow sensors. These sensors can then be connected directly to the bridge pier as depicted in the figure, or on a sturdy, corrosion resistant, steel post in an area susceptible to scouring.

### 1.3 Magnetostriction

Magnetostrictive materials are ferromagnetic metals or metal alloys that exhibit a coupling between magnetic inductance and stress forces. This coupling can be leveraged to allow the material to be used as either an actuator or a sensor.

#### **1.3.1 Joule Effect**

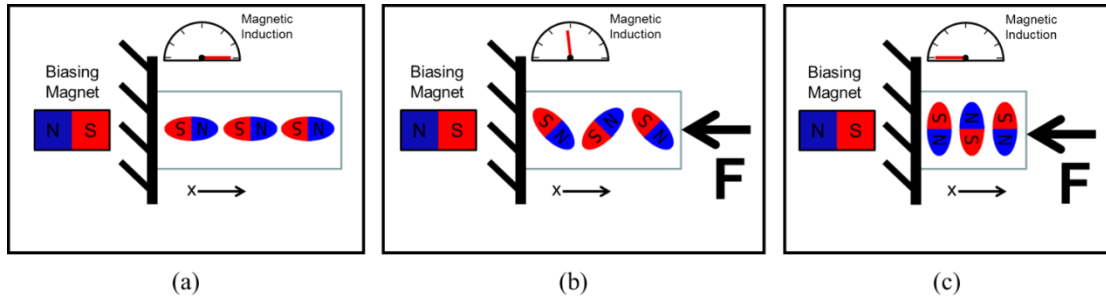
When acting as an actuator, magnetostrictive materials utilize the Joule Effect. In order to maximize the potential displacement and force when used as an actuator, the material must first be pre-stressed to align the magnetic dipoles of the material anti-parallel to one another. This alignment is depicted in Figure 4a. Given this alignment, a magnetic field can then be introduced along the length of the sample (+x direction in this example), causing these dipoles to rotate and produce an increase in both the magnetization and dimension of the material in this direction. The corresponding change in dimensions can be used to move or apply force to another object like the mass 'm' as depicted in Figure 4b and c.



**Figure 4.** Illustration of the Joule Effect: (a) Pre-stressed material, (b) Dipoles beginning to rotate due to external magnet, causing the material to elongate (c) Dipoles fully rotated achieving maximum elongation

### **1.3.2 Villari Effect**

Conversely, to act as a sensor, magnetostrictive materials utilize the Villari Effect. In this scenario, the magnetic dipoles are aligned into a single direction using a biasing magnet as depicted in Figure 5a. Stress imposed by external forces will now force the dipoles to rotate, causing an alteration of the material's magnetic induction as depicted in Figure 5b and c. The largest stress induced change is expected to arise as a reduction in magnetization along the length (the +x direction) of the sample. Energy minimization during this process would promote magnetic domain reorientation into anti-parallel domains, thus we would not expect a significant change in magnetization along the transverse directions of this sample. In practice, however, samples and domains are generally not perfectly symmetric, and thus tracking of the change in magnetization along the transverse direction has also been shown to provide a signal that correlates well to the changing applied stress field. The signal to noise ratio is smaller than for changes along the +x direction, however the signal is still useful.



**Figure 5.** Illustration of the Villari Effect: (a) Magnetic dipoles aligned by biasing magnet (b) Stress from the applied force causes dipoles to rotate and create magnetic inductance in the x-direction (c) Magnetic Dipoles are fully rotated achieving maximum change in magnetic induction in the x direction

Mathematically, for a linearized 1-D example, the magnetic induction,  $\beta$ , produced by the Villari Effect is represented in Equation 1.

$$\beta = \mu^T H + d * T \quad (1)$$

In this equation,  $\mu$  represents the permeability,  $H$  the applied magnetic field,  $d$  the magneto-mechanical coupling, and  $T$  the stress. The first term of the equation,  $\mu^T H$ , signifies the contribution of the permeability of the material and external magnetic field introduced by the biasing magnet to the overall magnetic induction of the material. The later term in the equation,  $dT$ , signifies the contribution of the material's magnetostrictive properties to the overall magnetic induction for a given stress state. A correlation between the stress state and the magnetic induction can be inferred from the equation.

### 1.3.3 Magnetostrictive Material Selection

There are several types of magnetostrictive materials to choose from as displayed in Table 1. The most popular and well known magnetostrictive material is

Terfenol-D. Although it possesses very high magnetostrictive properties, its very brittle nature would not allow for the robustness required of the sensor. Pure iron and nickel have the desired elastic characteristics, but have very little magnetostriction. Researchers at the Magnetic Materials branch of the Naval Surface Weapons Center, Carderock Division (NSWC-CD), were instrumental in recognizing Iron-Gallium alloys, now known as Galfenol, as the first of the family of structural magnetostrictive alloys. With the creation of Galfenol comes the adequate combination of strength, elasticity, and magnetostriction needed to create a robust flow sensor. Most importantly, Galfenol can be rolled into very thin sheets and cut into the thin flexible whiskers capable of deflecting in water flow. For these reasons, Galfenol has been selected as one of the materials to be used for this study.

**Table 1.** Properties of common magnetostrictive materials

	<b>Terfenol-D</b>	<b>Iron</b>	<b>Nickel</b>	<b>Galfenol</b>	<b>Alfenol</b>
Saturation Magnetostriction (ppm)	1600-2400	-24	-66	150-420	100-200
Modulus of Elasticity (GPa)	25-35	200	207	65	68
Ultimate Tensile Strength (MPa)	28	400	500	580	606
Hysteresis in $\lambda$ -H and B-H curves	Moderate	Low	Low	Very Low	Very Low
Mechanical Properties	Brittle	Flexible	Flexible	Flexible	Flexible

In an effort to create a material with even higher compliance while still maintaining adequate magnetostrictive properties, an Iron-Aluminum alloy, known as Alfenol, was investigated. With apparent higher resilience and flexibility, and only minor losses in magnetostriction, this is the primary material used in the study.

## 1.4 Design Requirements

The complexities of scour explained above, as well as the harsh and remote environment introduced by a river, require a scour monitoring system to have a stringent set of design requirements.

### **1.4.1 Sensor Sensitivity to water**

The most important and basic requirement for the project is to ensure that the sensors are capable of detecting flow. It is not necessary for the sensors to quantitatively detect the velocity of the flow, but only to distinguish between a buried sensor and a sensor that is exposed to the water. The sensors should have the ability to distinguish between these two states regardless of the velocity or steadiness of the flow.

### **1.4.2 Ten Year Lifespan**

One of the greatest benefits of a scour monitoring system, such as the one described in this study, is its ability provide scour severity data without a team needing to constantly visit the bridge and measure it with sounding rods. The convenience of such a system would quickly be compromised if it needed continual routine maintenance or replacement. As a result, it is a requirement that the system have at least a 10 year lifespan. In order to meet this requirement the system must be physically robust, resistant to rust and other corrosion, and must require a minimal amount of power to operate.

### **1.4.3 Simple Design**

While not a specified requirement, striving for a simple design helps to achieve the necessary lifespan for the system. Achieving a simple design primarily involves avoiding the addition of moving parts. The monitoring system is designed to remain buried in mud for the majority of its lifespan, which would allow dirt and moisture into the joints of any moving parts and likely cause them to prematurely fail. Upon being unearthed by scour, moving parts would risk further damage from debris floating down the river. This is why a solid state flow sensor which is impervious to water and tolerant of plastic deformation is ideal for the proposed monitoring system.

### **1.4.4 Low Power consumption**

The sensors used in the proposed scour monitoring system as well as the equipment used to log and transmit data inevitably consume power. As an isolated system buried under a riverbed, all of the power will likely be provided from a single battery source capable of storing enough energy to run the system for the full ten years. As a result, it is necessary for the system to operate while consuming as little power as possible.

Adding a power generating device to the system is desirable, but given the environment of the system is not very feasible. Most power generating devices, such as turbines, require moving parts that would not be ideal for the reasons listed in Section 1.4.3 above. Solar power does not have these moving parts, but would not be a viable option underwater. One promising source of power may lie in the thermal

differences between the top and bottom of the post, but at the time of this writing such devices are not developed enough for use in this study.

While power consumption will be considered and investigated, the Prototypes constructed for this study are connected to weather proof, bridge-side electrical boxes where batteries can be easily exchanged.

#### **1.4.5 Wireless Communication**

To monitor hundreds or thousands of scour sites in real time, each monitoring system must be capable of communicating to a centralized information hub. Without a wired infrastructure already present to connect each system, the most feasible option is to communicate wirelessly. Cellular networks are accessible from many bridge sites, allowing for a simple and cheap (~\$20 for a monthly data plan at the time of this writing) partial solution to the problem. For sites that do not have accessibility to cellular networks, there are several cheap, long range wireless communication devices available. If set up correctly these isolated sites would then be able to communicate to one of the sites connected to a cellular network, which could then communicate that information to the centralized hub. If it is important for every bridge site to have a direct line of communication, satellite communication via services such as Iridium could also be considered.

Our collaborators from Michigan Tech are working in parallel with this study to create such a network. Prototypes constructed for the current study simply save the data to a flash memory card for manual retrieval.



#### **1.4.6 Easily Installable**

Installation of the scour monitoring system would be very simple when implemented on newly constructed bridges. However, the majority of the bridges this system would be used for are aging bridges. With a possible need to install multiple scour posts at each installation location, ease of installation is imperative. A simplified install would not only help to reduce cost, but could also have implications with respect to permitting. Obtaining a permit to drill in the vicinity of a bridge site is much more difficult than obtaining a permit to drive a post into the ground like a nail. Drilling is necessary for the prototype installations performed in this study to protect the sensors, but a novel solution to protecting the sensors for future installation methods is introduced in Appendix B:

#### **1.4.7 Cost Effective**

In addition to all of the performance based requirements listed above, it is important that the cost of the scour monitoring system not become overly expensive to feasibly implement. Since the proposed system only provides information on the scour immediately around the post, it is likely that it will be necessary to have multiple posts at each bridge site. With thousands of bridges in each state of the United States alone, the cost for a local department of transportation can compound quickly. It is therefore necessary that the cost of each post remain inexpensive relative to the budget of potential users.

## Chapter 2: Sensor Design

Two types of bio inspired flow sensors have been created for the purposes of this study. A high flow velocity, whisker, sensor is discussed Section 2.1 and a low flow velocity, seaweed, sensor is discussed in Section 2.2.

### 2.1 Whisker Sensor

#### **2.1.1 Bio Inspiration**

Many aquatic creatures either navigate or supplement their navigation using cantilever beam-like structures commonly known as whiskers. One such creature, known as the Harbor Seal, Figure 6, has whiskers sensitive enough to detect and follow the invisible wake of a small submarine more than ten seconds after the submarine has passed (Dehnhardt, Bjorn, Hanke, & Horst, 2001). The impressive sensing abilities of such creatures provides the motivation for the whisker sensors used in this study.



**Figure 6.** Harbor Seal with highly sensitive flow detecting whiskers (Brenner, 2002)

The basic concept and design of the whisker is explained and analyzed extensively in Michael Marana's thesis, *Development of a Bio-Inspired Magnetostrictive Flow and Tactile Sensor* (Michael, 2012). A summary of this design and its utilization of magnetostriction is provided in this section.

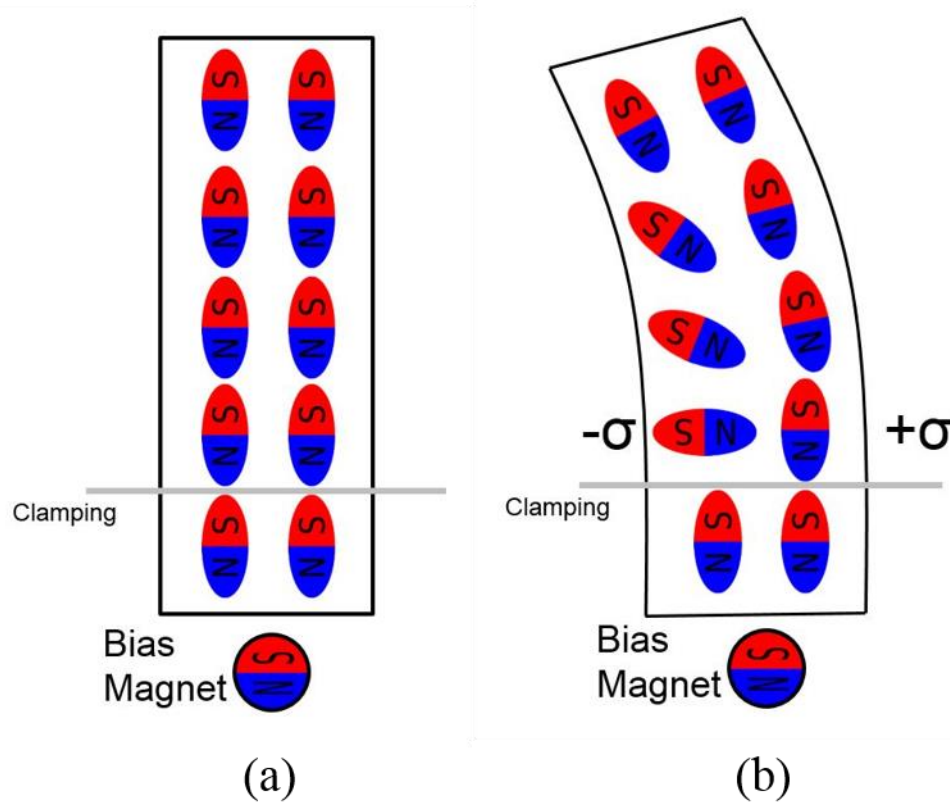
### **2.1.2 Magnetostriction within a Galfenol or Alfenol Whisker**

While a basic understanding of magnetostriction has already been introduced, it is helpful to illustrate the role of magnetostriction within the whisker itself. Because it is desired to use the whiskers as sensors, the Villari effect described in Section 1.3.2 will be utilized.

Mechanically, whiskers can be modeled as cantilever beams, with the root of the beam located where the whisker attaches to the animal. For the Alfenol and Galfenol whiskers the root is a clamping point where the whisker is immobilized. As with all cantilever beams, when the tip is displaced, compressive and tensile stresses develop on opposite sides of the beam, with the greatest magnitude of these stresses located at the root.

The resulting effect of these stresses on the magnetic dipoles, and thus the magnetic induction, is displayed in Figure 7. As depicted in Figure 7a, prior to the whisker being deflected, a biasing magnet keeps all of the dipoles aligned parallel to the length of the whisker. Upon deflection of the whisker, as depicted in Figure 7b, the dipoles located in the tensile region remain aligned with the length of the whisker and produce little to no change in the magnetic inductance. The compressive stresses

however, force the magnetic dipoles to rotate producing a measurable change in magnetic induction in the axis parallel to the length of the whisker. This change is highest at the root where the largest compressive stresses are experienced.

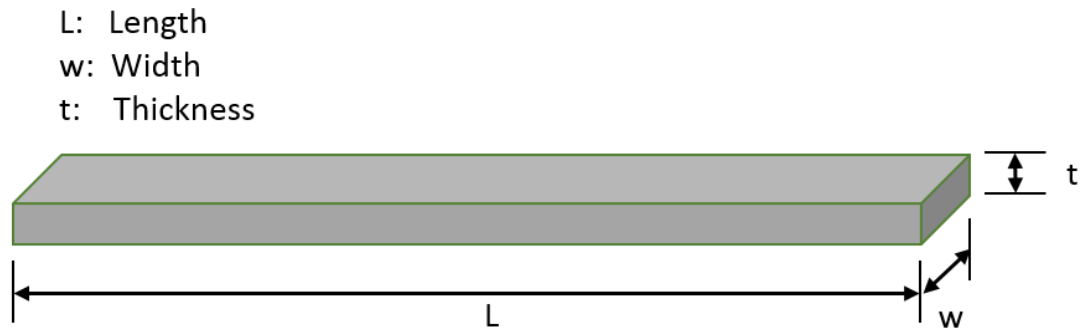


**Figure 7.** Arrangement of magnetic dipoles in an (a) undeflected, stress free whisker and (b) deflected whisker experiencing compressive ( $-\sigma$ ) and tensile ( $+\sigma$ ) stresses

### 2.1.3 Basic Sensor Setup

Several variations of the whisker sensor have been utilized and experimented with during the course of this study, but the overall design concept remains the same. In all descriptions of the whiskers used in this study, width, thickness and length will

be defined as depicted in Figure 8. That is to say the length will always be identifiable by the longest overall dimension of the whisker, width as the longest dimension of the whisker cross-section, and thickness as the shortest dimension of the whisker cross-section.



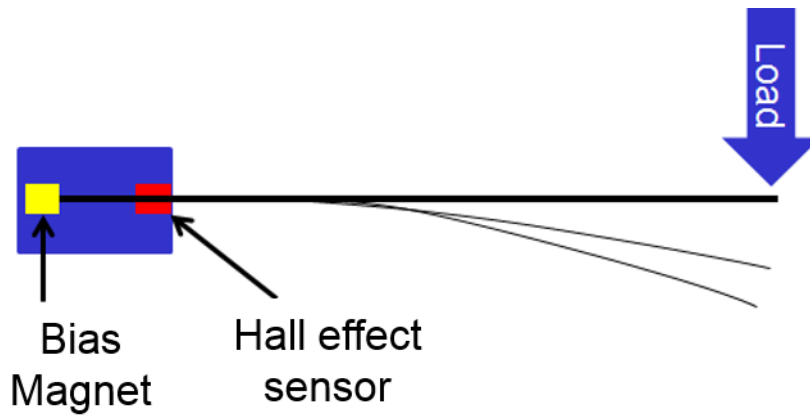
**Figure 8.** Whisker Dimension Definitions

The basis of each whisker sensor consists of four main components. A magnetostrictive whisker, a holder, a Hall Effect sensor, and a biasing magnet. The holder is used to hold the whisker in place and act as an anchor for the whisker, allowing the system to become a cantilever beam. This anchor point acts as the root of the cantilever beam, and as mentioned in the previous subsection, is paramount in its role of creating a high stress region in the whisker upon bending. The anchor point can be created by allowing the holder to clamp down on the whisker holding it in place, or by simply epoxying the whisker to the holder. For most situations, it is better to epoxy rather than clamp the whisker into place, as the clamping mechanism can add its own pre-stress and cause the problems that will be discussed in Section 4.4.2.

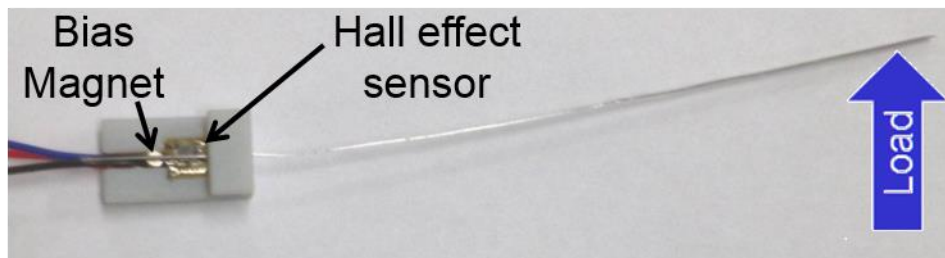
In order to detect the changes in magnetic induction, a hall sensor is embedded into the holder. The optimal placement of the hall sensor is as close to the high stress region, or anchor point, as possible. If design restrictions do not allow for such a placement, the sensor can still provide meaningful readings with the hall sensor located a few millimeters behind the high stress region, as long as it is still in contact with the whisker. The benefits of reading the magnetic induction traveling orthogonally through the width of the whisker versus orthogonally through the thickness of the whisker is currently being studied; although, preliminary results indicate that it is optimal to read the flux lines traveling orthogonal to the width of the whisker.

Finally, a biasing magnet must also be embedded into the holder and remain in contact with the whisker to align its magnetic dipoles and allow for the induction of the Villari Effect. Once again, the optimal location and strength of the biasing magnet is currently being investigated, but preliminary results indicate a 0.6 pull lbs magnet placed around 2-3 mm from the anchor point is optimal.

The basic concept of the whisker setup is illustrated in Figure 9, while a photograph of an actual whisker setup is presented in Figure 10. Figure 10 is an example of a setup in which the hall sensor is not located directly at the area of high stress concentration, but is still effective in providing readings of whisker deflection.



**Figure 9.** Illustration of basic whisker sensor concept



**Figure 10.** Photograph of basic whisker sensor setup

## 2.2 Seaweed Sensor

### **2.2.1 Motivation and Bio-Inspiration**

While testing the whisker design in different flow conditions, it became apparent that a separate sensor design may be required to detect flow speeds below 0.15 m/s. In order to detect smaller fluctuations this design needs to be as compliant as possible and buoyant enough to flex given the smallest alteration in flow velocity or direction. Such sensitivity to flow speed and direction is exhibited in nature through seaweed, thus providing the bio-inspiration for the second sensor.

### 2.2.2 Basic Design

As with the whisker sensor, several variations of the seaweed sensor have been used and experimented with during the course of this study, but the overall design concept remains the same. The seaweed sensor consists of a plastic holder, a strip of fabric, a small magnet and a hall sensor.

To best emulate the seaweed structure, a sheet of synthetic fabric is cut into a strip typically 5-8 cm long and 1-2 cm wide. This strip is then hung from the center of a plastic holder with a hall sensor embedded into it. The hall sensor is positioned to read the magnetic induction along the length of the of the fabric strip. Epoxied to the fabric strip 5mm below the hall sensor is a small 0.5 pull lbs magnet.

The seaweed design does not rely on magnetostriction, but simply on the variation of the magnetic field due to the movement of the magnet. This allows the sensor to pick up flow fluctuations in nearly stagnate water, creating a low speed sensor. An example of the seaweed sensor is depicted in Figure 11.



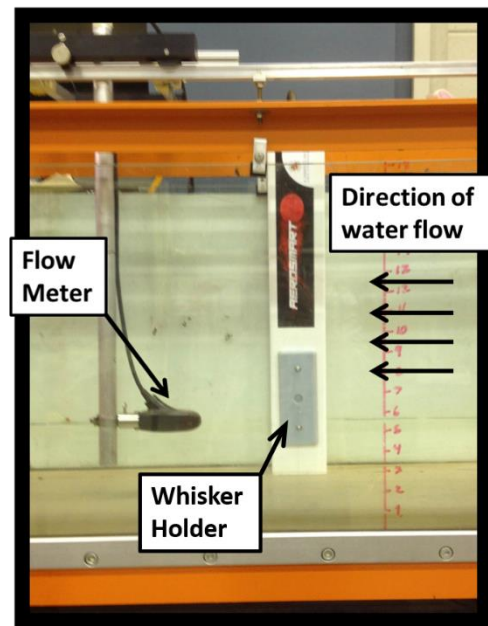
**Figure 11.** Photographs of a seaweed sensor with a holder for a vertical post



While the seaweed sensor is optimal for low velocity flow, it can become pinned against the holder in high speed flow, necessitating both the whisker and seaweed sensors be used to create a system optimized for all flow speeds.

### 2.3 Flume Testing

Flume testing was performed to investigate the effectiveness of each sensor in various conditions. A photograph of the flume setup can be viewed in Figure 12.



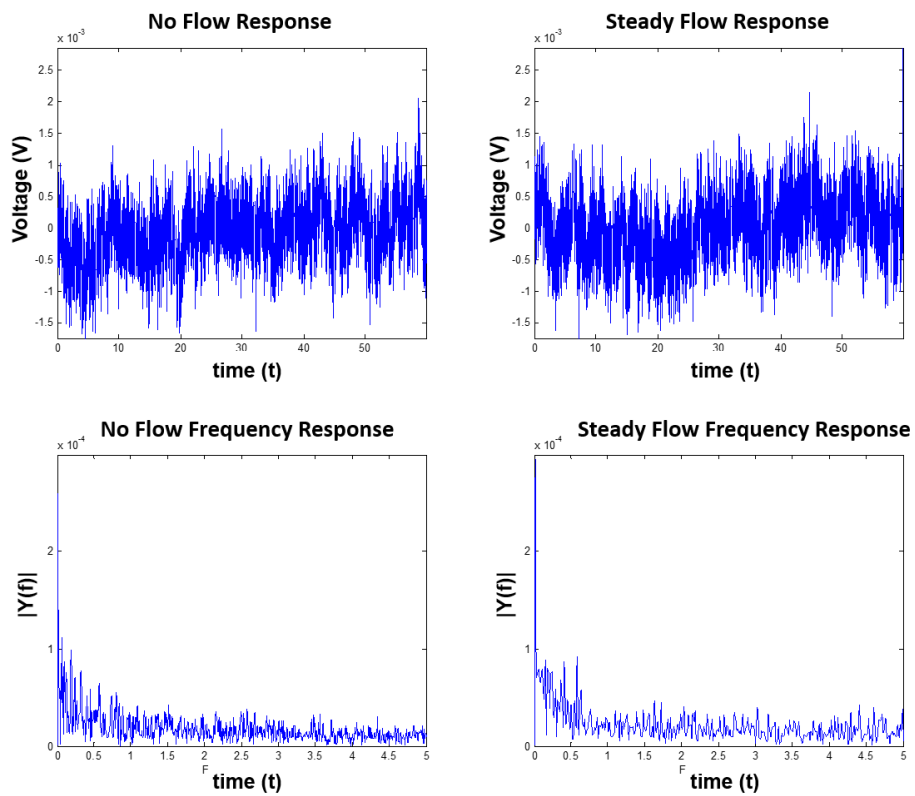
**Figure 12.** Setup for testing whisker performance in a flume

Results for each sensor are presented in the sections below.

#### **2.3.1 Whisker Sensor Flume Results**

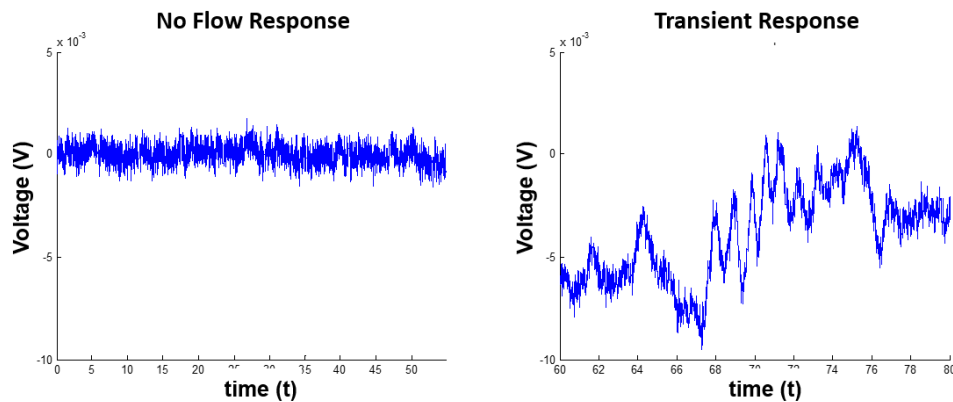
As mentioned above, the whisker sensor is optimized for high velocity flow. Although these sensors can successfully detect flow velocities greater than 0.15 m/s, the nature of the flow must still be considered; particularly the turbulence of the flow.

In extremely steady flow, such as the flow found in a flume, the whisker will simply reach a point of deflection and not oscillate around that point. Without such oscillations it is impossible to distinguish between a whisker that is being statically deflected by the flow and a whisker that is simply buried in a deflected state. Figure 13 illustrates this principle by displaying both the signal from a whisker continually being deflected by steady flow and the same whisker undeflected in air. The signals are indistinguishable. It is therefore necessary for the whisker to have a dynamic response.



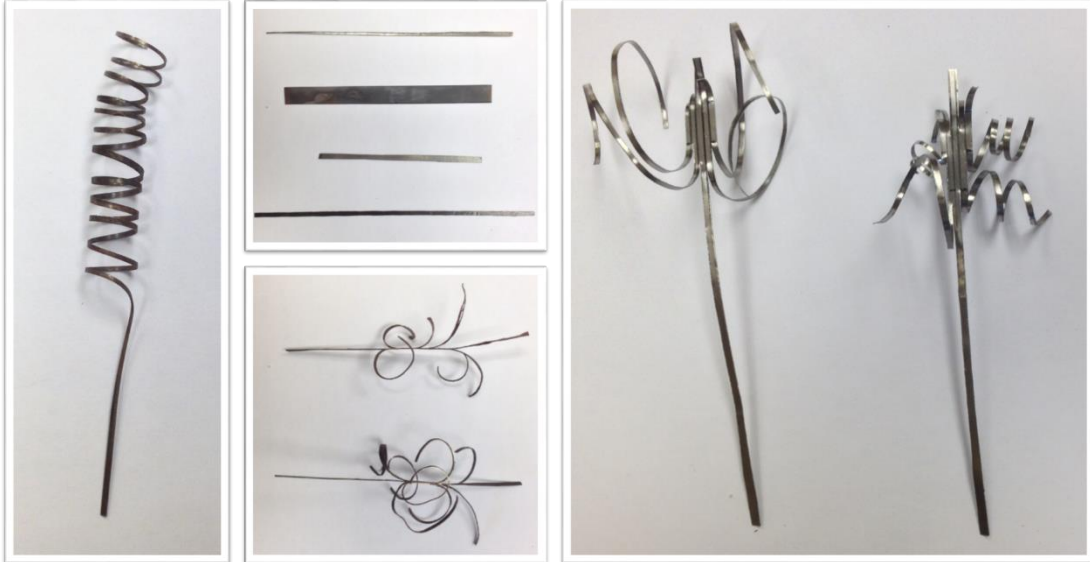
**Figure 13.** Comparison between a whisker being continuously deflected in steady state flow and an undeflected whisker in air

In practice, it is unlikely that the whiskers would experience such a steady flow in a river, especially at a location at risk for scour. The conditions experienced at such locations are better represented by the transient response of the whisker present during the startup of the flume. Such a response presents a clear differentiation between a stationary whisker and whisker in water flow. A sample transient response can be viewed in Figure 14



**Figure 14.** Transient response of the whisker as experienced during the flume startup (left) compared to a no flow condition (left)

In an attempt to optimize the whisker sensors for steady flow conditions, several methods were utilized to achieve a dynamic response. These methods primarily involved using different whisker lengths, widths and shapes in an attempt to create vortex shedding. Examples of these unique whisker geometries are presented in Figure 15.



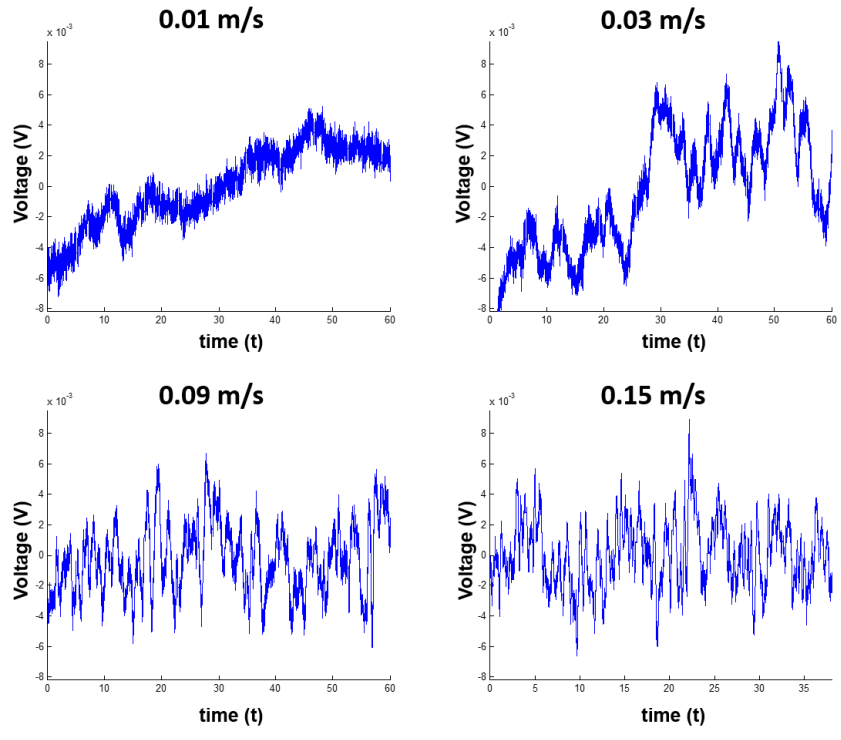
**Figure 15.** Unique whisker geometries used in an attempt to induce oscillations

Despite looking promising visually, the whiskers depicted above did not produce the desired dynamic response upon testing. A dynamic response was eventually achieved in steady state conditions by attaching an unstable airfoil, and is discussed in detail in Appendix A:.

### **2.3.2 Seaweed Flume Results**

The seaweed sensors are designed to be optimized for flow that is too slow for the whisker sensors to detect ( $<0.15\text{m/s}$ ). Due to the extremely high compliance of the fabric used for the seaweed sensor, it does not experience the same difficulties under steady flow conditions as the whisker sensor.

Through the flume testing, it was determined that the seaweed sensors could detect flow velocities less than  $0.01\text{ m/s}$ . Figure 16 displays results depicting the seaweed sensor performance at speeds between  $0.01\text{ m/s}$  to  $0.15\text{ m/s}$ .



**Figure 16.** Seaweed sensor flume results at 0.01 m/s, 0.03 m/s, 0.09 m/s and 0.15m/s

The motion of the seaweed is clearly evident in each of the plots. It can also be noticed that as the velocity increases, the oscillations become more random and more increasingly difficult to discern. Under these higher velocity conditions, it would be preferential to have the more consistent and lower frequency response of the whisker sensor.

## Chapter 3: Data Acquisition System (DAQ) Development

### 3.1 DAQ Requirements

As indicated in Section 1.4.4 the proposed scour monitoring system has very stringent power consumption requirements. In addition to these requirements, physical size, analog to digital conversion resolution and sampling rate must also be considered. The final physical size of the DAQ system is dictated by the size of the final post dimensions, and has yet to be determined. However, with the minimal footprint required by modern electronics, rearranging the components of the DAQ system to the necessary dimensions is not anticipated to be a problem.

#### **3.1.1 ADC Resolution and Sampling Rate**

The resolution of a given analog to digital converter, or ADC, is provided in units of bits. The number of bits required for a desired measurement resolution depends on the voltage range output of the sensor being read. The upper limit of this voltage range is identified for the ADC of the DAQ either internally or using an external voltage as a reference. The ADC can then obtain a reading from the sensor by receiving the voltage being output and comparing it to this upper limit. The ADC then outputs an integer between 0 and a maximum integer defined by its bit resolution that is proportional to the voltage read and the defined upper voltage limit. The

number of integer increments of voltage will be  $2^n$  for an n-bit ADC (i.e. 4,096 for a 12-bit ADC). With higher bit resolutions, larger maximum integers can be represented and greater resolutions achieved.

For example, the maximum number of integers that can be represented by 10-bits is  $2^{10} = 1024$  (integers: 0-1023), and the sensors used in this study output voltages between 0V and 5V. Therefore, a 10-bit DAQ will output an integer using Equation 2,

$$ADC\ Output = \frac{V_s}{5} * (1024) \quad (2)$$

where  $V_s$  is the voltage being output by the sensor.

Using this formula one can discern that using 10-bit DAQ, a common resolution value for ADCs found on microcontrollers, and a 5 V sensor gives a resolution of approximately 5-mV. This resolution is adequate for the large voltage fluctuations output by the seaweed sensor, but not for the small voltage oscillations output by the whisker sensor. A 16-bit ADC with a resolution of approximately 0.1 mV is much more desirable for the whisker sensor.

The minimum necessary sampling rate is defined by the Nyquist frequency, or twice the highest frequency expected in the signal ( $f_{max} = f_{Nyquist} = f_{Sample\ rate}/2$ ). The oscillations from both the seaweed and whisker sensors are expected to be very low, <10 Hz, so a sampling rate of 20 Hz would be sufficient. While this is the minimum sampling rate required for detection of a signal of 10 Hz, it will provide only two samples per cycle of oscillation at this frequency. A general rule of thumb is to target

closer to 10 samples per cycle of interest, and thus a minimum sample rate of 200 Hz would be desirable for a 10 Hz signal. There is a tradeoff associated with file size going up as sample rate goes up. While providing improved fidelity of a signal in the time domain, a file of one minute of data acquired at 500 Hz will contain 3000 data points, while one minute of data acquired at 200 Hz will contain only 1200 data points, which will likely be “good enough” from a system design perspective. For this study, the DAQs are set to achieve a frequency of around 500 Hz. This is the maximum rate achievable by the DAQs for recording 10 sensors and is well above the required Nyquist Frequency. It is likely that for future field deployments this sample rate will be reduced, however for the preliminary investigation and proof of concept work in this thesis, the larger file set was manageable and desirable from the perspective of learning more about how the system performs.

### **3.1.2 Sleep Mode and Sensor Power Control**

While scour constantly fluctuates, these fluctuations are not instantaneous, especially in the absence of adverse weather conditions. It is therefore not necessary that a scour monitoring system continuously record data without pause. Instead it is more logical for the system to conserve energy and only take data samples at predetermined time intervals with power down sleep cycles in between those intervals.

While operating at 5V, the hall sensors used in this study consume approximately 9mA, and account for a large portion of the power consumption. It is



important that any DAQ constructed for the scour monitoring system not only be capable of powering itself down for sleep cycles, but also have the capability of powering down the sensors as well.

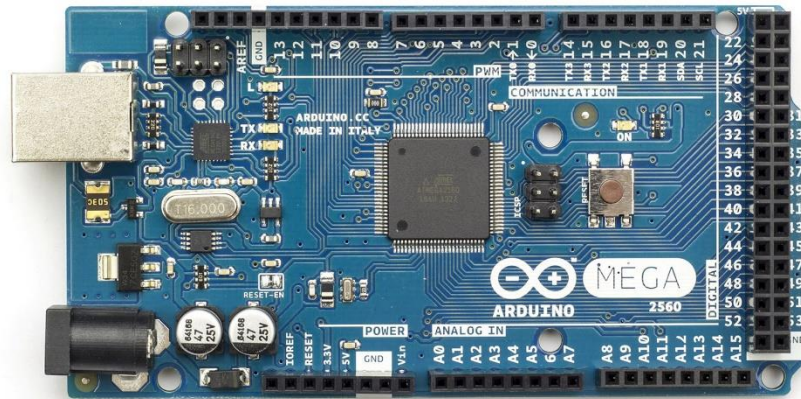
### 3.2 Basic Arduino Setup

#### **3.2.1 Arduino Platform**

Coding microcontrollers using C can be tedious and time consuming in nature. One must manually look up and manipulate registers for the features of the microcontrollers one would like to use and pass those register values to the microcontroller in machine code. Although there are typically code libraries for a given microcontroller to ease this process, computing platforms can alleviate this process even further by standardizing sets of functions across multiple microcontrollers, effectively creating its own programming language. Knowledge of how to use the platform allows users the capability to program multiple microcontroller packages without needing to learn new syntax. This ability to change hardware without needing to write completely new code offers useful flexibility for prototyping new electronic systems.

The Arduino platform was selected for developing the prototype DAQ system in this study for its simplicity and the large, easily accessible knowledge base that has been created as a result of its popularity. As defined by the Arduino website, “It’s an open-source physical computing platform based on a simple microcontroller board, and a development environment for writing software for the board” (Arduino, n.d.).

The platform is available through both the purchase of a pre-constructed development board like the one depicted in Figure 17 or by downloading the source code for free and boot loading it onto a compatible microcontroller of your own.



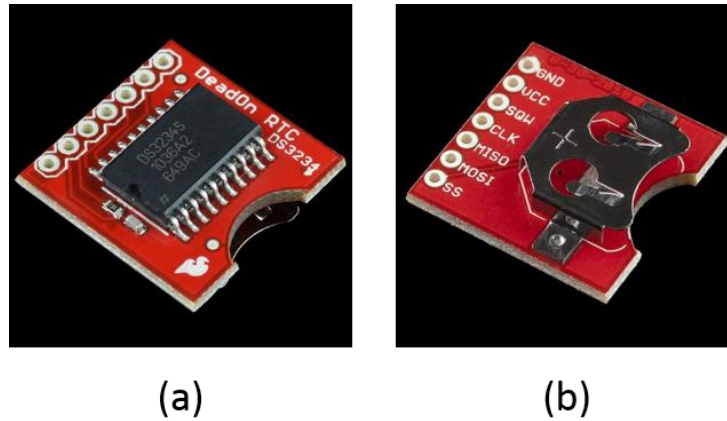
**Figure 17.** A pre-constructed Arduino development board, the Arduino Mega 2560 (Arduino, n.d.)

### 3.2.2 DAQ Components

The development board used in the construction of the studies most basic DAQ prototypes is the one pictured in Figure 17, the Arduino Mega 2560. The development board includes a 16 MHz ATmega2560 processor and 16 ADC input pins. In addition to the components already provided by the board, the system needs a way to track the time of day that the data samples are taken and a place to store recorded information to create a fully functional DAQ.

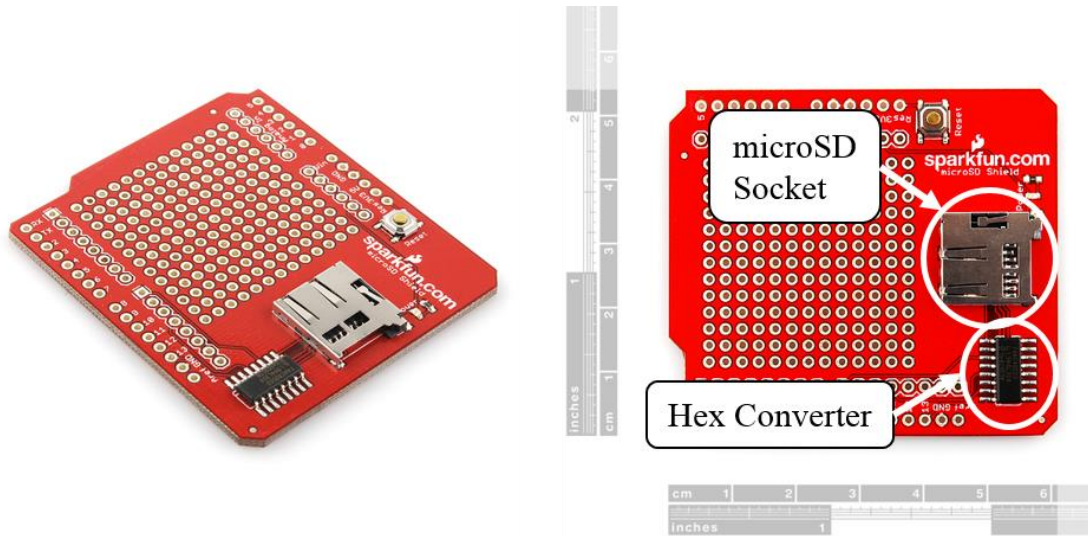
To keep track of when data samples are taken, the DAQ system utilizes a surface mounted real time clock, or RTC. In particular, the systems used in this study

use the DS3234 mounted onto a SparkFun Electronics™ breakout board. The breakout board provides easy access to the pins of the RTC package as well as a holder for a 12 mm coin cell battery for backup power. The complete package used is presented in Figure 18. Communication with the RTC is performed via a Serial Peripheral Interface Bus, or SPI, protocol.



**Figure 18.** DS3234 RTC with SparkFun Electronics™ breakout board (a) DS3234 RTC (b) 12mm coin cell battery holder (SparkFun Electronics, n.d.)

To store recorded data, the DAQ system uses a microSD card which also communicates using an SPI protocol. An external circuit is required for the development board to communicate with the microSD card. For this a microSD “shield” like the one produced by SparkFun Electronics™ and pictured in Figure 19 can be used. This shield provides a socket for a microSD card to be inserted into, a hex converter to step down the 5V logic levels from the development board to the 3.3V levels required by the microSD card, and the connections required for powering and communicating with the microSD card.



**Figure 19.** Sparkfun Electronics™ microSD Shield with Hex Converter and microSD Socket  
(SparkFun Electronics, n.d.)

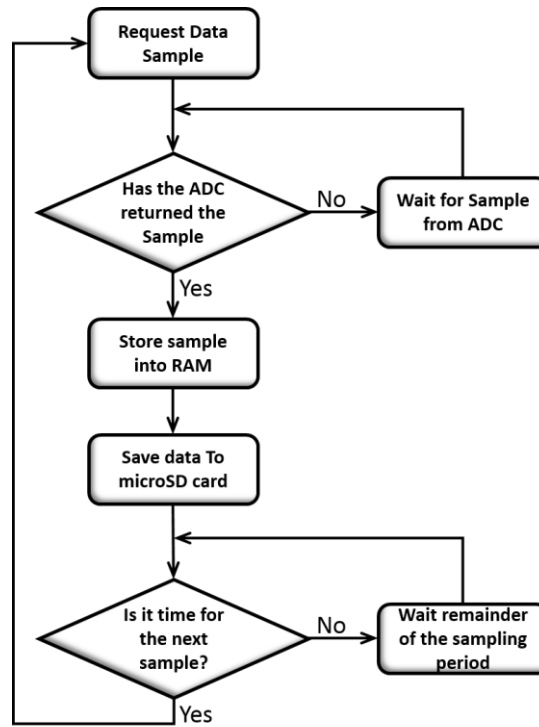
Using these rudimentary and relatively inexpensive electronics, a basic data recording system can be constructed. To create a powered down sleep cycle, a few extra components are required. Different methods were used to achieve these cycles and will be covered in the sections describing those respective prototypes.

### 3.2.3 Basic DAQ procedure and SD Card Bottleneck

For a typical data logging system using the components listed above, the procedure is as follows. First the microcontroller requests a reading, or readings in the case of multiple sensors, from the ADCs. The microcontroller then waits the necessary time for each ADC to accept the command, take a reading from the sensor, and return the resulting value, which it stores in its random access memory or RAM. Next, the microcontroller sends these values to the microSD card to be stored. Finally, upon the completion of these tasks the microcontroller will simply wait the

appropriate amount of time as dictated by the sampling rate to begin the next sample.

This process has been illustrated for the reader in Figure 20.



**Figure 20.** Visualization the data logging process for a simple DAQ

If the time it takes to complete the process outlined above is longer than the input sampling rate, the microcontroller will simply start the new data sample as soon as it is able. This will cause the actual sample rate to fall below the rate desired. Furthermore, the time it takes to complete the process of recording a single data point can be affected by external factors, meaning there will not be a uniform sampling period between each data point. For this reason, it is advisable to ensure that the requested sampling rate does not exceed the limitations of the system.

As with many processes a single feature can be identified as the primary limiting factor to performance, commonly referred to as a “bottleneck”. For the DAQs identified in this study, this bottleneck feature is the speed at which data can be stored to the microSD card. While this bottleneck can be partially mitigated by using SD cards with faster write speeds, it remains the limiting factor.

### **3.2.4 Utilization of NiRTOS and a FIFO buffer**

To further mitigate the microSD data saving problems, the DAQ system utilizes a real time operating system, or RTOS. With an operating system, the programming for the DAQ can utilize threads, effectively allowing the system to multitask. The operating system used in the current study is niRTOS created by Giovanni Di Sirio, and ported to the Arduino platform by Bill Greiman (Sirio & Greiman, 2013). niRTOS was selected for its minimal consumption of flash memory. The only tradeoff of such a small size is that it provides only the most basic operating system functions, which is all that is required to create a data recording system.

By using threads, procedures can be divided into priority levels where higher priority tasks have the ability to interrupt tasks of a lesser priority. This along with the implementation of a niRTOS’s first in first out, or FIFO, buffer allows for a reduction in the limiting capacity of the microSD card. This paper will provide a simplified overview of how these principles work, but for a more in depth understanding, the reader should research threading and FIFO buffering on their own.

First it is necessary to explain how the system uses a FIFO buffer. The buffer is allocated a predetermined amount of RAM memory. For the system in this study, it is allocated all of the remaining available RAM not used to store or run the code. Unlike storing data in a memory card, loading the data to the microprocessor's RAM is nearly instantaneous and is something the microprocessor must do before saving it to the microSD card anyway. Now, however, when the microprocessor stores the data into its RAM, it stores it with an identifier that can be used to find the data later. This way, if the processor is unable to finish saving the sample to the microSD card in the time allotted by the sampling rate, it can temporarily suspend the saving operation while it gathers the next data point. When the processor returns to the point of saving data to the microSD card, it will complete saving the previous point to the microSD card and erase it from its RAM before moving onto the next one; hence the nomenclature "first in, first out". The data point that the processor is currently saving can be several samples behind the data point currently being taken, creating a "buffer" between the two.

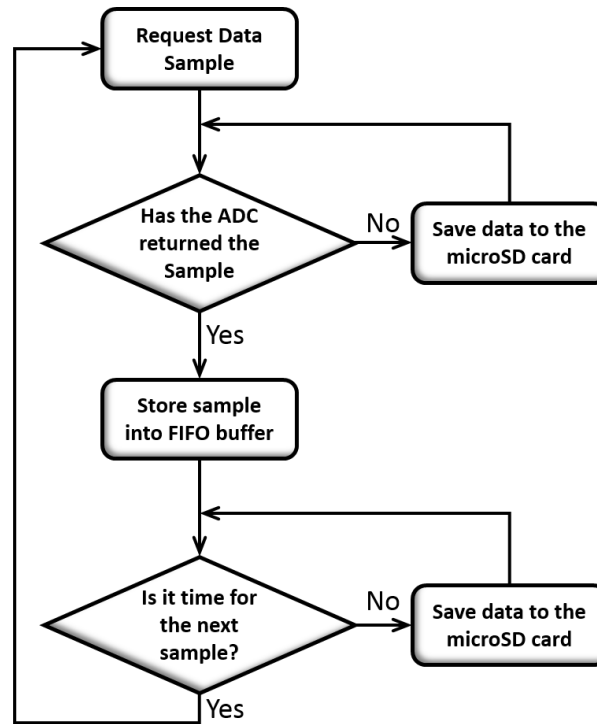
It should be noted that while this can significantly increase the maximum achievable sampling rate, a limit still exists when the buffer becomes so large that it uses up all of its allocated space in the RAM. In the event that this happens the system will simply skip taking new data points until enough of the allocated memory is available. The system records the number of data points skipped as "overruns" so that the user can use this knowledge along with the sampling rate to determine the time gap between points.

A single core processor is only capable of performing one task in a given moment, so in order to apply a FIFO buffer, the system must be able to utilize prioritized threads. In other words it must have the capability to interrupt lower priority threads in the middle of their process to complete higher priority threads, and return to the lower priority thread where it left off.

The current system only utilizes two threads. A high priority thread responsible for collecting and saving data points and low priority thread responsible for saving those points to the microSD card. In effect this means that the system is constantly saving data whenever the high priority thread has no tasks to perform. Logically this includes when the processor is waiting the requisite sample time before taking the next sample, but also includes when the processor is waiting for the conversion results from the ADC.

The new process including the niRTOS implementation is illustrated in Figure 21. This is the process used to program the DAQ systems in this study. The code used for the system is available in Appendix C:. Minor changes are required based on the DAQ version used, but the majority of the code is identical. The changes required based on the DAQ used are noted in the code.





**Figure 21.** Visualization of niRTOS modified data logging process

### 3.3 First Full Function DAQ

The first prototype DAQ utilized all of the exact components described in Section 3.2.2 as well as a few extra components.

#### **3.3.1 First Prototype Sleep Cycle**

The AVR microcontroller used in the Arduino platform does have low power sleep modes that can be used, but they do not have an effect on the other components present on the development platform. These components account for much of the power consumption, especially the FTDI board responsible for facilitating the USB communication between the microcontroller and computer. To temporarily fix this

problem for the first prototype, a rudimentary external circuit consisting of an electric relay and another small, low powered microcontroller to control it is used. Two 5 V regulators are also added to the system to provide regulated power to the sensors and the added microcontroller.

The added microcontroller is an Atmel ATtiny 85 and is used solely to switch the relay on and off. As with the other microcontrollers used in this study it is boot loaded with the Arduino platform for ease of use. The code used to run the microcontroller can be found in Appendix C:.

The double pole single throw (DPDT) relay used in the circuit is an NTE R40-11D2-5 with a 5 V switching voltage. When the required voltage is supplied by the microcontroller the relay directly connects the DAQ circuit to the battery. The power from the battery is then able to provide power to both the Arduino and the 5 V regulator connected to the sensors. This way all power consumption is eliminated during the sleep cycle, except the minimal amount needed to run the ATtiny micro controller, which can be reduced even further by putting it into a sleep mode as well. A photograph of the first prototype DAQ is provided in Figure 22.

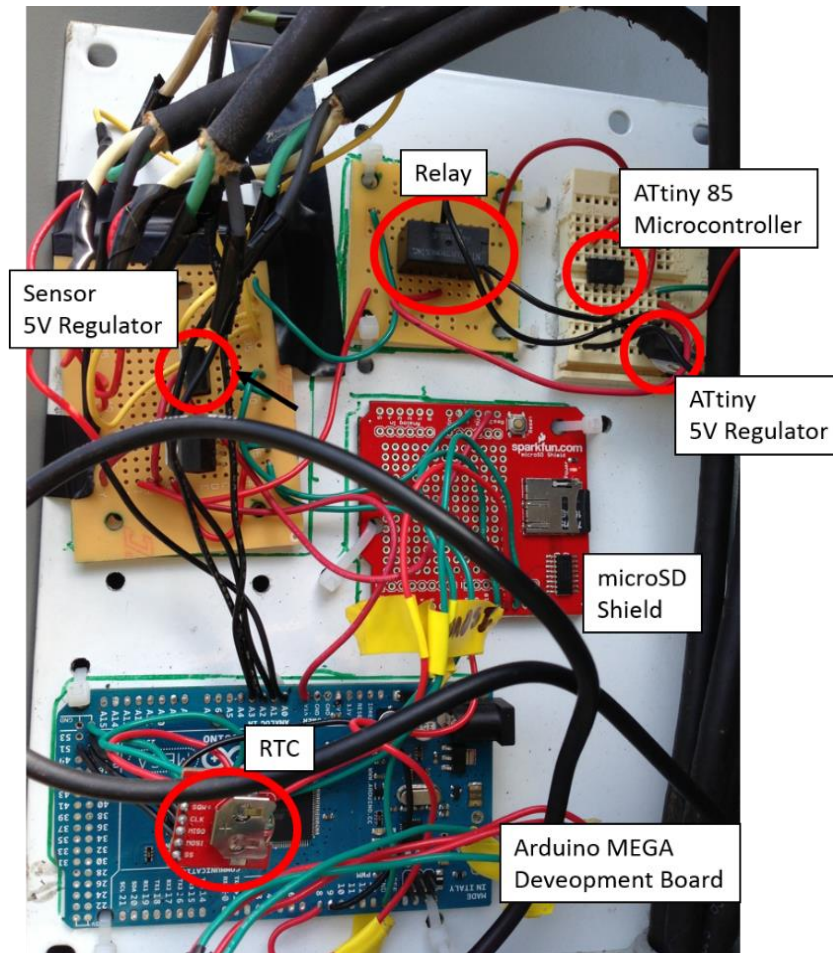


Figure 22. Photograph of the initial DAQ prototype with labeled components

### 3.3.2 Lesson Learned: Continuous Reset

During the initial operation after the installation of the first prototype DAQ it did not appear that the ATtiny microcontroller used to switch the system on and off was properly performing its function. Instead of continually switching on the DAQ once every hour for a minute long sample like it was programmed, there would be long periods in which the DAQ never shut off. This allowed data to still be gathered, but caused the batteries to die very quickly.

After construction of the “Hand Built” DAQ described in the next section, it became apparent that the problem was emanating from the lack of both a decoupling capacitor to stabilize the power, and a pull up resistor on the reset pin. These are elements that are built into Arduino development boards, but are required to be added to a bare microcontroller. It is likely that the power disruptions and drifting voltages on the reset pin were causing the microcontroller to continuously restart. The ATtiny is programmed to begin with the pin connected to the relay set to output 5 V, and the restarts were likely quick enough to never disrupt power to the main DAQ system or sensors. Only when the system was fortunate enough to have a stable power input and the correct reset pin voltage, did the system properly takes the data samples once every hour. The systems seems to operate correctly with the addition of the decoupling capacitor and pull up resistor.

### 3.4 Hand Built DAQ

#### **3.4.1 Hand Build DAQ Motivation**

The prebuilt Arduino development board is designed to contain a sufficient number of features to easily accommodate projects of all types and varieties for prototyping purposes. The downside to this approach is that it consumes additional power for unneeded electrical components and requires external circuitry to create a low powered sleep cycle. It is therefore advisable to create one’s own circuit with only the necessary components.

Recreating the DAQ from the most basic level also allows for the consideration of additional functionality. One of the most notable additions is the use of 16-bit ADCs to achieve resolution high enough to read the whisker sensors.

### **3.4.2 Hand Built DAQ Components and Construction**

Construction of the hand built DAQ began with replicating the necessary components from the development board, starting with the microcontroller. The ATmega2560 microcontroller used in the development platform is replaced with the ATmega1284P. The ATmega1284P has twice the amount of RAM, which can be used to increase the size of the FIFO buffer and the maximum sampling rate. The ATmega1284P also costs about half as much as the ATmega2560P. The features lost by switching to the ATmega1284P, such as extra digital input/output pins or UART channels, are not necessary for the DAQs constructed in this study. The required 16 MHz clocking crystal, decoupling capacitors, pull up resistors and other basic components required for the microcontroller to operate properly were also added to the system. These are the same basic components required for the PCB DAQ described in the next section and can be viewed in detail in the schematic presented in Figure 65 found in Appendix D:

The Mighty 1284P platform is used to run Arduino software on the ATmega1284P. Mighty 1284P is an open source platform created by the anonymous user “maniacbug” that once boot loaded, ports the Arduino platform to the

ATmega1284P, making it possible continue to use nilRTOS and the code created for the previous DAQ. (maniacbug, 2011)

The ADS1115 breakout board from Adafruit™ is used to achieve the desired 16-bit resolution required by the whisker sensors. The breakout board contains a surface mounted ADS1115 as well as all of the basic electrical components required to ensure a clear signal. Each ADS1115 has four analog inputs, communicates via an inter-integrated circuit (I<sup>2</sup>C), and has a sampling rate of 866 samples per second. Each ADS1115 also includes an address pin capable of changing its I<sup>2</sup>C address based on which other pin you connect it to. This allows for up to four distinct addresses to be utilized, permitting the use of four ADS1115 ADCs per microcontroller. For a single microcontroller this translates to 16 analog input channels.

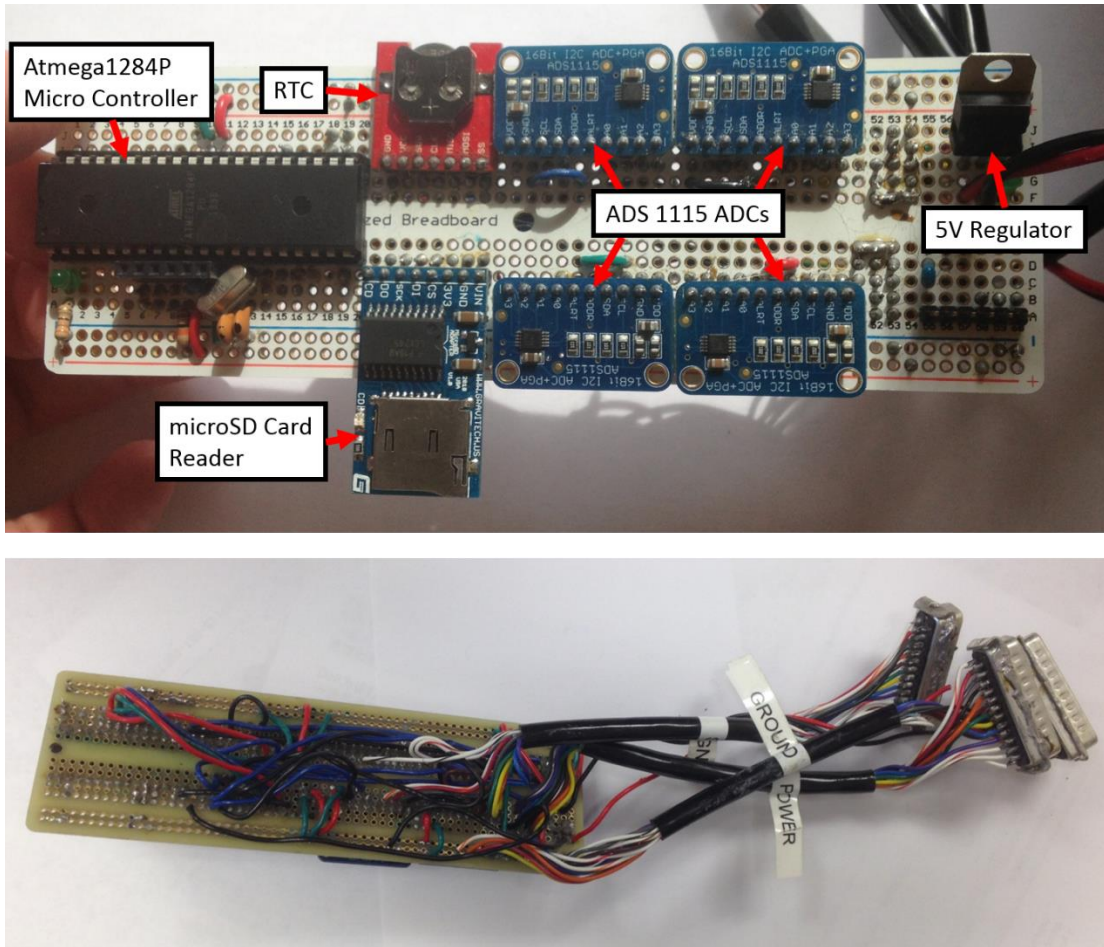
It should be noted that although each ADS1115 has four analog input channels, it only has one ADC which switches between the input channels. Therefore, if all four channels are used, the maximum sampling rate is cut by a quarter to approximately 216 samples per second. In order to keep a sampling rate of 500 samples per second, the hand built DAQ has four consecutive minute long sampling periods as opposed to the one sampling period used before. The consequence of having four consecutive sampling periods is that the high power consumption cycle lasts four times as long.

As with the initial prototype, the hand built DAQ has both an RTC and microSD card reader. The RTC is the same SparkFun Electronics™ DS3234

breakout board as used before. The microSD card reader is switched for a reader with the same capabilities but a smaller footprint, the Gravitech™ MicroSD Card Adapter. The smaller footprint allows it to more easily fit onto the hand built DAQ circuit board.

The microcontroller can be programmed via an external FTDI microchip such as SparkFun Electronics™ FTDI Basic Breakout. The omission of a continuously powered FTDI microchip allows for a low powered sleep cycle without the use of an external relay and microcontroller. The DAQ now experiences significant power reduction from simply putting the microcontroller into a sleep cycle and using a transistor to control power to the sensors.

The power is provided to the system via a battery supply regulated by a 5 V regulator. A photograph of one of the constructed hand built DAQs created is depicted in Figure 23.



**Figure 23.** Photograph of one of the hand built DAQs from the front (top) and back (bottom)

### 3.4.3 Problems Encountered

Two chief issues were encountered while working with the hand built DAQs; they would continuously restart or short. The first issue, the DAQ continually restarting, was sporadic, making it very hard to recreate the problem for investigation. This resulted in the cause of the issue not being discovered until the hand built DAQ was no longer in use and it began appearing in other DAQ revisions. The restarting



was determined to be a result of the power supply and will be discussed in detail in Section 3.7.

The second issue, shorting, was determined to have two fairly straightforward causes. The most obvious cause was the excessive amount of external wire necessary, as clearly visible in Figure 23. Although the wires are insulated, it is easy for exposed sections to accidentally come into contact with one another during normal handling. The less obvious cause of the shorting was the use of excess low viscosity soldering flux. The flux used was thin enough that it was easy for it to drip down the circuit board unnoticed, bridging sensitive connections. Often times, when the DAQ was plugged in after such an occurrence the flux quickly vaporized without causing damage. If the flux did not quickly vaporize, the connections created from the excess flux shorted the ADC boards causing them to fail. This problem can be easily mitigated in future prototypes using a “no clean” flux which does not conduct electricity.

### 3.5 PCB CAD DAQ

#### **3.5.1 PCB DAQ Description**

After a prototype is created by hand it is a natural progression to then transfer the design to a printed circuit board (PCB). Using a printed circuit board has several benefits over a typical hand built prototype. Having metal traces as opposed to wires completely eliminates the shorting problems due to handling of the DAQ described in Section 3.4.3. Copper fills allow for the creation of power planes, allowing

components to easily connect to both power and ground sources. Designing the circuit as a PCB also decreases the overall size of the footprint used, especially when using surface mount (SMT) components. Finally, having the connections between the components already manufactured within the board significantly reduces the time required to construct each DAQ. Ordering manufactured PCB circuits can also cut cost depending on the quantity ordered.

The primary components used in the PCB DAQ, such as the ADC microchips and RTC, are the same as those used in the hand built DAQ. Except now, instead of using break out boards provided by SparkFun Electronics™ and Adafruit Industries™, the basic components are placed directly onto the PCB. Other components like the microcontroller are simply the SMT counter parts of the ones used with the hand built DAQ.

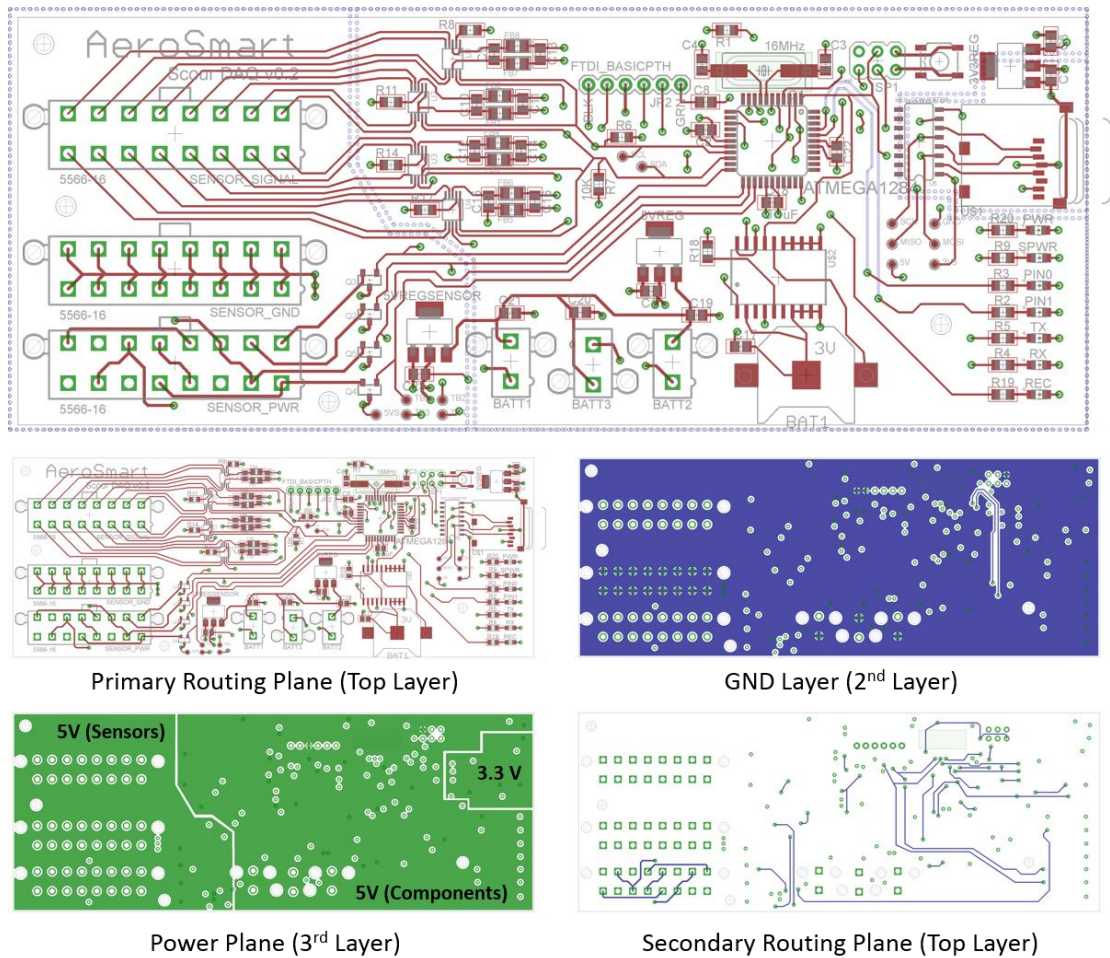
The PCB DAQ was designed using Cadsoft™ EAGLE. It consists of four different copper layers. The top and bottom layers are simply used for routing signal traces with all of the components mounted on the top layer. The second layer provides a global ground as well as electromagnetic insulation between the power layers and signals running through the traces. Finally, the third layer provides power to the components and is divided up into three sections. Two of the sections provide 5 V power, one to the sensors and one to the 5 V onboard components. These are each supplied from two different voltage regulators to avoid overheating. The third section supplies 3.3 V, once again supplied by its own regulator. Each PCB layer is represented in Figure 24. The schematic for the PCB and a bill of materials can be

found in Appendix A: At the time of this writing, the boards are waiting to be manufactured and have not yet been tested.

### **3.5.2 Additional Features**

The PCB DAQ is designed to have a few minor but helpful additional features when compared to the hand built DAQ. The most obvious of these are the onboard connectors for the battery and the sensors. The board has three separate battery connectors linked in parallel to permit the addition of extra batteries to increase power capacity without increasing voltage. It is not required however, to have more than one battery connected for the DAQ to become operational.

It should be noted that each sensor has its own power and ground connection present on the board. While it may be simpler and more compact to have only one power and one ground connector to supply all of the sensors, the individual connectors serve two purposes. First, it allows each sensor to be treated individually; therefore, if one sensor is malfunctioning, it can easily be completely severed from the system to avoid any disturbance to the other sensors. Also, like the hand built DAQ, four consecutive sampling periods are required to retrieve data from all available sensors. Having separate power connections for each sensor allows the capability to switch on only the sensors needed for each individual sampling period, resulting in significant power reduction, especially when extrapolated over time.

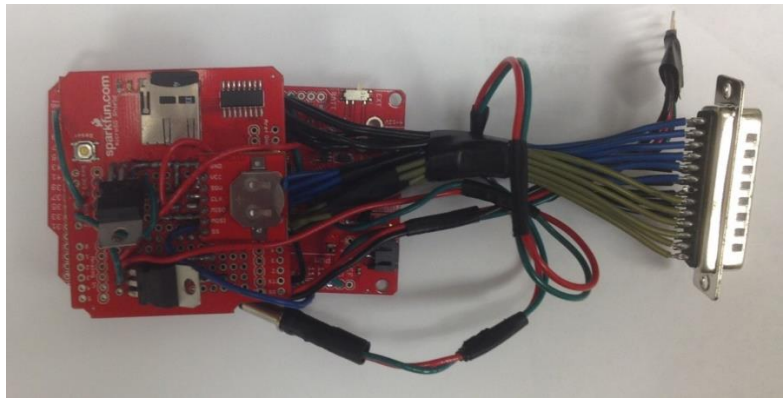


**Figure 24.** CAD drawings of the PCB DAQ board, including individual representations of each copper layer. The three segregated power planes have been labeled for the reader's convenience

### 3.6 Temporary Development Board DAQ

With the hand built DAQs needing continual repair due to shorting components, it was decided to temporarily return to DAQs similar to the initial prototype while waiting for the PCB DAQ to be manufactured. The primary improvement of this temporary DAQ over the initial prototype is the use of a new development board that eliminates the need for an external relay and microcontroller

to enter a sleep mode. The development board used is SparkFun Electronic's™ “pro” version of the Arduino Mega used before. The pro version simply strips out many of the components used to simplify use of the board for new electronics hobbyists, including the FTDI microchip mentioned before. This reduces the extraneous power consumption used by the board and allows it to achieve a low power sleep cycle. Although an improvement over the initial design, the power savings are not as great as expected from the PCB DAQ. An example of the temporary DAQ is presented in Figure 25.

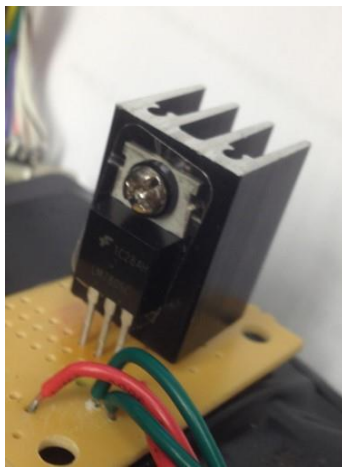


**Figure 25.** Temporary DAQ created using SparkFun Electric's™ Arduino Mega Pro

### 3.7 Batteries and Overheating

Lead acid batteries have been chosen to supply power to the DAQs used in this study for their reliability and availability in long life capacity. Lead acid batteries are primarily available in 6 V and 12 V options, although many others exist. The 12 V batteries were initially used in order to ensure that the 5 V regulators could achieve the desired 5 volts after compensating for energy dissipation during regulation.

It was discovered however that the use of a voltage over twice the required voltage needed was the cause of the sporadic restarting experienced by both the hand built DAQ and temporary DAQ mentioned above. While the 5 V regulators used in the study are rated to be able to handle such a drop in power, they could not do so without overheating and temporarily cutting the power. The problem was temporarily fixed by applying heat sinks to the regulators as pictured in Figure 26. The final solution involves switching to 6 V batteries so that the regulators do not have to work as hard and do not require heat sinks. Examples of the 6 V and 12 V batteries used in the study are depicted in Figure 27.



**Figure 26.** Heat sink used to prevent overheating of the 5V regulators



**Figure 27.** Typical batteries used to power the DAQs in this study. 12V-35amp-hr (left) 6V-13amp-hr (right)

The problem being caused by overheating also explains the sporadic nature of the restarts. The onset of overheating is greatly affected by two conditions, ambient temperature and the number of sensors connected to the power source. Changes in ambient temperature mean that when the DAQs are tested on a cool day or in an air-

conditioned lab, overheating is not an issue, or is at least delayed long enough to go unnoticed. On a hot day the onset of overheating in the regulator is very quick and obvious. Adding more sensors to the system draws extra power that the voltage regulator must adjust, causing it to dissipate more heat. This explains why the issue was never observed with the initial prototype, as it was only ever connected to four sensors. Also, much of the testing done in the lab was performed with fewer sensors to simplify problems that needed troubleshooting. Testing using the complete number of sensors was performed, but failure was not observed due to the air-conditioned environment.

The two reasons listed above caused the failure to be observed only sporadically, making it very hard to recreate and troubleshoot. The cause was only discovered when a gust of wind caused the system to temporarily recover. These issues have not reappeared since the switch to 6 V batteries. As an additional safety measure, separate voltage regulators are now used for the sensors and other 5 V onboard components.

## Chapter 4: First Installation – Bacon Ridge

### 4.1 Install Site Description

#### **4.1.1 Site Selection**

The first installation site selected is a tidal site, Bridge No. 02072, located on MD450 over Bacon Ridge Branch near Annapolis Maryland, in which the direction of the water flow changes in correlation with the tide. The selection of a tidal site, was based on the assumption that the constant flux of flow direction and a riverbed composition of primarily loose sediment would create an environment of constant scouring and refilling. The average depth of the water around the bridge is around 1 m. Photographs of the first installation site can be observed in Figure 28.

#### **4.1.2 Flow Speeds**

As measured by an OTT MF pro flow meter with a resolution of 0.01 m/s, typical flow speeds at the tidal site continuously changed between extremely low, approximately 0.01 m/s, to unmeasurable. It became apparent that the whisker sensors would not operate in these extremely low velocity conditions and that a new design would be required. It was necessary that this sensor remain as compliant as possible, allowing it to deflect in response to the slightest fluctuation in velocity. The necessity for this type of sensor provided motivation for the creation of the "seaweed" sensor described in Section 2.2.2.





(a)



(b)

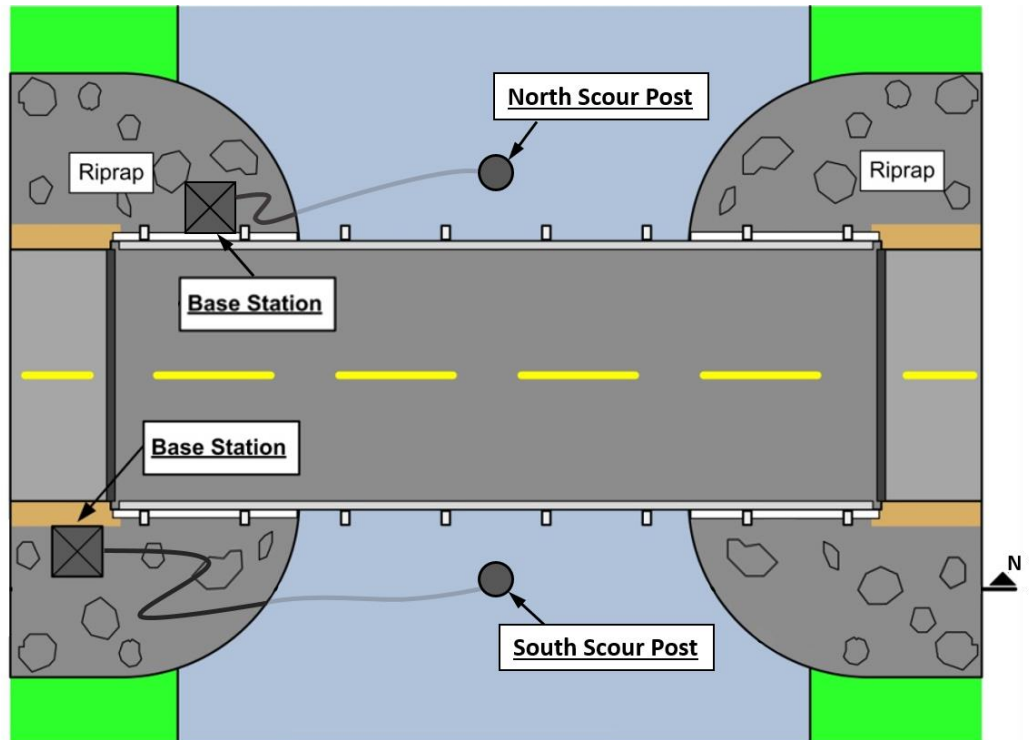


(c)

**Figure 28.** First install site at Bacon Ridge Branch tidal bridge. (a) North face of the Bridge (b) South side of the bridge (c) View of the bridge from the north looking south

## 4.2 Scour Posts

Two posts are installed at this location, each centered between the river banks and located approximately 1.8 m (6 ft) from opposite sides of the bridge. An illustration of the install site is presented in Figure 29 to provide the reader with better idea of the placement of each component described in the following sections.

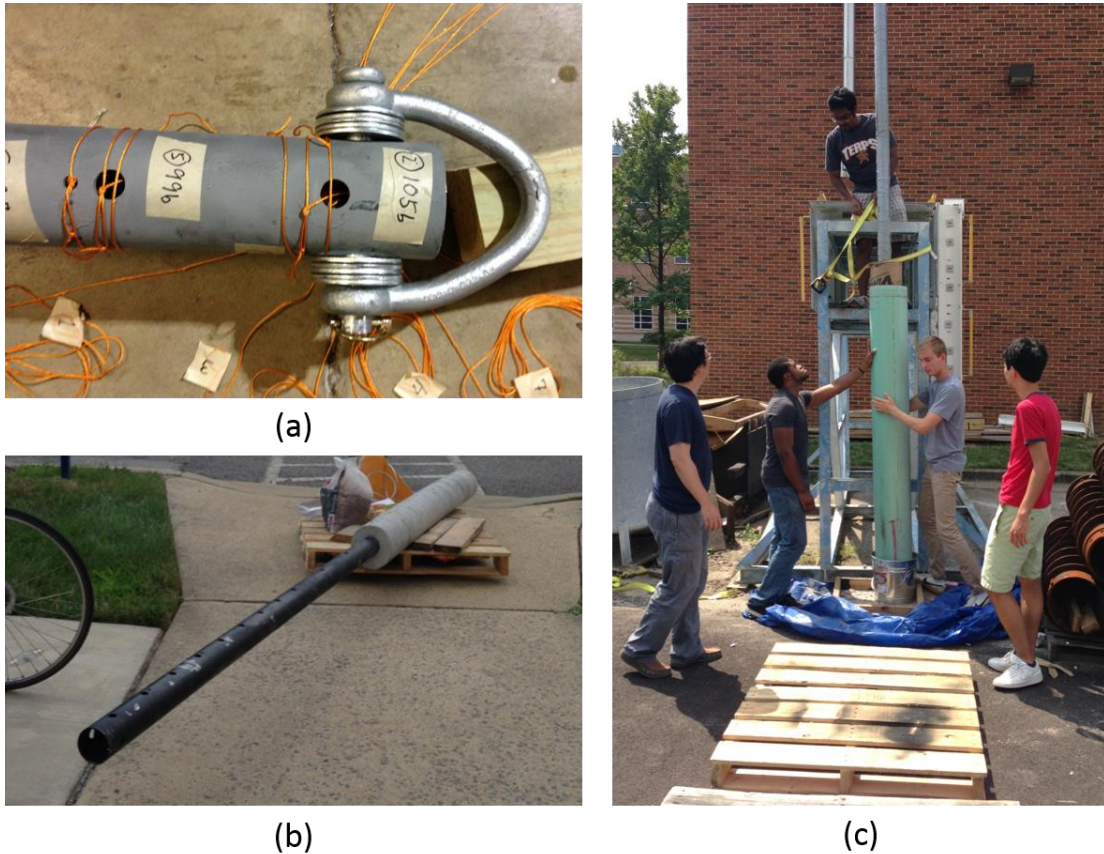


**Figure 29.** Illustration of the first install site at Bacon Ridge depicting the general placement of each component

### **4.2.1 Structural Characteristics**

The basis of the first Scour post prototypes consist of a 4.3 m (14 ft) long schedule 40 stainless steel post with a 7.6 cm (3 in) diameter. The bottom half of the post is encased in a concrete cylinder to ensure the stability of the post when struck

by large objects floating down the river. A clevis is installed 6.35 cm (2.5 in) from the top of the post, creating an easy attachment point for picking it up. Photographs of the structural components of the post can be viewed in Figure 30.

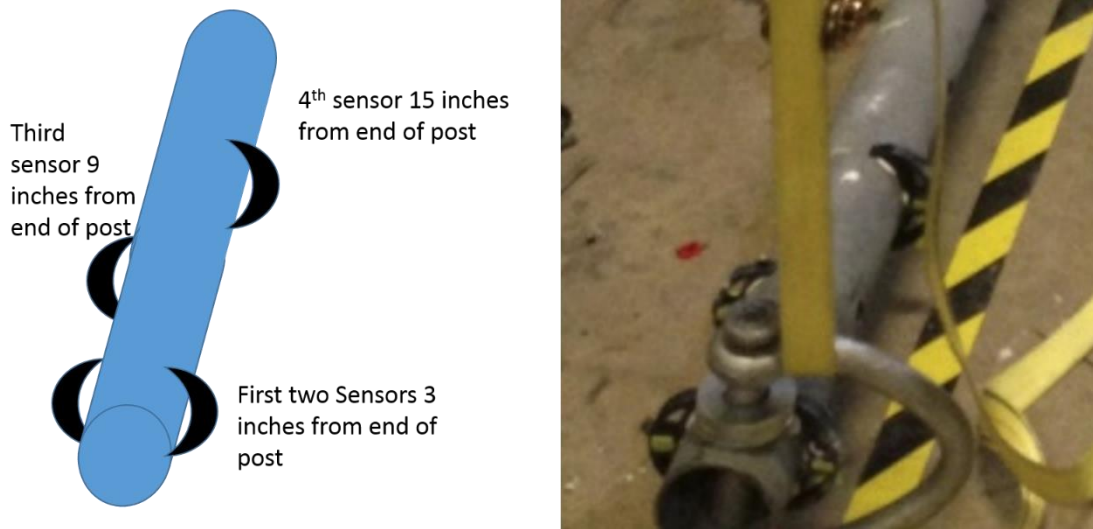


**Figure 30.** Structural components of the first prototype scour post. (a) Clevis used to hoist the post (b) Bare scour post encased with concrete (c) Process of encasing the scour post in concrete by vertically standing it inside a Sano tube and pouring in concrete.

#### 4.2.2 Sensors and Wiring

As depicted in Figure 31, four seaweed sensors are installed into each post, with the first two sensors installed 7.6 cm (3 in) from the top and each subsequent

sensor placed in 6 inch increments thereafter. The sensors alternate sides of the post so that two sensors are present on opposite sides of the post, and when the post is installed in the water, all sensors are positioned so that they are perpendicular to the mean flow direction.



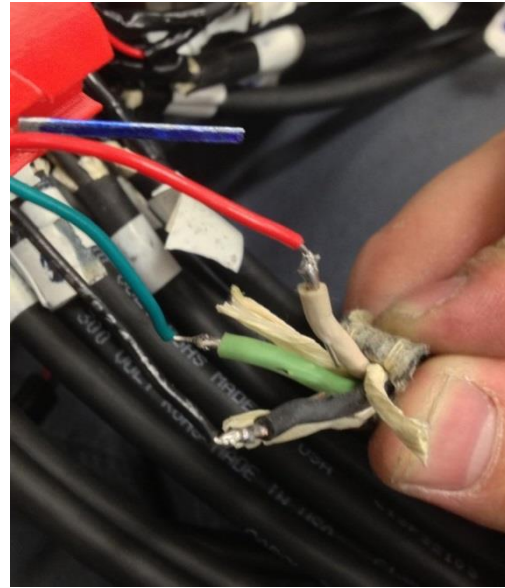
**Figure 31.** Illustration and photograph of seaweed sensor placement for the first post installation

The basic seaweed sensor design needed to be modified to adapt to the curved surface of the scour post. This task was greatly simplified with the use of a 3D printer. The sensor was designed as a crescent moon, with its inner curved surface matching the outer surface of the post. An opening in this curved surface allows access to the hall sensor connections. These connections are then covered with a water proofputty that solidified upon curing. Small holes have been placed at ends of the holder to allow it to be screwed directly into the post. A layer of waterproof putty is also added between the interface of the holder and post, to better secure this attachment. The synthetic fabric used to create the seaweed portion of the sensor is

approximately 5 cm (2 in) long and 1.9 cm (0.75 in) wide. Finally, the magnet is hung 5 mm from the hall sensor. An example of this holder is depicted in Figure 32.



**Figure 32.** Example of the seaweed sensor holders used on the first post installation



**Figure 33.** 22 gauge wire inserted and soldered into 18 gauge wire to allow for connection to hall sensors and DAQ

Each post is internally wired slightly differently, but in each case the wires from the post are safely routed to the shore through a 2.5 cm (1 in) conduit which acts as protection against objects floating down the river that could cut or catch onto the wire. The conduit is a large enough diameter to fit a total of four cables through it allowing 14 connections. This includes three cables containing three conductors and one cable containing four conductors. In the post on the north side of the bridge, the wired connections from the sensors are routed directly from the sensors and through conduit to a land based electrical box located on the side of the bridge. On the south side post the sensors are first wired to a small circuit board contained within the post

that provides a shared power and shared ground to the sensors. Utilizing this setup eliminated the need for routing the power and ground connections for each sensor through the conduit, thereby increasing the number of allowable sensors from four to eleven, with the extra availability intended to be used for whisker sensors. These sensors were not added for reasons explained in Section 4.4.2. For waterproofing, the internal PCB and its connections were completely encased in epoxy.

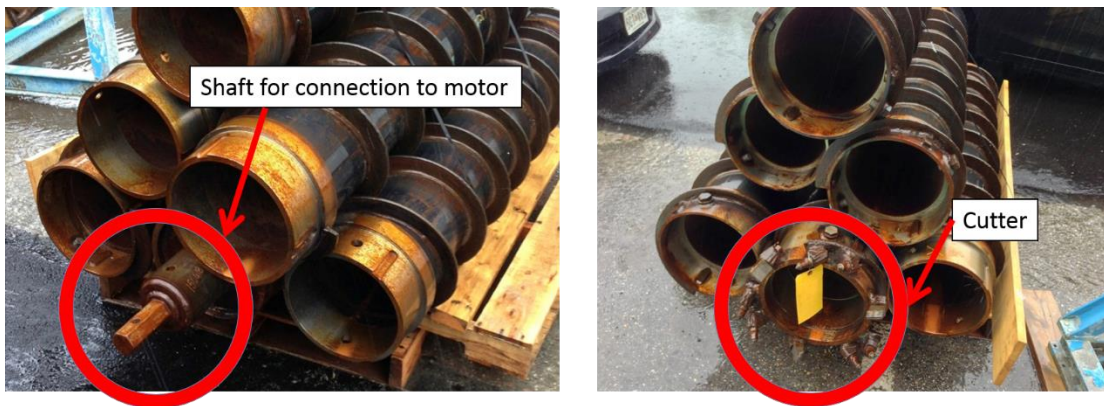
The electrical components are wired using 18 gauge Viper® SJOOW wire manufactured by Southwire. This wire is designed for use in wet environments, but not guaranteed for use in submerged settings. While not ideal, the wire was selected based on installation time constraints and the inability at that time to find a supplier with truly submersible cable.

The wire is also a much lower gauge than desired making it too large to solder into the plated holes in the sensors and DAQ. To compensate for this gauge difference, solid core 22 gauge wire was stripped and inserted in to the strands of the of the 18 gauge wire as depicted in Figure 33. The soldered connections, exposed electrical components, and short strands of 22 gauge wire were then covered in a water proof putty.

### 4.3 Installation

Due to the heavy weight and large size of the initial scour post, heavy duty construction equipment was required to install it. The largest of which being an excavator and hollow stem auger. The hollow stem auger acts as a large, hollow drill

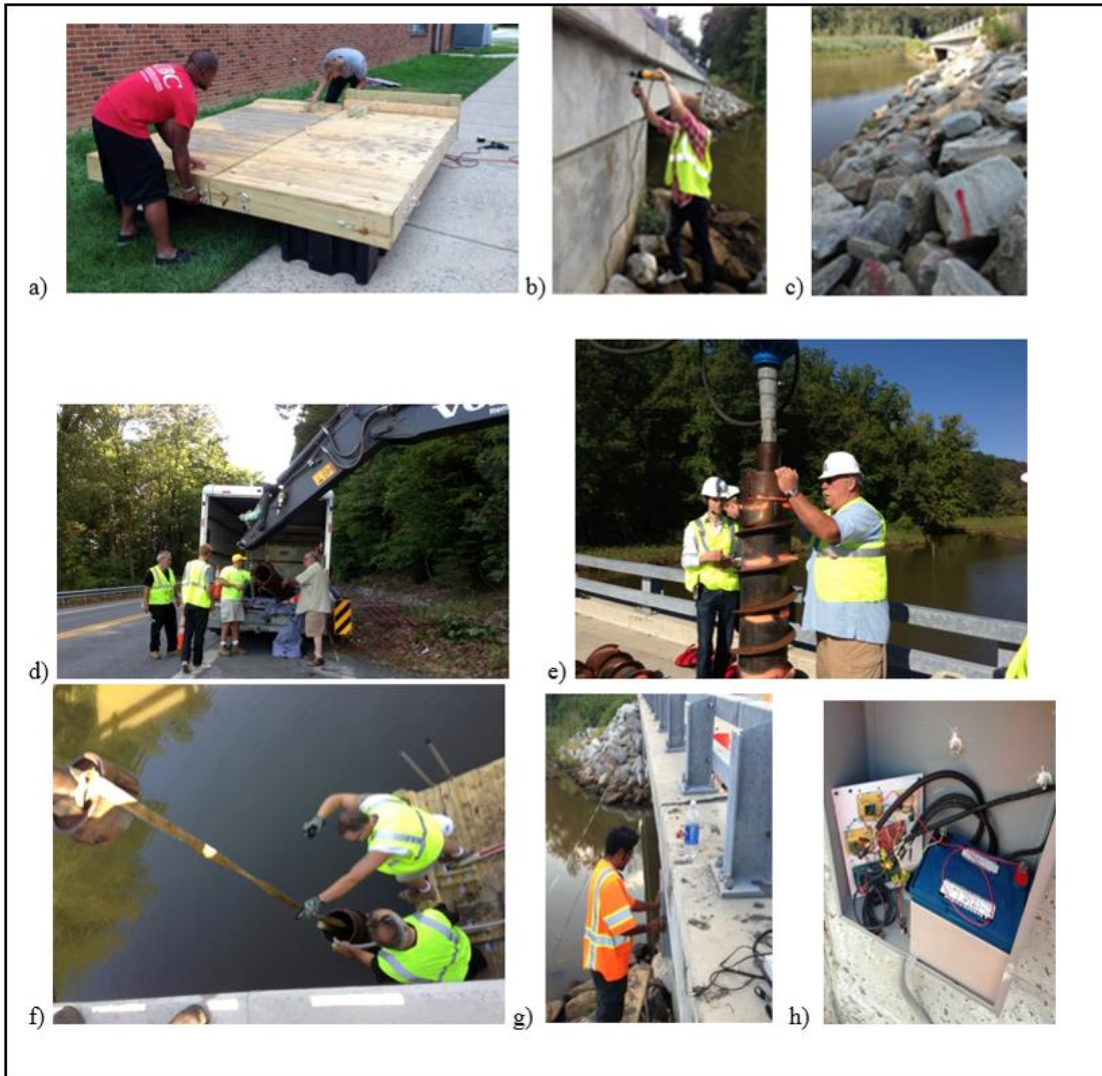
that the post can be dropped into. It comes in 1.5m (5 ft) sections that are attached as it is drilled deeper into the riverbed. The auger was held and rotated by a specialized excavator attachment via a shaft present on the top auger section. To avoid allowing the riverbed to fill the hollow auger, the bottom section was compression fitted with a disposable wooden plug. Upon drilling to the required depth, the auger attachment was removed so that the excavator could be used to place the scour post and conduit containing the wiring inside. A long steel pole and mallet were then used to knock the wooden plug from the bottom of the auger so that it could be removed without removing the scour post along with it. The wooden plugs were soaked in dawn soap for over 24 hours prior to the installation and coated with Crisco shortening immediately before the installation to help facilitate its unplugging. The elements of the Hollow stem auger are depicted in Figure 34.



**Figure 34.** Hollow stem auger section with labeled shaft connector and cutter

The conduit containing the wiring was run to a weather proof utility box bolted to the side of the bridge containing the DAQ system and battery. Once connected to the utility box, the above water portion of the conduit was covered with

the surrounding rip rap to avoid creating a tripping hazard. The underwater portion of the conduit was connected to a heavy chain to encourage the conduit to bury itself in the river bed, out of the way of debris floating down the river. Much of this process was performed using a floating platform constructed specifically for this installation. Photos highlighting key stages of the installation process are provided in Figure 35.



**Figure 35.** Photos of full-scale installation at Bridge No. 02072 on MD450 over Bacon Ridge Branch. a) students building installation working platform; b) installation of electronics housing on bridge structure; c) contact Miss Utility well in advance



as fiber optic cable had to be avoided on the south side of the bridge; d) deploy hardware to installation site; e) assemble auger on bridge deck; f) once hollow stem auger is to appropriate depth, knock loose plug at base of auger and with excavator, place sensor post into position; g) after removing auger, run wiring to data acquisition system on bridge wall; h) install battery; retrieve data card periodically to download data recorded from flow sensors for one minute every hour until such time that a wireless data logger is added to allow for interrogation of sensors from a remote location.

#### 4.4 Lessons Learned

Analyzing the difficulties experienced in building and installing the first prototype offers invaluable information for future installations. This section describes the most substantial of these lessons.

##### **4.4.1 Simplification of Initial Prototype**

Many of the initial lessons learned involved remembering not to lose sight of the number of unique and new techniques being applied to perform the first installation. Individually, the hurdles of incorporating these new techniques seems easily manageable, but they can quickly compound together into much more difficult obstacles. Below are a few ways the first installation could have been simplified to lessen the compounding of obstacles.

As mentioned in Section 4.1.1, a tidal site was chosen for the first installation site because it was believed that, with its loose sediment and reversal of flow direction in correlation to the tide, the height of the riverbed would constantly fluctuate. While in theory this sounds like a promising environment to test a scour monitoring system, it should have been noticed that the extremely low flow speeds

would not be ideal for the initial proof of concept prototype. Furthermore, the expected daily fluctuation in riverbed height was not observed.

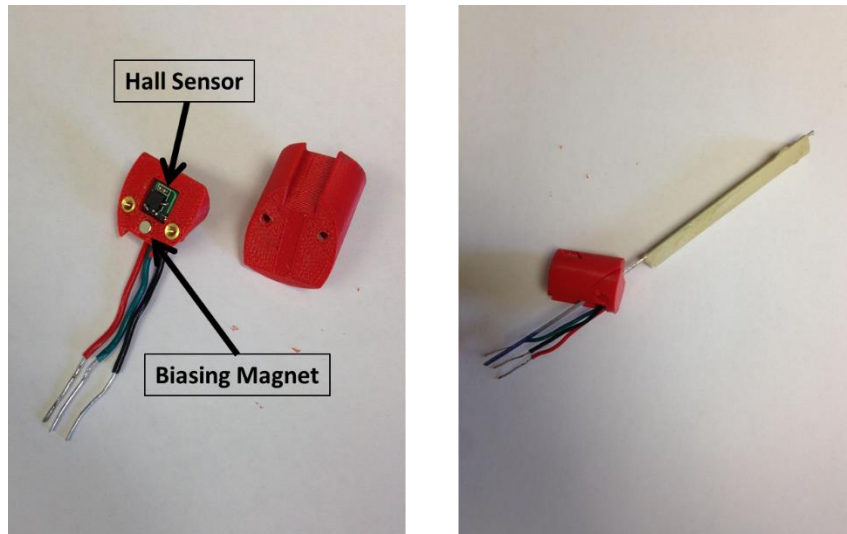
In hindsight, being the first installed prototype, it may have been wiser to use an incremental process by first focusing on simply proving the system's ability to discern which of its sensors are in the presence of flowing and which sensors are buried underground. This would have entailed searching for an install site with ideal flow velocity and not being concerned with its probability of scour. The post then could have been designed to ensure that a few sensors were well within the water flow and a few sensors were deeply buried. Using this simplified proof of concept post to work out bugs and flaws in the system, it would become easier to then use future installments to prove the detection of true scour and to optimize for extreme, low or high velocity conditions.

In anticipation of having a constantly fluctuating initial test bed, it was originally planned to have as many as 16 sensors installed on each post. Because it was believed that sensor construction had been mastered, this represented the maximum number of sensors that could be connected to the DAQ. However, applying the sensors to the actual post itself and ensuring the water proofed integrity of every connection proved to be a sizeable task. Given the time constraints of the install date and a problem encountered with the installation of the whisker sensors discussed in the next subsection, it was decided to reduce the number of sensors to only four seaweed sensors. This made it much more manageable to address some of the other unforeseen problems also discussed in this section.

#### **4.4.2 Whisker Pre-stress**

Prior to the construction of the initial full scale scour posts, increasing the clamping pressure applied to the whiskers in the whisker sensors always proved advantageous. With increased clamping pressure, the whisker becomes more restricted at the clamping point, thereby also increasing the stress generated upon bending. Following this logic, the sensor's plastic holders were designed as cylinders that had a gradually increasing circumferential thickness from back to front. This way when they were forced into the drilled holes of the steel post, the tight fit at the end of the cylinder would clamp onto the whisker with extremely high pressure. The addition of a waterproof putty to cement the holders into the post further tightened the fit increasing the pressure even more.

Upon the installation of the whisker sensors using this method, the whiskers became more brittle and susceptible to plastic deformation than had ever been previously observed. The whiskers began breaking at the clamp point in response to very small deflections, when they had previously been observed to be bent into 90 degree angles without breaking. An example of the whisker holder used is presented in Figure 36.



**Figure 36.** Whisker sensor used for the first installation prototype. The whiskers were angled at 45 degrees to allow them to fit into the auger

It was determined that the newly induced fragility was likely due to the excessive amount of pre-stress placed on the whisker by the clamping mechanism. By creating such a tight clamp on the whisker it is probable that the whisker was near its maximum stress in an undeflected state. Deflecting the whisker further increased this pressure to a point where it is quickly work hardened and snapped.

To avoid creating high pre-stresses in future whisker designs, clamping mechanisms have been abandoned. The whiskers are instead encased in a block of epoxy at the desired clamped point. With epoxy's high structural stiffness and ability to bond directly with the whisker, the whisker becomes highly immobilized without the addition of any pre-stress whatsoever.

### **4.4.3 Wiring Lessons Learned**

Many of the difficulties encountered during the first installation can be attributed to the use of the oversized, 18 gauge wire. These include problems dealing with the physical dimensions of the wire as well as with the process of effectively increasing the gauge of the wire to fit smaller connections.

One of the first problems encountered involved simply feeding the wire through the conduit. While the wires were able to fit through the 2.5 cm (1 in) conduit, it was with a very tight tolerance. “Fish tape” was used to facilitate the task. The stiff fish tape was first fed through the empty conduit and taped to the end of the wires. The fish tape and wires were then forcefully pulled through the conduit while being heavily coated with lubricant; a process that could have been made much easier with the use of a thinner cable consisting of higher gauge wires. This would also allow for the cross-sectional size of the post to be decreased as well, significantly easing the installation process as a whole.

As mentioned above, to increase the gauge of the wire from 18 to 22, smaller 22 gauge wires were partially stripped and inserted into the strands of the 18 gauge wire. Besides being a more time consuming process than being able to connect the wires directly to the sensors and DAQ, this process initially did not appear to have any major pitfalls. But, upon testing the sensors many failed to produce a signal. It was determined that in several cases, where the 22 gauge wire was inserted into the 18 gauge wire, it often pierced through the casing of the wire it was being inserted into and penetrated into the casing of an adjacent wire causing a short. These bridges

between conductors initially went unnoticed due to the fact that they occurred inside the cables outer shielding.

Given the lessons learned about the wiring discussed in this section it became evident that finding a higher gauge and submersible class wire needed to become a top priority. Through extensive searches prior to the initial installation, such a commercially available wire could not be located. Many suppliers would offer cables for wet environments but not assure their capability in submersible environments. An alternative was discovered through ordering custom made cables from Mercury Wire, a company specialized in submersible wiring. These are the wires used in the second installation and are described in Section 5.2.4.

Not related to the gauge of the wire, it was discovered that the putty used as a waterproofing and adhesion agent for the seaweed holder and wire connections was not aptly suited for the task. Shortly after the first installation, it was discovered that the power connection to one of the top seaweed sensors had become disconnected as displayed in Figure 37. This is likely a result of the putty not having enough adhesion to the sensor holder and the post, and becoming extremely brittle upon curing, causing it to easily break apart and the wire to break away with it.



**Figure 37.** Broken seaweed sensor with disconnected wire from first installation

#### **4.4.4 Other Lessons Learned**

There were other lessons learned during the first installation which do not require in depth explanation. Two of these lessons are presented below.

Upon close examination a drift is evident in the data presented in Section 4.5. This can be avoided in future installations by tying the ground of the DAQ to the earth. This would involve driving a copper pole into the terrain and extending a wire from the pole to the DAQ's ground.

When the south post was drilled into the ground the auger was drilled roughly a foot deeper than on the north side of the bridge to facilitate removal of the wooden plug from the submerged end of the hollow stem auger. Gravel was poured into the auger to backfill the hole to the same elevations as the north post hole. While this appeared to work during the installation, within less than two weeks, the loose sediment and gravel allowed the post to sink, causing it to become completely buried and leave no sensors exposed to the water flow.

#### 4.5 Results

Data from the seaweed sensors are shown in Figure 38 for the Bacon Ridge Branch site and provides a clear demonstration of the technology performing as intended. This figure shows data from three seaweed sensors on the north post as collected by the first generation prototype DAQ described in Section 3.3. The top sensor with a severed connection alluded to in the lessons learned section has been omitted. For this post, all but the top ~22-23 cm of the post was buried.

The individual graphs are of 60-second long data traces taken hourly, starting at low tide at 12:43 (left traces), and ending at high tide at 19:55 (right traces). The top row of traces are from the sensor 7.5 cm (3 in) below the top of the sensor post, the middle row of traces is from the sensor 22.9 cm (9 in) below the top of the sensor post, and the bottom row of traces is from the sensor 38 cm (15 in) below the top of the sensor post.

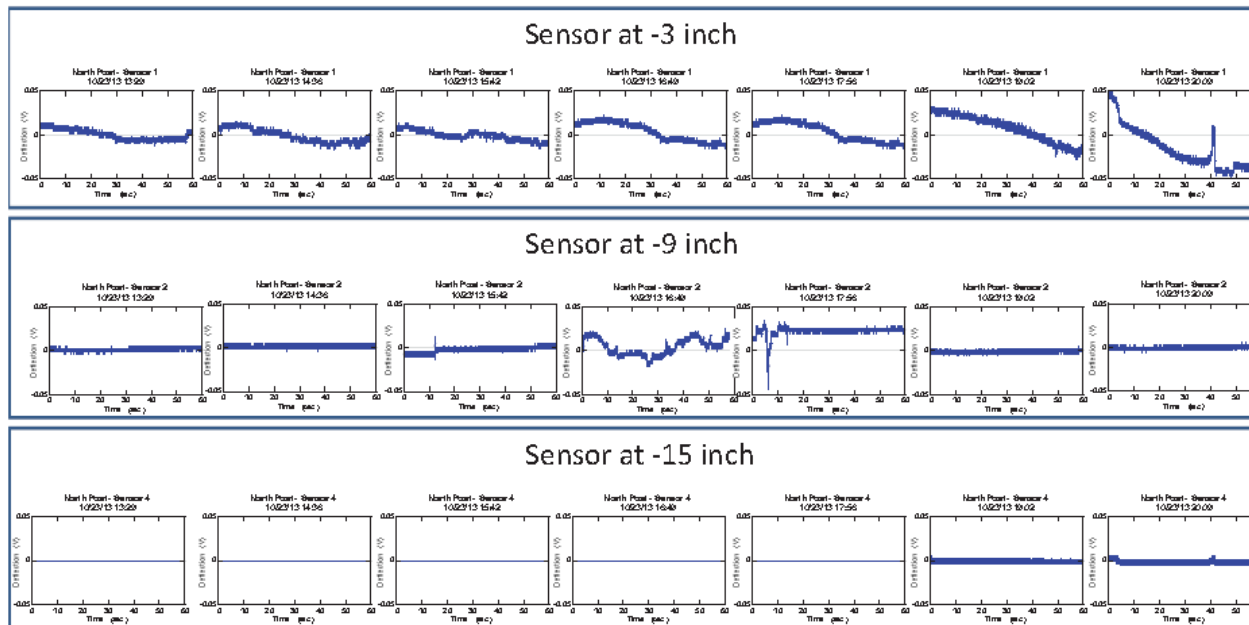
All seven data sets from the sensor 7.5 cm below the top of the sensor post show the sensor is in water because the response exhibits flow induced motion. The sensor at 22.9 cm below the top of the post is just barely buried and only shows motion at the time of highest flow velocity, between low and high tide. The sensor that is 38 cm below the top of the post is fully buried and shows no motion. Such data confirms the ability of the proposed scour monitoring system to detect scour.



↙
↘

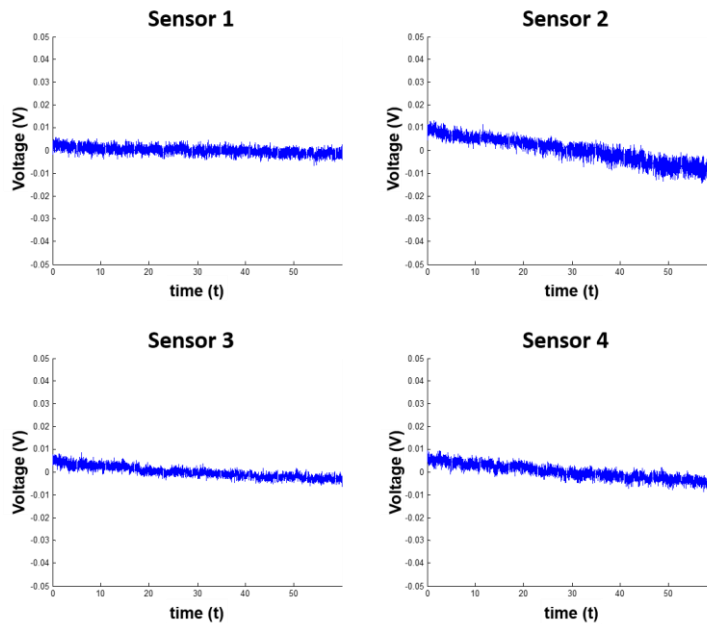
Low tide 10/23/13 - 12:43  
 High tide 10/23/13 - 19:55

TIME  
 13:29      14:36      15:42      16:49      17:56      19:02      20:09



**Figure 38.** Preliminary results from the sensor post on the north side of the Bacon Ridge Branch Bridge. All seven data sets from the sensor 7.5 cm (3 inches) below the top of the sensor post show the sensor is in water because the response exhibits flow induced motion. The sensor at 22.9 cm (9 inches) below the top of the post is just barely buried and only shows motion at the time of highest flow velocity, between low and high tide. The sensor that is 38 cm (15 inches) below the top of the post is fully buried and shows no motion.

The South post has always remained buried, and consistently outputs a static signal for every data set. The plots in Figure 39 are examples of what the sensors read during each sampling period. The slight drop in voltage is drift due to the absence of an Earth ground as alluded to in Section 4.4.4.



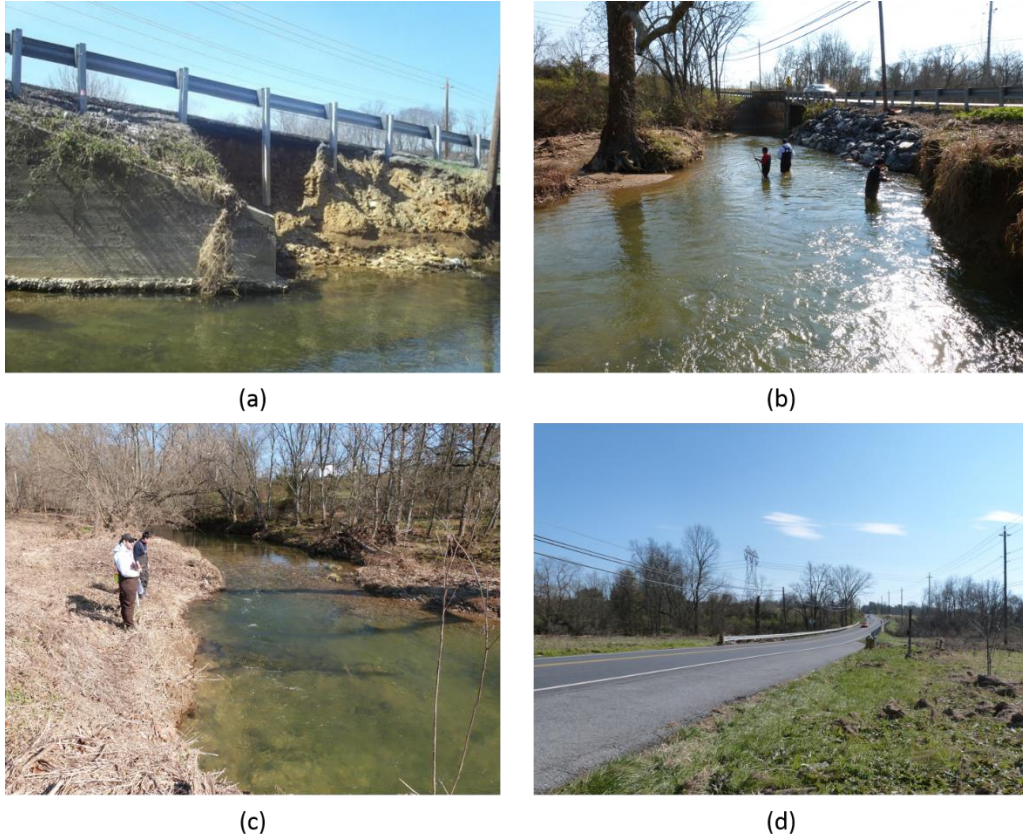
**Figure 39.** South post sensors reading constant static signal

## Chapter 5: Second Installation – Bennett Creek

### 5.1 Install Site Description

The second installation site selected is, Bridge No. 1008600, located on MD355 over Bennett Creek near Frederick Maryland. The site was selected for its propensity toward lateral riverbed migration. Different from conventional scour, lateral riverbed migration occurs when the water flow erodes a river bank, effectively causing the river to shift to a new location. Photographs of the first installation site, including dangerous effects of lateral riverbed migration can be observed in Figure 40.

The location also has the advantage of much higher flow velocities compared to the first installation site. Typical flow velocities observed at the site are roughly 0.3 m/s (1 ft/s) to 0.46 m/s (1.5 ft/s).



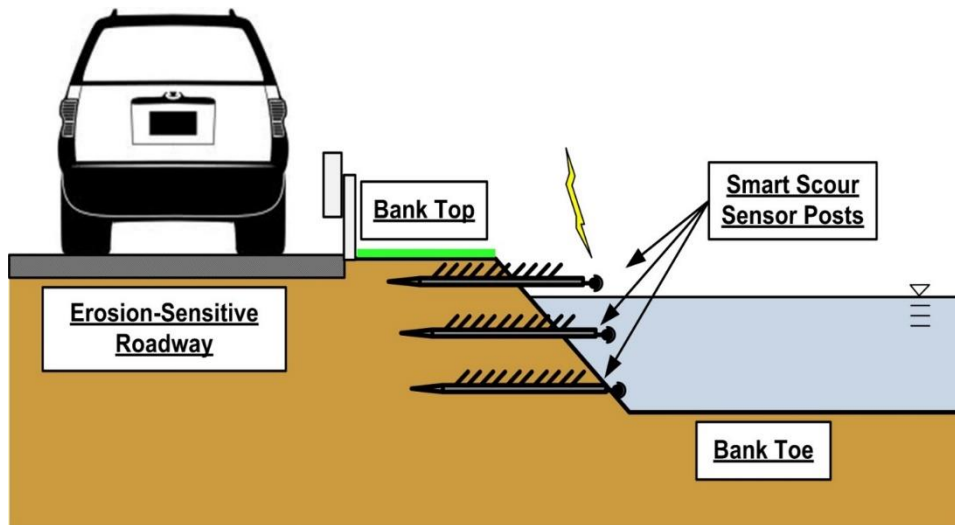
**Figure 40.** Photographs of the second installation site before installation. (a) Exposed guard rail due to lateral riverbed migration before the addition of rip rap protection. (b) Installation site as viewed from up stream. (c) View of upstream conditions as viewed from the installation site. (d) Bridge No. 1008600 viewed at a distance

## 5.2 Scour Posts

### **5.2.1 Method for Measuring Lateral Riverbed Migration**

Unlike the posts for conventional scour, the lateral riverbed migration posts are installed horizontally as opposed to vertically, although the basic concept remains the same. The sensors are installed along the length of the post so that as the river

bank erodes away, the extent of this erosion can be inferred by the number of sensors exposed. This basic concept is illustrated in Figure 41.



**Figure 41.** Illustration of horizontal post installation for detection of lateral riverbed migration

Two posts are installed for the purpose of the current study. To understand whether the proposed system can be utilized in air as well as water, one of the posts is located several feet above the average water level, while the other post is located underwater as indicated in Figure 42.



**Figure 42.** Installation locations of the lateral riverbed migration posts

### **5.2.2 Structural Characteristics**

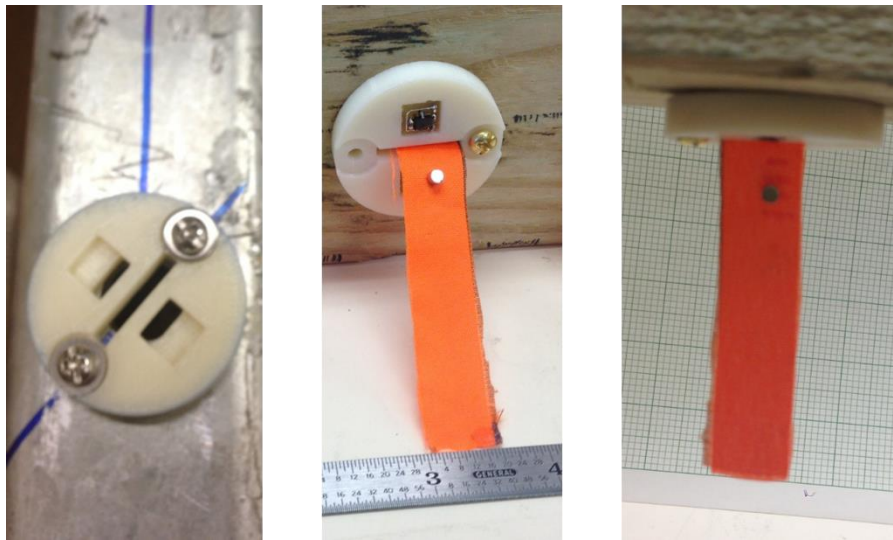
A 3 m (10 ft) long, stainless steel post with a 5.08 cm (2 in) square cross-section is used for the lateral migration posts. The flat outer surface of the square cross-section greatly eases the process of installing the sensors to the post compared to the previously used circular cross-section. The concrete basin was deemed not to be required for this installation making the post much lighter and capable of being moved by hand. Five holes are drilled into the post to allow for the wiring from the attached sensors to run inside of the post. The first hole is 15.25 cm (6 in) in from the end of the post and the four subsequent holes spaced in 30.5 cm (1 ft) increments behind it.

### **5.2.3 New Seaweed Sensor Design**

The scour posts are designed to be fitted with five seaweed sensors and the capability to add on three whisker sensors after the installation. To accommodate the horizontal placement of the posts, the seaweed sensor holder design needed to be altered. This alteration actually simplified the sensor design into the shape of a large coin that can be attached to the flat surface of the post. An approximately 5 cm long by 1.5 cm wide strip of synthetic fabric is epoxied to the holder and dangled from a slit centered on its circular face, creating the artificial seaweed.

One feature of the new seaweed sensor design includes using two hall sensors per seaweed as opposed to one. Using two sensors acts as a safety redundancy in case one sensor fails, and also allows for experimenting with adding the two signals

together in an attempt to achieve a higher signal to noise ratio in the data. The hall sensors are embedded into a shallow square cutout of the sensor face and coated with epoxy for waterproofing and protection. This positions the hall sensors so that they are reading the magnetic induction in the axis along the seaweed length. Finally, two magnets, one epoxied to each side of the fabric, are hung 5 mm below the hall sensors. Photographs of the new seaweed sensor design are presented in Figure 43.

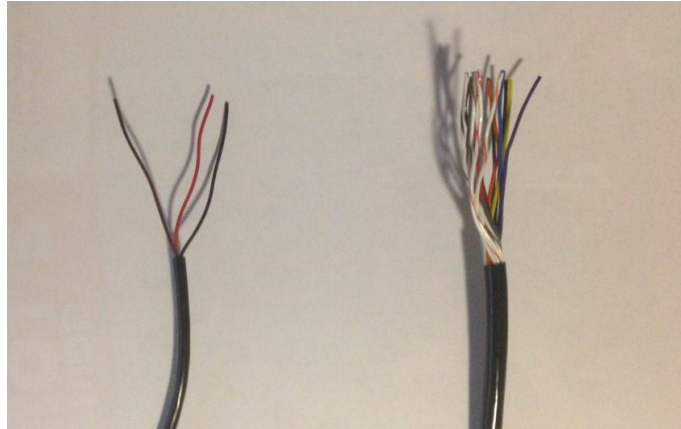


**Figure 43.** Seaweed sensors specially designed for the horizontal posts

### 5.2.4 Wiring

The higher gauge, smaller diameter and guaranteed submersible cable required for the second installation is custom built for this project by Mercury Wire. Two variations of the cable are used. One variation consists of three conductors and is used to connect directly to the sensors. The other variation consists of 13-conductors and is used to combine the signals from the three-conductor cables into a smaller diameter to be transferred through the conduit to the DAQ system. Other

than the number of conductors and their outer diameter, the cables are identical. A photograph of the new cables is presented in Figure 44, and the datasheet for each wire can be found in Appendix E:.



**Figure 44.** Submersible wire used in the second installation, consisting of a 3 conductor wire (left) and 13-conductor wire (right)

As mentioned in the paragraph above, each hall sensor is connected to its own the three-conductor cable. The connections are coated with epoxy for waterproofing, being sure to cover the entire portion of the cable's striped external casing. While the outer casing of the wire package is submersible, the casings around each individual conductor are not. If the epoxy is not applied so that it completely covers this area, the capillary effect can cause the outer casing to fill with water and eventually soak through the casing of each individual conductor.

The cable from each sensor is then fed through the post to a junction where they are connected to three 13-conductor wires. They are connected in such a way that the each 13-conductor wire contains only power, ground or signal connections. Connecting the sensors this way allows for a logical organization of the wires. Each

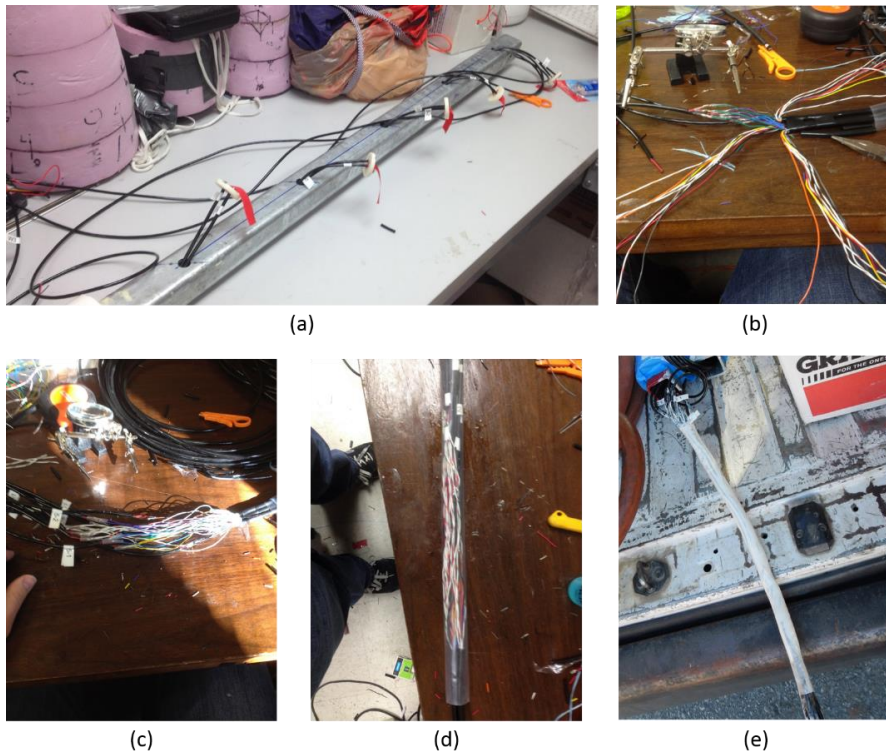


of the conductor casings inside the 13-conductor cables possesses its own unique identifying color. With each of the 13-conductor cables being composed of the same array of conductor colors, it makes it possible to assign each color to a sensor. For example, the ground connection from Sensor 1 would be connected to the red conductor of the ground cable, the signal connection from Sensor 1 would be connected to the red conductor of the signal cable, and the power connection from Sensor 1 would be connected to the red conductor of the power cable. This makes it easy to sort out what wires belong to which sensor when connecting to the DAQ, so long as the function of each 13-conductor cable is correctly labeled.

Utilization of three 13-conductor cables provides enough connections for 13 hall sensors, via 13 three-conductor cables, to be connected to each scour post. Ten of these cables are used to connect the five seaweed sensors. The ends of the three remaining cables are epoxied over and left unconnected inside the post. After the installation, a cap with whisker sensors attached was added to the post to which these cables are then connected to as discussed in 5.6. Until the addition of this cap, the end of the post was covered with a cut open tennis ball.

Special attention must be given to connecting the wires at the junction between the three-conductor cables and the 13-conductor cables. The conductors must have secure connections, be protected from the elements and must not short into one another. To create a secure connection, the conductors were twisted together and soldered. Heat activated shrink tube is then used to cover and isolate the connections from one another. To help insure the isolation of each wire connection, as well as to

decrease the total diameter of the junction, the connections were staggered ~1 in from each other. This created a total junction length of a little over a foot. In order to waterproof and protect the junction, a large heat activated shrink tube is placed over all of the connections and filled with epoxy. This outer shrink tube is then heated before the epoxy has a chance to cure, causing air bubbles and excess epoxy to squeeze out of the junction. Photos highlighting the key stages of wiring the post are presented in Figure 45.



**Figure 45.** Second post wiring process (a) Seaweed sensors are fed through the post (b) three-conductor and 13-conductor cables are soldered together (c) Shrink tube on individual conductors heated (d) Large shrink tube placed around connection bundle before being filled with epoxy (e) Completed junction with cured epoxy

### 5.3 Installation

Being much smaller than the post used in the first installation and light enough to be moved by hand, the amount of heavy construction equipment needed was greatly minimized for the lateral migration posts. A horizontal drilling company was hired to perform the drilling required to install the post (BelAir Underground Services Inc., Joppa Md). They provided careful depth control and horizontal placement of the two sensor posts. For each post the drilling was initiated approximately 6 m (30 ft) from the river bank and concluded once the drill penetrated the riverbank wall.

Before retracting the drill head, it was attached to the end of the conduit containing the post wiring. This way, while the drill was pulled back through the drill hole, the conduit would be pulled through with it to be connected to an electrical box installed where the drilling began. The conduit continued to be pulled through the hole during the insertion of the post, helping it feed through the drill hole as well. Both posts were installed leaving two exposed seaweed sensors and three buried seaweed sensors. This proved to be much easier to achieve with the horizontal posts compared to the previously installed vertical posts. Photos highlighting the key stages of the installation process are provided in Figure 46.



**Figure 46.** Photos of full-scale installation at Bridge No. 1008600 on MD355 over Bennett Creek. a) Jeff Knaub of MDSHA showing UMD students target location for sensors; Rip rap protecting bank from prior scour event at top left of photo; b) installation of turbidity curtain on morning of installation; c) BelAir drill rig ~9.2m (30 ft) from where sensor will protrude from bank; d) sensor used to track depth and lateral position of drill tip; e) feeding wiring and sensor post into bank ~60 cm (2 ft) above nominal water level as drill bit is retracted; f) admiring successful installation of the in-air sensor post; g) feeding wiring and sensor post into bank at depth of ~15.25cm (6 inches) below nominal water level for this site.

Finally, as depicted in Figure 47, a weather proof electrical utility box was erected near the area the drilling began to contain the DAQ components. Copper rods

were driven into the ground near the box and connected to it via a copper wire to provide an earth ground for the DAQ systems.



**Figure 47.** Electrical box for storing DAQ and electrical components for the second installation

#### 5.4 Lessons Learned

The lessons learned from the first installation were applied to the second installation and proved to be very useful. The time and effort spent constructing and installing the second scour post prototypes was significantly reduced while the integrity of the system achieved a higher standard. As would be expected, the number and severity of lessons learned decreased with the subsequent installation. That being stated, several valuable lessons were still learned with the installation of the second post, with the most pertinent ones discussed below.

##### **5.4.1 Erosion Due to Drilling**

The most visibly evident lesson learned involved erosion around the riverbank wall as a result of the drilling. After drilling and the insertion of the post, the outer

opening of the drill hole was packed with mud from the river while natural settling of the foundation was left to fill in the rest. Upon the first return to the install site, it was noticed that while settling appeared to have buried the portion of the post deep within the foundation, the dirt that was packed around the opening of the drill hole by hand had eroded away. This left undesirable “coves” in the foundation around the post as depicted in Figure 48. It should be studied how to prevent such coves in future horizontal scour post installations, as they could have the adverse effect of contributing to lateral riverbed migration.



**Figure 48.** Residual cove formed from drilling

#### **5.4.2 Ice Formation around the Post**

One unexpected phenomenon observed involved the formation of ice around the underwater post. While it was expected that the post would be surrounded by ice when the river itself became frozen, a thick coating of ice appeared to form around the post while the surrounding water remained unfrozen. The reason for the buildup of ice is not known.

One possible explanation is that while the movement of the water causes it to remain unfrozen in subzero temperature, the presence of the post may cause the water to become slow enough to freeze in its immediate vicinity. Another explanation may involve the ground temperature having a lower temperature than the flowing water, causing the highly conductive post to also have a lower temperature and freeze the surrounding water. Whatever the cause of the ice formation, it is reason for concern, as a sensor frozen in a block of ice would produce a false positive for a buried sensor. Future research should involve the brainstorming of ideas to prevent this ice formation, possibly by using specialized coatings to decrease freezing temperature.

#### **5.4.3 Ferromagnetic Particle Clumping**

Another natural occurrence not previously considered is the presence of small ferromagnetic particles in the stream. These particles do not appear to have any immediate effect on the system, but have a tendency to build up around the epoxy surrounding the magnets on the seaweed sensors. No noticeable degradation in signal is observed from the buildup and the particles are easily scraped away by hand, but an investigation of the effects of these particles over time should be conducted.

#### **5.4.4 Underwater Post Specific DAQ Problems**

The last lesson learned to be discussed was only recently discovered at the time of this writing. It appears as though something about the underwater scour post causes the DAQ systems to prematurely fail. This has been primarily studied using the temporary DAQ systems described in Section 3.6, but may also explain some of

the failures experienced when attempting to use the hand built DAQs. The failure would not happen immediately but would instead be noticed when returning to the DAQs to collect data cards. It always appeared as though the DAQ connected to the underwater post stopped recording data after only a few hours. To rule out the DAQ as the source of the error, it was switched with the DAQ reading the in-air post. In both cases, only the DAQ connected to the water post failed. It is uncertain whether the underwater post somehow expends all of the battery power in that amount of time or simply causes a failure within the DAQ to stop it from recording.

It is worth noting that at some point before this discovery, it was discovered that the DAQs connected to the in water post were only receiving  $\sim 3$  V instead of the expected 5 V. It was suspected that there may be short in the system, and upon disconnecting the power to one of the hall sensors on the 5<sup>th</sup> (the most deeply buried, seaweed sensor) the voltage partially recovered. The voltage then fully recovered upon disconnecting the second hall sensor on the same seaweed sensor. To test whether the problem actually lay within the 5<sup>th</sup> seaweed sensor and was not just the result of the number of sensors connected, one of the hall sensors from the 5<sup>th</sup> seaweed sensor was reconnected and a hall sensor from the 4<sup>th</sup> seaweed was disconnected. In this scenario, the voltage remained below expected, leading to the assumption that the problem did indeed lie within the wiring for the 5<sup>th</sup> seaweed sensor. It is unknown whether this issue is related to the constant failure of the underwater post DAQ systems.



## 5.5 Second Prototype Results

### **5.5.1 System Verification**

The preliminary data presented in this section is recorded by a high powered Texas Instruments DAQ as opposed to one of the DAQs constructed for this study. While only feasible for use when a user is present and with a large power source, the DAQ's high resolution, high sampling rate, and ability to output a real-time graph in LabView are desirable for the initial study of the signals. Data as recorded by one of the temporary DAQs is available in Section 5.2.2.

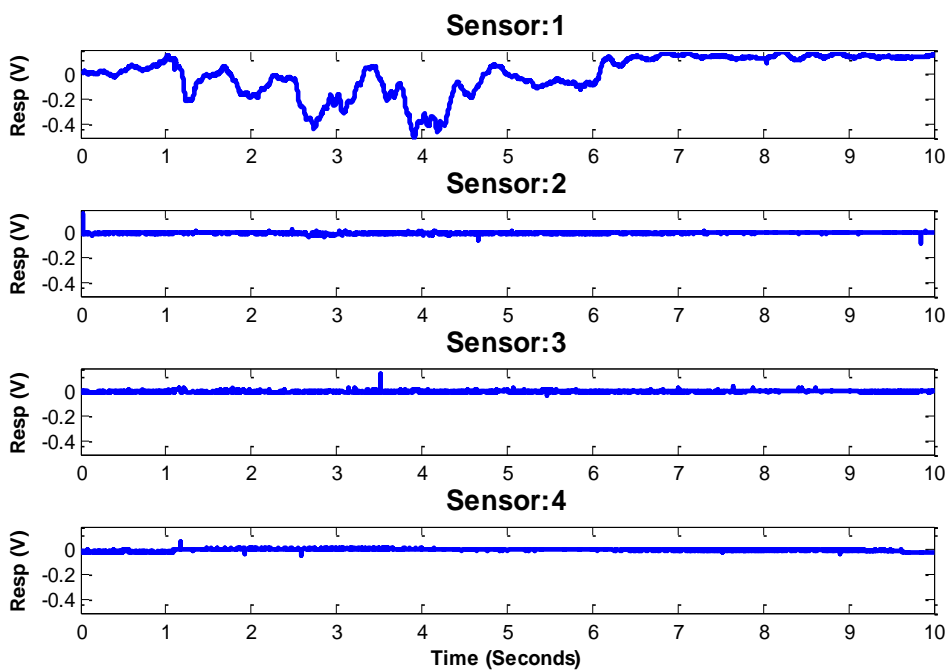
Figure 49 depicts the state of the two installed posts located at the Bennett Creek installation site at the time of the recorded data.



**Figure 49.** State of the lateral riverbed migration scour posts upon taking of data

Preliminary data from the first four sensors in the in-air post are provided in Figure 50. A comparison between the photograph in Figure 49 and the output data in Figure

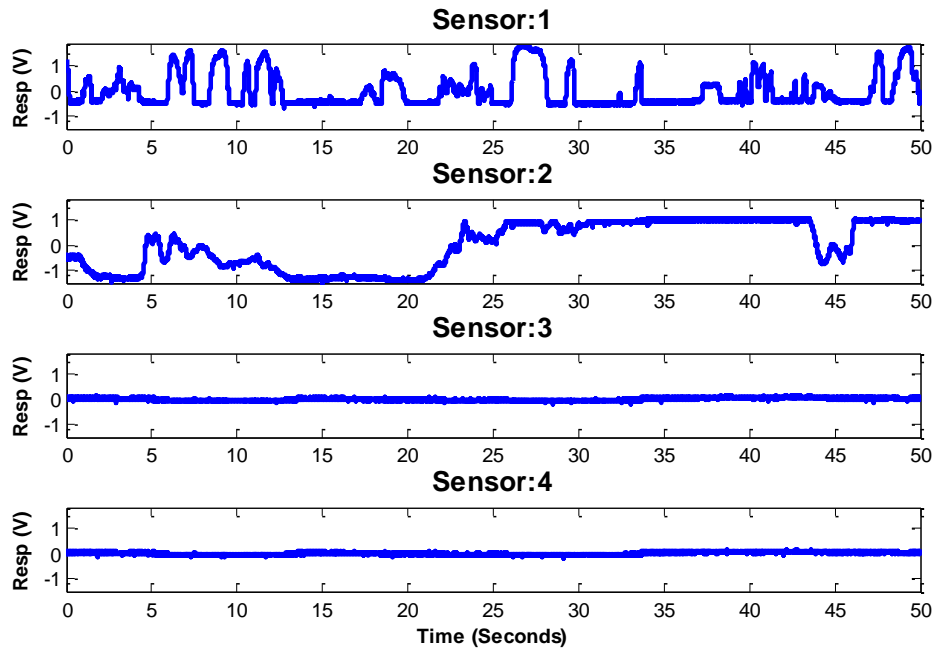
50 displays a strong correlation. Oscillations are only evident in the time-data response for Sensor 1, the only sensor completely unearthed and exposed to the airflow. While Sensor 2 is also unearthed, it remains protected from the airflow by the small cove in the bank and is not exposed to the air flow, causing it to remain stationary. Sensor 3 and Sensor 4 remain completely buried as indicated by both the photograph and the static signal.



**Figure 50.** Data from the riverbed migration in air post recorded using a high powered DAQ

Preliminary data from four of the sensors in the water post are provided in Figure 51. While the state of the sensors cannot be ascertained from the photograph presented in Figure 49, a firsthand inspection of the underwater post revealed a completely unearthed Sensor 1, a mostly unearthed Sensor 2, an almost completely buried Sensor 3, and a completely buried Sensor 4. Once again a strong correlation

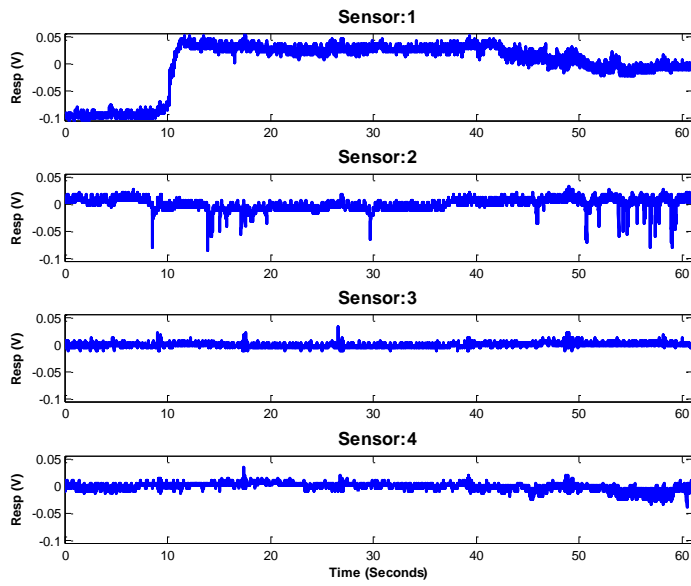
between the visual inspection of the post and the recorded data is present. Dynamic responses are only present in Sensor 1 and Sensor 2 as these are the only sensors exposed to the flow enough to produce strong oscillations in the seaweed.



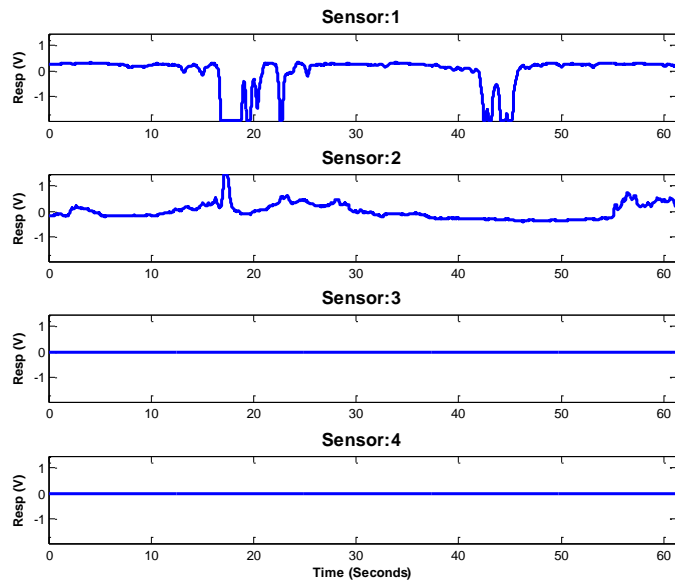
**Figure 51.** Data from the riverbed migration underwater post recorded using a high powered DAQ

### 5.5.2 DAQ readings

Figure 52 and Figure 53 display typical data traces taken by the temporary DAQ at a later date than above. A comparison with the data taken from high end TI DAQ in the previous section provides a verification of the temporary DAQ system. It can be ascertained from the in-air post data, that while there was less movement in Sensor 1, indicating a less windy day, there is more movement in Sensor 2, indicating possible further erosion of the riverbed.



**Figure 52.** Data from the riverbed migration in air post recorded using the temporary DAQ

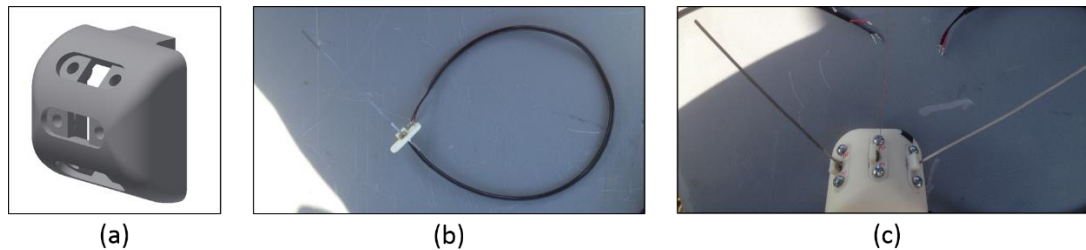


**Figure 53.** Data from the riverbed migration underwater post recorded using the temporary DAQ

## 5.6 Whisker Post Cap Addition

### **5.6.1 Post Cap Description and Attachment**

To test the capabilities of the whisker sensors in river flow, the tennis balls on the end of the post were replaced by a 3D printed plastic cap as represented in Figure 54a. The dome shape of the cap contains three placeholders where exchangeable whisker inserts are screwed into place. The whisker inserts utilize the basic sensor design described in Section 2.1.3, with the hall sensor positioned directly under the area of high stress concentration. Abiding by the lesson learned from the first installation, the whiskers are epoxied into a small rectangular opening on the face of the whisker instead of clamped in place. The whisker is positioned so that the hall sensor is sensing the magnetic inductance on an axis orthogonal to the whisker width. Finally, all of the electrical connections are epoxied over for water proofing and physical protection. An individual insert and completely assembled post cap can be observed in Figure 54b and c respectively.



**Figure 54.** Whisker Cap components (a) Cap design with place holders for whisker sensors (b) Insertable whisker sensor (c) Complete whisker cap assembly

Three Alfenol whiskers were installed into the cap. The properties of each whisker are presented in Table 2.

**Table 2:** Properties of the whiskers used on the scour post whisker caps

Whisker	Thickness (mm)	Width (mm)	Length (mm)	Cross section Description	Post Placement
1	0.25	2.2	143	Flat	Water Top
2	0.25	4.2	129	Flat	Water Middle
3	0.35	2.2	123	Flat	Water Bottom
4	0.3	6.25	141	L shape	Air Top
5	0.4	2.1	152	flat	Air Middle
6	0.3	7	137	S shape	Air Bottom

The post cap was attached to the end of the post using two zip ties fed through holes present in the cap and on the end of the post. The cap was installed so that the width of the whiskers are oriented parallel to the flow. Photographs of the caps attached to the posts are presented in Figure 55.



**Figure 55.** Whisker post caps attached to both the in-air and underwater posts via zip ties

## 5.6.2 Whisker Cap Results

The results presented in this section were once again measured using the high powered TI DAQ. The higher resolution of the DAQ is required to detect the small fluctuations in the whisker signal. The resolution provided by the PCB DAQ will be sufficient to take these data reading upon its completion.

With no movement visibly evident in the whiskers attached to the air post, the data collected from these sensors were used as a static control data sample. Figure 56 displays the time response of the three water sensors as well as a time response from the in air whisker to be used as the control.

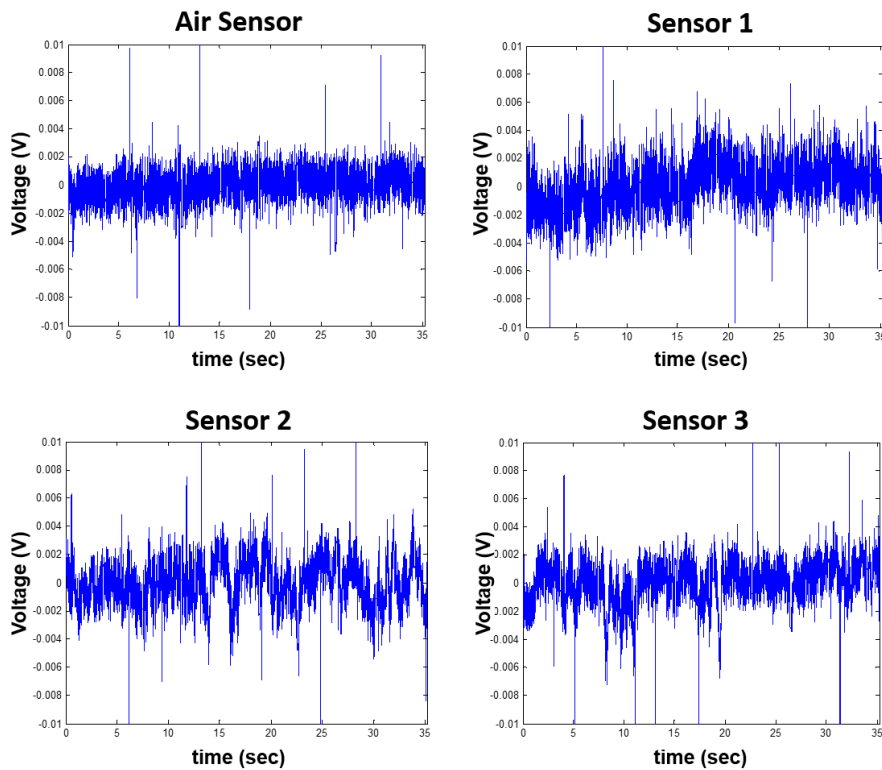
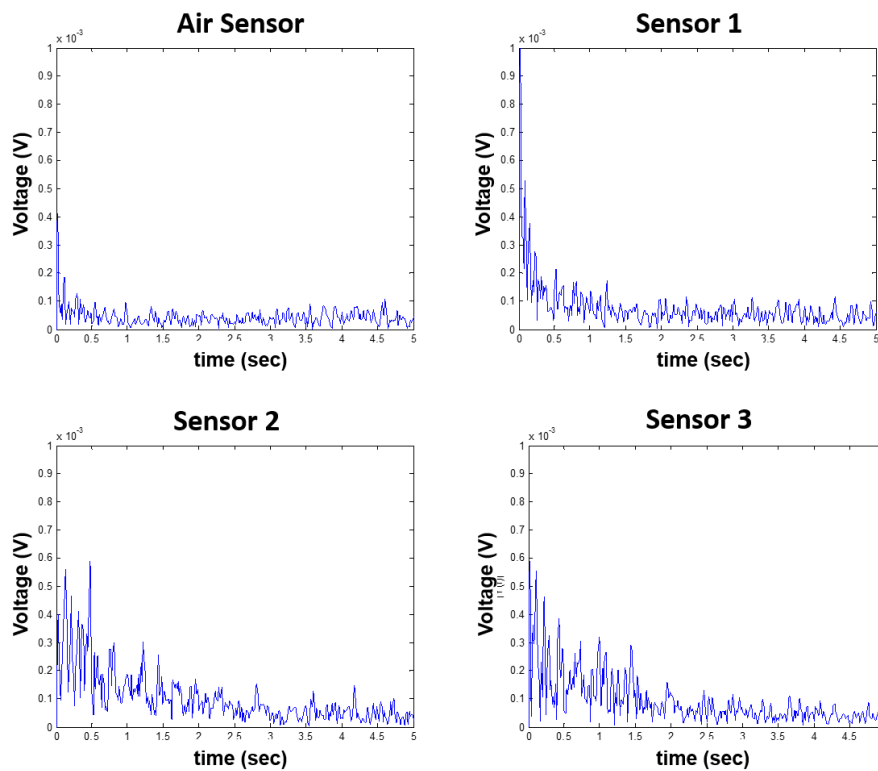


Figure 56. Time response data for the whiskers attached to the whisker post cap

While some movement may be observable from the time traces, it is much more useful to take the Fourier Transform of the data to obtain the frequency response. In examining the lower range of the frequency response, as presented in Figure 57, a distinct increase of magnitude is evident in the water post for these frequencies when compared to the air post control. The presence of this magnitude increase correlates to the low frequencies observed visually. It should also be noted that while this data was being taken, the water level was low enough that Sensor 1 was partially sticking out of the water. This may be a reason for its frequency response magnitude being lower than the other sensors, although it is still visibly higher than the air sensor.



**Figure 57.** Time response data for the whiskers attached to the whisker post cap



## Chapter 6: Conclusions

### 6.1 Summary

The current study proposed a solution to the complex task of monitoring scour remotely and in real time. This solution utilizes the magnetostrictive properties of Alfenol and Galfenol to create flow sensors inspired by the whiskers of sea mammals. These sensors are capable of sensing whether they are buried under a river bed or in flowing water. Using the readings from these flow sensors and knowledge of their depths, scour severity can be determined. Two different bridges sites have each been installed with two scour monitoring systems based on the proposed sensor post solution.

The first two posts were installed vertically at a tidal site near Annapolis Maryland to test for conventional scour. The low flow speeds of the site promoted the design of a new low flow velocity sensor inspired by the movement of seaweed. Utilizing this new sensor, the scour posts were successfully capable of determining the erosion state of the riverbed.

The third and fourth posts were installed horizontally at a bridge site near Frederick Maryland to test for lateral riverbed migration using both the seaweed sensors and whisker sensors. These posts proved capable of successfully determining the erosion state of the riverbank using both the whisker sensors and seaweed sensors independently.

As a result of this study, the following milestones have been accomplished:

- A solution for continuous monitoring of scour utilizing flow velocity sensors was proposed and design requirements for the solution defined.
- Two variations of bio-inspired flow sensors have been designed and constructed. The first sensor, inspired by the whiskers of aquatic mammals, utilizes magnetostriction and is optimized for flow velocities greater than 0.15 m/s. The second sensor, inspired by seaweed, utilizes only magnetics and is optimized for velocities less than 0.15 m/s
- To record data from the sensors several revisions of a low powered data acquisition system were designed, constructed and tested. A final PCB version of this system was designed using a culmination of the lessons learned from these revisions and presented in this study.
- Two conventional scour monitoring systems were installed near a tidal bridge. The lessons learned from this installation were documented and used to improve the overall system design.
- Applying the lessons learned from the first installation, two lateral riverbed migration scour posts were installed at a second site. Potential improvements for the system were once again documented.
- A specialized cap was added to the lateral posts at the second site to allow for the testing of whisker sensors in a natural river environment.
- Data from each installation site and the added whisker were presented and analyzed.

## 6.2 Future Work

The success of the initial scour monitoring system prototypes lends itself to extensive future work, much of which has been alluded to in the previous chapters of this study.

One of the most important focuses of future works should be to minimize the system's power usage. The most obvious way to resolve power consumption issues is to find ways to minimize the DAQ power consumption and find lower power hall sensors. However, the viability of power generation, possibly through thermal gradients, should still be considered.

Some additional work has already commenced through a concurrent study. Associates at Michigan Tech have begun to working on implementing wireless capability to the design. This includes the wireless systems for sending data to the hub and how best to process the data locally to minimize the amount of data transmission needed.

Separate from the wireless system to transmit data from the install sites to a base station, it may be advisable to investigate a method for wirelessly communicating between the scour post and a local base station at the install site itself. This would eliminate the need for submersible cable which can be expensive and susceptible to damage from floating debris. Standard wireless communication systems are not effective underwater, necessitating the need for a specialized solution. Currently the most promising solution available seems to be acoustic modems. Acoustic modems are commercially available but extremely expensive and

overdesigned for the needed application. A cheap alternative may be to create a simplified version of such a system especially suited to the needs of this project.

Finally, future studies could strive to increase sensor reliability and sensitivity. This could include studies to make the whisker sensors thinner, and therefore more susceptible to flow induced vibrations, without losing significant amounts of magnetostriction. Thinner whiskers would also be more flexible and less susceptible to plastic deformation and breaking. Similar means may also be achieved by including additives to the magnetostrictive alloys.

# Appendices

## Appendix A: Airfoil Study

### A.1 Introduction of Airfoil Study

The experiment below was performed to investigate ways to improve the signal from the sensors. While the final design was not used in the study, it is a helpful solution to keep in mind if a more oscillatory response is needed.

### A.2 Necessity of Oscillatory Response

It is important for the magnetostrictive sensors in this study to not only deflect when introduced to water flow, but to also produce some sort of dynamic or oscillatory response. As alluded to in the introduction of this study, the sensors may be struck by large debris floating down the river. As a result, the magnetostrictive sensors will likely experience small plastic deformations, altering the properties of the material and therefore altering the value of magnetic induction produced by the whisker in an undeflected state. As a result, a baseline reading from the sensor cannot be ascertained, causing a quasi-statically deflected whisker signal to be indistinguishable from an undeflected whisker signal. A constantly changing, or dynamic, signal must therefore be produced to ascertain whether or not water is flowing past the whisker.

### A.3 Unstable Airfoil Concept

#### **A.3.1 Static Margin**

In an effort to force such an oscillatory response, the study employs the use of hydrodynamic airfoil stability. The principle of static margin is a topic taught in all basic aerodynamic and hydrodynamic stability courses. The principle relies on the placement of the center of gravity of an airfoil to be forward of its neutral point. This introduces inherent torsional stability to the airfoil, allowing it to naturally return to a neutral angle of attack upon deflection. By reversing this relationship and placing the center of gravity aft of the neutral point, the airfoil will become unstable and will not naturally settle to a neutral angle of attack. For the purposes of this study, this unstable configuration is produced by fixing the magnetostrictive whisker to the trailing edge of the airfoil.

#### **A.3.2 Experimental Setup**

The sensor construction for this study utilizes the design described above. A 7.87mil thick, 78.7mil wide, and 6in long rectangular whisker is used, which has been galvanized to avoid the negative effects of corrosion. The holder for keeping the whisker in place is created out of plastic using a Stratasys EDEN350 3D printer. The face of the holder has a vertical 0.06in x 0.4in rectangular slit cut into its center, into to which the Galfenol whisker can be inserted and secured with epoxy. After

insertion into the holder, the whisker protrudes 4in. The face of the plastic holder also features eight “fingers” extending outward in a circular pattern to identify premeasured increments of 45 degrees.

A platform extruding out of the back of the holder contains the hall sensor and biasing magnet. An EQ-430L hall sensor manufactured by Asahi Kasei Microdevices is centered 0.454in behind the face of holder, and oriented to read the magnetic inductance along the width of the whisker. The hall sensor has a sensitivity of 130mV/mT when operated at 5v, as it is in this experiment. The cylindrical biasing magnet is located 0.83in behind the face of the holder with the flat of its surface in contact with the thickness of the whisker. The magnet is 0.1in thick with a radius of 0.125in and has a strength of 0.6 pull lbs. A photo of one such holder used in this study is presented in Figure 7.

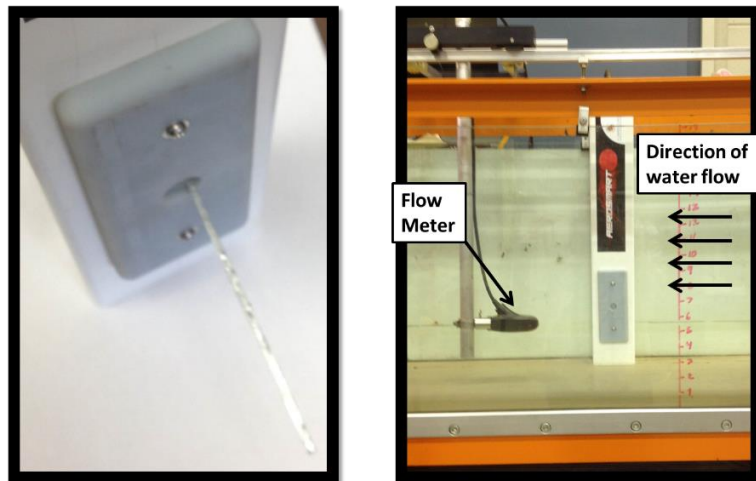


**Figure 58.** Whisker holder used in the experimental setup: side view (left), front view (Middle), top view (Right)

The plastic holder described above is compression fit between a plastic fence post and a mounting plate to keep it secure in the flow of the water. The 1.7ft long fence post has a rectangular cross section measuring 3.5in x 2in and has 0.125in thick walls. The mounting plate is a 0.4in thick, 2.46in x 6.132in 3D printed solid rectangle with a cutout matching the shape of the eight fingered face of the whisker

holder etched 0.3in through the plate's thickness. A 0.6in hole is drilled through the remainder of the plate thickness in the center of the cutout, allowing the whisker to protrude out into the flow. Small pieces of electrical tape are added to the tips of the fingers of the plastic holder in an attempt to increase the tightness of the compression fit and reduce vibrations.

Finally, to simulate a steady state river flow condition, the entire setup is placed into a flume with the top of the assembly clamped to the top edge of the flume. The flume is an Armfield S6 Glass sided tilting flume with a 1ft x 1.5ft cross section. The whisker is placed into the flume with its width horizontal to the floor and tested at 0, 0.33, 0.65 and 0.82 ft/s. These speeds are verified by using an OTT MF pro flow meter with a resolution of 0.01 ft/s. The full setup is depicted in Figure 59.



**Figure 59.** Assembled experimental setup: close up of mounting plate configuration (left), Flume Setup (right)



#### A.4 Plastic Molded Airfoils

The airfoil chosen for the experiment has a NACA 0050 symmetric profile with a 0.5in chord. The airfoil is applied by placing the whisker into a silicon mold of the airfoil and pouring in a plastic resin. After the resin cures, the whisker is removed from the mold with a plastic airfoil attached to the last three inches of its length. When the whisker is placed into the flume, the leading edge of the airfoil is oriented into the flow. A photo of a whisker with an airfoil attached is presented in Figure 60.

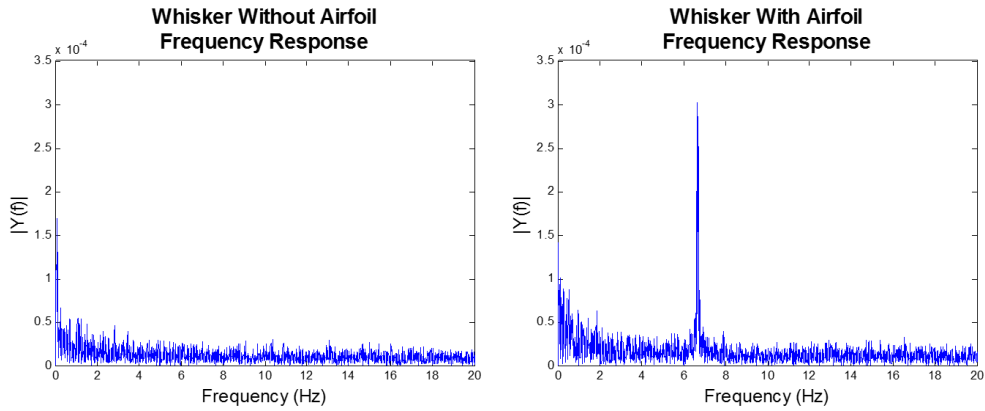


**Figure 60.** Galfenol Whisker with attached airfoil.

#### A.5 Results

##### **A.5.1 Data Format**

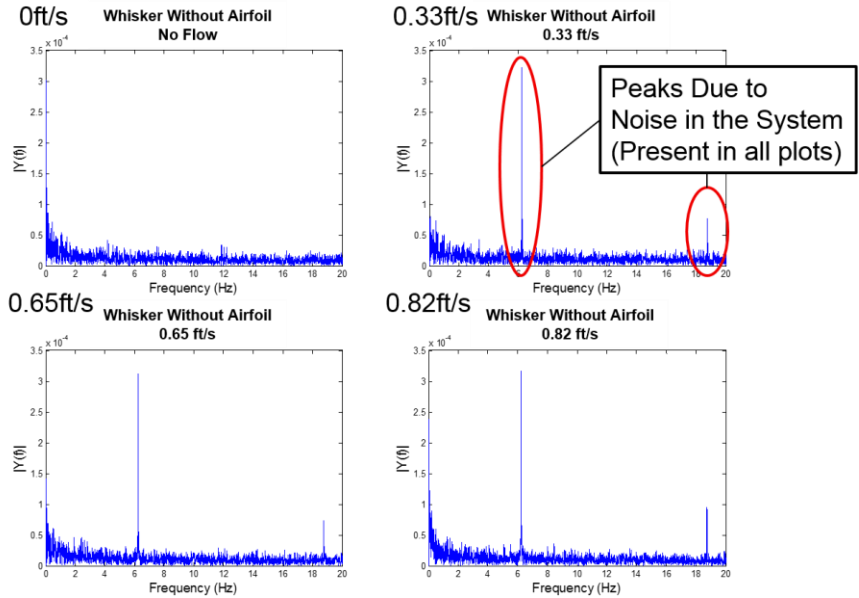
An inspection of the time displacement results does not provide discernable and meaningful data; therefore a frequency response is required. Figure 61 presents a comparison between a typical non-vibrating (left) and vibrating (right) sensor. A strong output peak is clearly visible in the vibrating whisker at approximately 6.5 Hz, whereas no peaks are visible in the non-vibrating whisker data.



**Figure 61.** Comparison between stationary whisker (left) and oscillating whisker (right)

### A.5.2 Results for No Airfoil Configuration

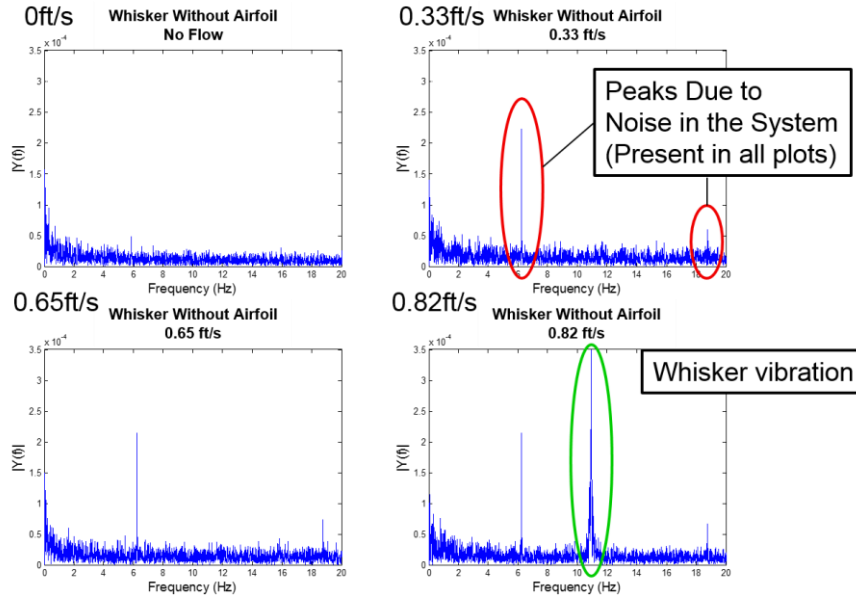
The data for the whisker without an airfoil is presented in Figure 62 below. Speeds from 0ft/s to 0.82 ft/s are represented. Peaks due to noise are present in the system at 6Hz and 19Hz and should not be confused with an oscillating whisker response. It is hypothesized that this noise is a result of looseness in the compression fit between the whisker holder and attachment plate. Other than the peaks observed due to noise, no significant response is visible in flow speeds at or below 0.82 ft/s. A visual inspection of the whisker during the experiments agrees with the findings presented in the plots below.



**Figure 62.** Frequency responses of a whisker without an airfoil for flow rates from 0 ft/s to 0.82 ft/s

### A.5.3 Results for Airfoil Configuration

The data for the whisker with an airfoil is presented in Figure 63 below. These results experience the same peaks due to noise as the system without an airfoil. Also similar to the system without an airfoil, no response is evident at flow speeds at or below 0.65 ft/s. But, when the system reaches 0.82ft/s a large vibration appears at 11Hz. Once again, a visual inspection of the whisker during the experiment agrees with the findings presented in the plots below.



**Figure 63.** Frequency responses of a whisker with an airfoil for flow rates from 0 ft/s to 0.82A ft/s

### A.6 Airfoil Study Conclusions

A study has been performed to investigate a magnetostrictive flow sensor for use in a scour monitoring system. The sensor was tested both with and without the presence of an attached unstable airfoil at various flow velocities. Three primary conclusions can be inferred. First, the study has confirmed that Galfenol has the structural properties necessary to create a tactile sensor. Second it has been demonstrated that this tactile sensor is capable of being sensitive to water flow. Finally, it has been determined that alterations to the geometry of the whisker, specifically the addition of an unstable airfoil, can create the necessary dynamic response required for such a sensor.

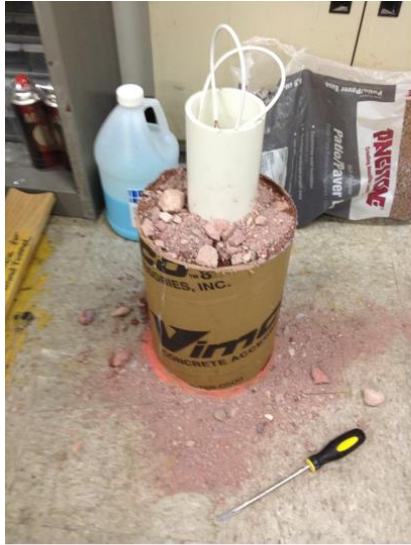
## Appendix B: Sensor Protection Using Rock Salt

As mentioned in Section 1.4.6, the desired installation method for the scour posts would be to simply pound them into the ground like a nail. The process of pounding poles into the ground is well established and could easily be performed using a hand held Rhino™ post driver. The difficulty lies in protecting the sensors from breaking off when exposed to the extreme shearing forces experienced while being pounded into the ground.

While brainstorming for a solution, the desire for some kind of a hard casing that dissolves in water was continually mentioned, but no commercially available option could be found. In an attempt to create an in house dissolvable casing, it was decided to attempt to use the super saturation properties of sodium acetate. When sodium acetate trihydrate crystals are heated they melt into liquid form. However, as the solution cools down past solidification temperature it will become supersaturated and in liquid form until a seed crystal is added. Upon the addition of this seed crystal, the entire solution rapidly solidifies.

These solidified Sodium Acetate crystals had the desired characteristic of being soluble in water, but did not prove to be hard enough to use as a casing for the scour posts. It was discovered however, that when the hot, aqueous sodium acetate was poured over a mix of dirt and rocks, a very hard shell could be formed. This shell also kept the advantage of remaining very soluble in water.

To test the newly discovered “rock salt”, it was used to encase an approximately 2 ft section of PVC pipe containing two whiskers sensors. This pipe was then placed into a very low velocity stream and left to sit overnight. Upon returning in the morning, the rock salt had dissolved away leaving the whiskers intact and undamaged. Photographs depicting the process of encasing the PVC pipe with rock salt are presented in Figure 64 below. Further testing must be performed to determine feasibility of the dissolvable rock salt encasement, but the solution seems promising.



(a)



(b)



(c)



(d)

**Figure 64.** Rock salt encasement procedure (a) Hot aqueous sodium acetate is poured over dirt and rocks contained in a Sano tube (b) Sano tube is removed after rock salt mix cools (c) Rock salt remains attached when lifting by the PVC pipe (d) Rock salt dissolving in low flow velocity water

## Appendix C: DAQ Code

### C.1 DAQ Code

```
#####  
//Libraries  
#####  
// Simple ADC data logger that demonstrates NilAnalog, NilFIFO, and  
NilTimer1.  
#include <SdFat.h>  
#include <NilRTOS.h>  
#include <NilAnalog.h>  
#include <NilFIFO.h>  
#include <NilTimer1.h>  
#include <SPI.h>  
#include <stdlib.h> // for the atol() function  
#include <Wire.h>  
#include <Adafruit_ADS1015.h>  
#include <avr/wdt.h>  
// Use tiny unbuffered NilRTOS NilSerial library.  
#include <NilSerial.h>  
#include <MemoryFree.h>  
  
#####  
//Logger Properties  
#####  
//Is this the temp DAQ?  
const boolean tempDAQ = true;  
  
// Time between points in microseconds.  
// Maximum value is 4,194,304 (2^22) usec.  
const uint32_t PERIOD_USEC = 2500; //Less is faster (1000 = 1  
reading every millisecond)  
//Calculate Hz by 1,000,000/period  
  
// Number of ADC channels to log  
const uint8_t NADC = 3;  
  
// FIFO buffer size. Adjust so unused idle thread stack is about 100  
bytes.  
const size_t FIFO_SIZE_BYTES = 2000;  
  
//How long to sample for in seconds  
const uint8_t SamplePeriod = 60;  
  
// Time between samples in minutes
```



```

const uint8_t SleepTime = 5;

//-----
// Type for a data record.
struct Record_t {
    uint16_t adc[NADC];
    uint8_t ovr;
};

// Number of data records in the FIFO.
const size_t FIFO_DIM = FIFO_SIZE_BYTES/sizeof(Record_t);

// Declare FIFO with overrun and minimum free space statistics.
NilStatsFIFO<Record_t, FIFO_DIM> fifo;
//-----

#####
//Defined Functions
#####

void(* resetFunc) (void) = 0; //declare reset function @ address 0

#####
//I2C Definitions
#####

int8_t Aadd = (0x0048);
int8_t Badd = (0x0049);
int8_t Cadd = (0x004A);
int8_t Dadd = (0x004B);

Adafruit_ADS1115 adsA(Aadd); /* Use this for the 16-bit version */
Adafruit_ADS1115 adsB(Badd);
Adafruit_ADS1115 adsC(Cadd);
Adafruit_ADS1115 adsD(Dadd);

uint16_t BBC = ADS1015_REG_CONFIG_CQUE_NONE | // (0x0003) (0011)
Disable the comparator (default val)
                ADS1015_REG_CONFIG_CLAT_NONLAT | // (0x0000) Non-
latching (default val)
                ADS1015_REG_CONFIG_CPOL_ACTVLOW | // (0x0000)
Alert/Rdy active low (default val)
                ADS1015_REG_CONFIG_CMODE_TRAD | //
(0x0000)Traditional comparator (default val)
                (0x0E0) | // (0x0E00)(1110 0000) 860 samples per
second (default)

```

```

                ADS1015_REG_CONFIG_MODE_CONTIN | // (0x0000)(0000
0000 0000) Continuous mode
                ADS1015_REG_CONFIG_PGA_6_144V; //(0x0000) +/-6.144V
range = Gain 2/3

#####
//Definitions
#####

// Macro to redefine Serial as NilSerial to save RAM.
// Remove definition to use standard Arduino Serial.
#define Serial NilSerial

// SD file system.
SdFat sd;

// Log file.
SdFile file;

//second,minute,hour,null,day,month,year
int DateTime[7];
String adStr;
String FullDnT;
String Day;
String Mo;
String Yr;
String Hr;
String Mn;
String Sec;

#####
//Pin Definitions
#####

//I/O pin connected to reset
int resetPin = 44;

// SD card chip select pin.
const uint8_t sdChipSelect = 20;

//RTC Chip Select
const int RTC_CS=13;

//Pin to activate transistor giving the sensors power
int pwrPin = 19;

// Maximum SD write latency.
uint32_t maxLatency = 0;

```

```

#####
//Define Thread Working Area
#####
// Declare a stack with 16 bytes beyond context switch and interrupt
needs.
// The highest priority thread requires less stack than other
threads.
NIL_WORKING_AREA(waThread1, 256);

#####
//Thread 1
#####
// Declare thread function for thread 1.
NIL_THREAD(Thread1, arg) {

    //Create Pointer to
    char* sc;

    // Start timer 1 with a period of PERIOD_USEC.
    nilTimer1Start(PERIOD_USEC);

    //Set timing variables for sampling
    uint32_t StartTime;
    uint32_t ChkTime;
    uint32_t RunTime= SamplePeriod * 1000;

    if (tempDAQ){
        StartTime = millis();
        ChkTime = millis();

        //reinitialize the FIFO
        fifo.reinit();

        //record data for predefined time
        while (RunTime>ChkTime-StartTime) {

            // Sleep until it's time for next data point.
            nilTimer1Wait();

            // Get a free buffer.
            Record_t* p = fifo.waitFree(TIME_IMMEDIATE);

            // Skip the point if no buffer is available , fifo will count
            overrun.
            if (!p) continue;

            // Read ADCs

```

```

    for (int i = 0; i < NADC; i++) {
        p->adc[i] = nilAnalogRead(i);
    }

    // Save count of overruns since last point in high 6-bits of
adc[0].
    uint16_t tmp = fifo.overrunCount();
    p->adc[0] |= tmp > 63 ? (63 << 10) : tmp << 10;

    // Signal SD write thread that new data is ready.
    fifo.signalData();

    ChkTime = millis();

}

Serial.println(F("Finished"));

// Done, close the file and print stats.
file.print(F("Max Write Latency: "));
file.print(maxLatency);
file.println(F(" usec"));
nilPrintUnusedStack(&file);
fifoprintStats(&file);

file.close();
Serial.println(F("Done!"));
Serial.print(F("Max Write Latency: "));
Serial.print(maxLatency);
Serial.println(F(" usec"));
//
nilPrintUnusedStack(&Serial);
nilPrintStackSizes(&Serial);
fifoprintStats(&Serial);
}
else{
//Start Sensor For loop here
for(int si = 0; si<4; si++){

    //Reset Fifo statistics
    fifo.reinit();

    //Convert sensor set number to a character for folder naming
    sc = itoa(si,0,10);
    char adChar[12] = {'S','e','n','s','o','r','*',sc,'.','C','S','V'};

    //Open file save to on the SD card
    if(!file.open(adChar, O_CREAT | O_WRITE | O_TRUNC)) {
        Serial.println(F("SD problem"));
    }
}
}

```

```

        //if there is an error, delay a short period and restart the
system
        delay(5000);
        resetFunc();
    }

    // Write the file header.
    file.print(F("PERIOD_USEC,"));
    file.println(PERIOD_USEC);
    file.print(F("Date,"));
    file.println(FullDnT);
    for (int i = 0; i < NADC; i++) {
        file.print(F("ADC"));
        file.printField(i, ',');
    }
    file.println(F("Overruns"));

    Serial.println(adChar);
    //Set Channel of the ADCs
    adsA.setCh(si, BBC);
    adsB.setCh(si, BBC);
    adsC.setCh(si, BBC);
    adsD.setCh(si, BBC);
    fifo.reinit();
    StartTime = millis();
    ChkTime = millis();

    // Record data until serial input is available.
    while (RunTime>ChkTime-StartTime) {

        // Sleep until it's time for next data point.
        nilTimer1Wait();

        // Get a free buffer.
        Record_t* p = fifo.waitFree(TIME_IMMEDIATE);

        // Skip the point if no buffer is available , fifo will count
overrun.
        if (!p) continue;

        // Read ADCs
        //for (int i = 0; i < NADC; i++) {
        // p->adc[i] = nilAnalogRead(i);
        //}

        p->adc[0] = adsA.ReadContADC();
        p->adc[1] = adsB.ReadContADC();

```

```

        p->adc[2] = adsC.ReadContADC();
        p->adc[3] = adsD.ReadContADC();

// for (int i = 0; i < NADC; i++) {
//     p->adc[i] = I2CADCRead(i);
// }
//Serial.println("I2C Gathered");
// Save count of overruns since last point in high 6-bits of
adc[0].
uint8_t tmp = fifo.overrunCount();
//p->adc[0] |= tmp > 63 ? (63 << 10) : tmp << 10;
p->ovr = tmp > 255 ? 255 : tmp;
//Serial.println("ovrs saved");
// Signal SD write thread that new data is ready.
fifo.signalData();

    ChkTime = millis();

}

Serial.println(F("Finished"));

//Let Save loop finish
//nilThdSleepSeconds(10);

// Done, close the file and print stats.
//Serial.println(F("Done!"));
file.print(F("Max Write Latency: "));
file.print(maxLatency);
file.println(F(" usec"));
nilPrintUnusedStack(&file);
fifoprintStats(&file);

file.close();
Serial.println(F("Done!"));
Serial.print(F("Max Write Latency: "));
Serial.print(maxLatency);
Serial.println(F(" usec"));
nilPrintUnusedStack(&Serial);
fifoprintStats(&Serial);
} //End for Sensor Select for loop here
}

//Transistor Power Off
Serial.println("Transistor Power Down");
digitalWrite(pwrPin,LOW);

//Break for the predetermined sleep time
for(int x = SleepTime; x > 0; x--){
    delay(60000);

```

```

        Serial.print("Miniues Left");
        Serial.println(x-1);
    }

    Serial.println("resetting");
    resetFunc(); //call reset
    Serial.println("this never happens");
}

//#####
//Thread Prioritization
//#####
/*
 * Threads static table, one entry per thread. A thread's priority
is
 * determined by its position in the table with highest priority
first.
 *
 * These threads start with a null argument. A thread's name is
also
 * null to save RAM since the name is currently not used.
 */
NIL_THREADS_TABLE_BEGIN()
NIL_THREADS_TABLE_ENTRY(NULL, Thread1, NULL, waThread1,
sizeof(waThread1))
NIL_THREADS_TABLE_END()
//-----
-----

//#####
//%%%%%%%% %%%%%%%%% %%%%%%%%% %%%%%%%%% %%%%%%%%%
//%%      %%          %%      %%      %%  %%
// %%%%  %%%%%%%%%  %%      %%%%%%%%% %%%%%%%%%
//      %%  %%          %%      %%      %%
//%%%%%%%% %%%%%%%%%  %%      %%%%%%%%% %%
//SETUP FUNCTION
//#####
void setup() {

    Serial.begin(9600);
    delay(4000);
    Serial.print("freeMemory(=)");
    Serial.println(freeMemory());
    Serial.println(F("Begin"));
}

```

```

delay(2000);

//Initialize RTC
RTC_init();

//Get Date and Time
ReadTimeDate(DateTime);

//Save Data and Time
Yr = String(DateTime[6]);
Mo = String(DateTime[5]);
Day = String(DateTime[4]);
Hr = String(DateTime[2]);
Mn = String(DateTime[1]);
Sec = String(DateTime[0]);

//Format Printable Date and Time
FullDnT = "20" + Yr + "/" + Mo + "/" + Day + "/" + Hr + ":" + Mn +
":" + Sec;

//Format Date and Time Filename
if (Mo.length() < 2){
    adStr = "0";
    adStr+= Mo;
}
else{
    adStr = Mo;
}

if (Day.length() < 2){
    adStr += "0";
    adStr += Day;
}
else{
    adStr += Day;
}

if (Hr.length() < 2){
    adStr += "0";
    adStr += Hr;
}
else{
    adStr += Hr;
}

if (Mn.length() < 2){
    adStr += "0";
    adStr += Mn;
}
else{

```



```

    adStr += Mn;
}

//Add .CSV to the file name
adStr += ".CSV";
Serial.println(adStr); //Print File Name
char adChar[adStr.length()+1]; //Convert to Chars
adStr.toCharArray(adChar, adStr.length()+1); //Extra cell needed
in str array
Serial.println((adChar)); //Print Char array

//Begin SD communications
if (!sd.begin(sdChipSelect)|| !sd.mkdir(adChar) ||
!sd.chdir(adChar)) {
    Serial.println(F("SD problem"));
    sd.errorHalt();
}

//If temp DAQ then open file now
if (tempDAQ){
    // Initialize SD and create or open and truncate the data file.
    if (!sd.begin(sdChipSelect)
        || !file.open(adChar, O_CREAT | O_WRITE | O_TRUNC)) {
        Serial.println(F("SD problem"));
        sd.errorHalt();
    }
    // Write the file header.
    file.print(F("PERIOD_USEC,"));
    file.println(PERIOD_USEC);
    file.print(F("Date,"));
    file.println(FullDnT);
    for (int i = 0; i < NADC; i++) {
        file.print(F("ADC"));
        file.printField(i, ',');
    }
    file.println(F("Overruns"));
}

//Begin I2C Channels
Wire.begin();

//Set Channel of the ADCs
adsA.setCh(0, BBC);
adsB.setCh(0, BBC);
adsC.setCh(0, BBC);
adsD.setCh(0, BBC);

//Power On Sensors
Serial.println("Sensor Power On");
pinMode(pwrPin, OUTPUT);

```

```

digitalWrite(pwrPin, HIGH);

Serial.println("Warming up");
for (int gg = 1; gg < 8; gg++){

    delay(1000);
    Serial.println(7-gg);

}

Serial.println("Taking Data");

// Start kernel.
nilSysBegin();
}

#####
//%%          %%%%          %%%%          %%%%
//%%          %%%          %%%          %%  %%
//%%          %%  %%  %%  %%  %%  %%
//%%          %%  %%  %%  %%  %%%
//%%%%%%%%          %%%          %%%          %%
//%%%%%%%%          %%%          %%%          %%
//LOOP FUNCTION
#####
// Write data to the SD in the idle loop.
//
// Loop is the idle thread. The idle thread must not invoke any
// kernel primitive able to change its state to not runnable.
void loop() {

    // Record data until serial data is available()
    while (1) {

        // Check for an available data record in the FIFO.
        Record_t* p = fifo.waitData(TIME_IMMEDIATE);
        //Serial.println(("Loop"));
        // Continue if no available data records in the FIFO.
        if (!p) continue;
        //Serial.println(("Past p"));
        // Write start time.
        uint32_t u = micros();

        // Overruns are in the high 6-bits of adc[0].
        //uint16_t overruns = p->adc[0] >> 10;
        uint16_t overruns = p->ovr;
        //p->adc[0] &= 0X3FF;
    }
}

```

```

    //Serial.println("Save");
    for (int i = 0; i < NADC; i++) {
        // Print ADC value and a comma.
        file.printField(p->adc[i], ',');
    }
    // Print overrun count and CR/LF.
    file.printField(overruns, '\n');

    u = micros() - u;
    if (u > maxLatency) maxLatency = u;

    // Signal the read thread that the record is free.
    fifo.signalFree();
}

//while (1) {}

}

#####
//ADC Read Function
#####

uint16_t I2CADCRead(uint8_t adcNum){

    uint16_t adc;

    if (adcNum < 4){
        adc = adsA.readADC_SingleEnded(adcNum);
    }
    else if (adcNum < 8){
        adc = adsB.readADC_SingleEnded(adcNum-4);
    }
    else if (adcNum < 12){
        adc = adsC.readADC_SingleEnded(adcNum-8);
    }
    else{
        //adc = adsD.readADC_SingleEnded(adcNum-12);
    }
    return adc;
}

#####
//RTC FUNCTIONS
#####
//=====
int RTC_init(){
    pinMode(RTC_CS,OUTPUT); // chip select
    // start the SPI library:

```

```

    SPI.setDataMode(SPI_MODE3);
    SPI.begin();
    SPI.setBitOrder(MSBFIRST);
    SPI.setDataMode(SPI_MODE3); // both mode 1 & 3 should work
    //set control register
    digitalWrite(RTC_CS, LOW);
    SPI.transfer(0x8E);
    SPI.transfer(0x60); //60= disable Oscillator and Battery SQ wave
    @1hz, temp compensation, Alarms disabled
    digitalWrite(RTC_CS, HIGH);
    delay(10);
}
//=====
int SetTimeDate(int d, int mo, int y, int h, int mi, int s){
    int TimeDate [7]={s,mi,h,0,d,mo,y};
    for(int i=0; i<=6;i++){
        if(i==3)
            i++;
        int b= TimeDate[i]/10;
        int a= TimeDate[i]-b*10;
        if(i==2){
            if (b==2)
                b=B00000010;
            else if (b==1)
                b=B00000001;
        }
        TimeDate[i]= a+(b<<4);

        digitalWrite(RTC_CS, LOW);
        SPI.transfer(i+0x80);
        SPI.transfer(TimeDate[i]);
        digitalWrite(RTC_CS, HIGH);
    }
}
//=====
void ReadTimeDate(int TimeDate[7]){
    //char[] temp;
    //int TimeDate [7]; //second,minute,hour,null,day,month,year

    for(int i=0; i<=6;i++){
        if(i==3)
            i++;
        digitalWrite(RTC_CS, LOW);
        SPI.transfer(i+0x00);
        unsigned int n = SPI.transfer(0x00);
        digitalWrite(RTC_CS, HIGH);
        int a=n & B00001111;
        if(i==2){
            int b=(n & B00110000)>>4; //24 hour mode
            if(b==B00000010)

```

```

        b=20;
    else if(b==B00000001)
        b=10;
        TimeDate[i]=a+b;
    }
    else if(i==4){
        int b=(n & B00110000)>>4;
        TimeDate[i]=a+b*10;
    }
    else if(i==5){
        int b=(n & B00010000)>>4;
        TimeDate[i]=a+b*10;
    }
    else if(i==6){
        int b=(n & B11110000)>>4;
        TimeDate[i]=a+b*10;
    }
    else{
        int b=(n & B01110000)>>4;
        TimeDate[i]=a+b*10;
    }
}
//temp.concat(TimeDate[4]);
//temp.concat("/") ;
//temp.concat(TimeDate[5]);
//temp.concat("/") ;
//temp.concat(TimeDate[6]);
//temp.concat(" ") ;
//temp.concat(TimeDate[2]);
//temp.concat(":") ;
//temp.concat(TimeDate[1]);
//temp.concat(":") ;
//temp.concat(TimeDate[0]);
//return(TimeDate)
}

```

## C.2 ATtiny Code

```

//Select pin that the relay is hooked up to
int pwr = 1;

void setup() {
    // initialize the digital pin as an output.
    pinMode(pwr, OUTPUT);
}

// the loop routine runs over and over again forever:
void loop() {

```

```
digitalWrite(pwr, HIGH); // Switch Relay on
delay(70000);           // Sample for a minute
                        //(add a 10 second safety buffer)
digitalWrite(pwr, LOW); // Switch relay off
delay(3600000);         // wait for an hour
}
```

## Appendix D: PCB DAQ Schematic and BOM

**Table 3.** Bill of Materials for PCB DAQ

Description	QTY	Ref Des	Mfg P/N #	Distributor	Distributor P/N #
<b>ADS1015 - 12-bit 4-Channel I2C ADC with Internal PGA</b>	4	U1, U2, U3, U4	ADS1115IDGST	Digikey	296-24934-1-ND
<b>Ferrite Bead</b>	8	FB1, FB2, FB3, FB4, FB5, FB6, FB7, FB8	MMZ2012Y152B	Digikey	445-1560-1-ND
<b>LED</b>	7	PIN0, PIN1, PWR, REC, RX, SPWR, TX	150080RS75000	Digikey	732-4984-1-ND
<b>Momentary Switch</b>	1	S1	PTS525SM10SMTRLFS	Digikey	CKN9104CT-ND
<b>NPN Transistor</b>	4	Q2, Q3, Q4, Q5	BC817-40,215	Digikey	568-1631-1-ND
<b>CAPACITOR, American symbol</b>	4	C2, C8, C18, C22	08051C104KAZ2A	Digikey	478-3562-1-ND
<b>RESISTOR, American symbol</b>	8	R1, R6, R7, R8, R11, R14, R17, R18	ESR10EZPJ103	Digikey	RHM10KKCT-ND
<b>CRYSTAL</b>	1	Q1	ABLS2-16.000MHZ-D4Y-T	Digikey	535-9875-1-ND
<b>RESISTOR, American symbol</b>	7	R2, R3, R4, R5, R9, R19, R20	CRCW08051K00JNEA	Digikey	541-1.0KACT-ND
<b>CAPACITOR, American symbol</b>	16	C1, C6, C7, C9, C10, C11, C12, C13, C14, C15, C16, C17, C19, C20, C21, C23	0805ZD105KAT2A	Digikey	478-1412-1-ND
<b>CAPACITOR, American symbol</b>	2	C3, C4	C0805C220J1GACTU	Digikey	399-8035-1-ND
<b>CR1216/CR1220/CR1225 12mm 3V lithium coin cell</b>	1	BAT1	3000TR	Digikey	3000KCT-ND
<b>Mini FIT connector 16 pol</b>	3	SENSOR_GND, SENSOR_PWR, SENSOR_SIGNAL	39-29-9162	Digikey	WM7331-ND

<b>Mini FIT connector 2 pol</b>	3	BATT1, BATT2, BATT3	39-29-9023	Digikey	WM3853-ND
<b>AVR ISP HEADER</b>	1	ISP1	10-89-7061	Digikey	WM50022-06-ND
<b>SPI RTC module with battery backup and internal clock.</b>	1	U\$2	DS3234S#	Digikey	DS3234S#-ND
<b>90degree through hole header</b>	1	JP2	961106-5604-AR	Digikey	3M9471-ND
<b>Hex Converter</b>	1	U5	M74HC4050RM13TR	Digikey	497-1844-1-ND
<b>ATMEGA1284 Microcontroller</b>	1	ATMEGA1284	ATMEGA1284-AU	Digikey	ATMEGA1284-AU-ND
<b>Micro-SD / Transflash card holder with SPI pinout</b>	1	U\$1	2908-05WB-MG	Digikey	3M5607CT-ND
<b>800mA and 1A Low Dropout (LDO) Positive Regulator</b>	2	5VREG, 5VREGSENSOR	REG1117-5/2K5	Digikey	296-27924-1-ND
<b>800mA and 1A Low Dropout (LDO) Positive Regulator</b>	1	3V3REG	REG1117-3.3/2K5	Digikey	296-21321-1-ND



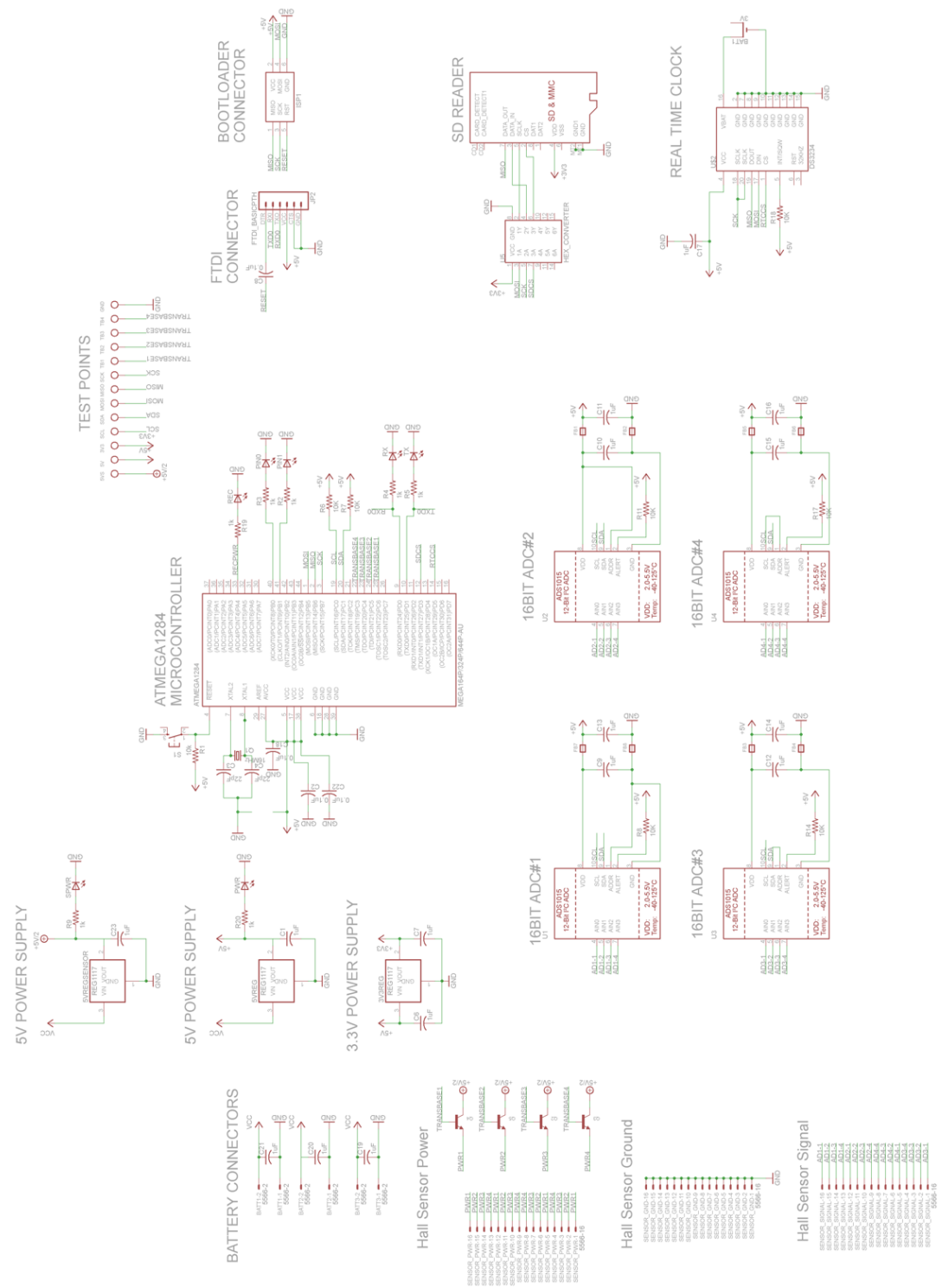


Figure 65. PCB DAQ Schematic

# Appendix E: Custom Submersible Wire Specifications


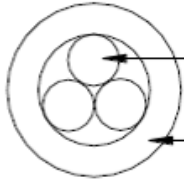

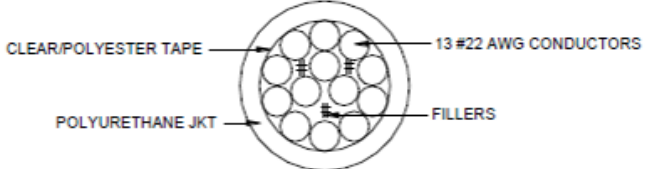
 <b>MERCURY WIRE PRODUCTS, INC.</b> SPENCER, MASSACHUSETTS <i>Manufacturers of Wire &amp; Cable</i>	<h2 style="margin: 0;">CABLE SPECIFICATION</h2>	MW#: 25254 ENGINEERED BY: DH DATE: 1/10/2014 SHEET 1 OF 1 REVISION: 01
<p><u>3/C #22 AWG CABLE</u></p> <p><b>Conductors:</b> #22 AWG 7/30 tinned copper</p> <p><b>Color Code:</b> 1. Black 2. Brown 3. Red</p> <p><b>Cabling Construction:</b> (3) #22 AWG conductors are cabled together LHL</p> <p><b>Jacket:</b> nominal .030" thickness, Black Polyurethane</p> <p><b>Cable OD:</b> .168" +/- .007"</p> <p style="text-align: center;"><u>Cross Section</u></p> <div style="text-align: center;">  <div style="display: flex; justify-content: center; gap: 50px; margin-top: 5px;"> <div style="text-align: center;"> <p>→ #22 AWG CONDUCTORS</p> </div> <div style="text-align: center;"> <p>→ POLYURETHANE JKT</p> </div> </div> </div>		
<div style="display: flex; justify-content: space-between;"> <div style="width: 45%;"> <p><b>PACKAGING:</b> BULK PUT-UPS, LONGEST LENGTHS POSSIBLE, 3 LENGTHS PER REEL MAXIMUM UNLESS OTHERWISE SPECIFIED ON PURCHASE ORDER. DIFFERENT PACKAGING MAY INCUR ADDITIONAL COSTS.</p> <p>THE PHYSICAL AND ELECTRICAL CHARACTERISTICS CONTAINED IN THIS CABLE SPECIFICATION ARE BELIEVED TO BE RELIABLE AND ARE DERIVED FROM VENDOR SUPPLIED DATA AND INDUSTRY STANDARDS. AS EACH APPLICATION IS UNIQUE, MERCURY WIRE CAN MAKE NO WARRANTIES AS TO THE SUITABILITY OF ANY PRODUCT FOR A PARTICULAR USE.</p> </div> <div style="width: 50%; border: 1px solid black; padding: 5px;"> <p>ACCEPTED: _____</p> <p style="text-align: center; margin-left: 100px;">COMPANY NAME</p> <hr style="border: 0; border-top: 1px solid black; margin: 5px 0;"/> <p>NAME (PRINTED) <span style="float: right;">DATE</span></p> <hr style="border: 0; border-top: 1px solid black; margin: 5px 0;"/> <p>NAME (SIGNATURE)</p> </div> </div> <p style="font-size: small; text-align: center; margin-top: 5px;">Mercury Wire Products, Inc. proprietary drawing. Not to be reproduced or disseminated without prior written permission.</p>		

Figure 66. Spec. sheet for the three-conductor submersible wire

 <p><b>MERCURY WIRE PRODUCTS, INC.</b> SPENCER, MASSACHUSETTS <i>Manufacturers of Wire &amp; Cable</i></p>	<h2>CABLE SPECIFICATION</h2>	<p>MW#: 25255 ENGINEERED BY: MD DATE: 1/10/2014 SHEET 1 OF 1 REVISION: 01</p>																											
<p><b><u>13/C #22 AWG CABLE</u></b></p>																													
<p><b><u>Conductors:</u></b> #22 AWG 7/30 tinned copper</p>																													
<p><b><u>Color Code:</u></b></p> <table style="width: 100%; border: none;"> <tr> <td style="width: 33%;">1. Black</td> <td style="width: 33%;">10. White/Black</td> <td style="width: 33%;"></td> </tr> <tr> <td>2. Brown</td> <td>11. White/Brown</td> <td></td> </tr> <tr> <td>3. Red</td> <td>12. White/Red</td> <td></td> </tr> <tr> <td>4. Orange</td> <td>13. White/Orange</td> <td></td> </tr> <tr> <td>5. Yellow</td> <td></td> <td></td> </tr> <tr> <td>6. Green</td> <td></td> <td></td> </tr> <tr> <td>7. Blue</td> <td></td> <td></td> </tr> <tr> <td>8. Violet</td> <td></td> <td></td> </tr> <tr> <td>9. Gray</td> <td></td> <td></td> </tr> </table>			1. Black	10. White/Black		2. Brown	11. White/Brown		3. Red	12. White/Red		4. Orange	13. White/Orange		5. Yellow			6. Green			7. Blue			8. Violet			9. Gray		
1. Black	10. White/Black																												
2. Brown	11. White/Brown																												
3. Red	12. White/Red																												
4. Orange	13. White/Orange																												
5. Yellow																													
6. Green																													
7. Blue																													
8. Violet																													
9. Gray																													
<p><b><u>Cabling Construction:</u></b> (13) #22 AWG conductors are cabled together LHL with fibrillated Polypropylene fillers</p>																													
<p><b><u>Binder:</u></b> Polyester tape, 25% coverage nominal</p>																													
<p><b><u>Jacket:</u></b> nominal .030" thickness, Black Polyurethane</p>																													
<p><b><u>Cable OD:</u></b> .279" +/- .010"</p>																													
<p><b><u>Cross Section</u></b></p>																													
																													
<p><b>PACKAGING:</b> BULK PUT-UPS, LONGEST LENGTHS POSSIBLE, 3 LENGTHS PER REEL MAXIMUM UNLESS OTHERWISE SPECIFIED ON PURCHASE ORDER. DIFFERENT PACKAGING MAY INCUR ADDITIONAL COSTS.</p> <p>THE PHYSICAL AND ELECTRICAL CHARACTERISTICS CONTAINED IN THIS CABLE SPECIFICATION ARE BELIEVED TO BE RELIABLE AND ARE DERIVED FROM VENDOR SUPPLIED DATA AND INDUSTRY STANDARDS. AS EACH APPLICATION IS UNIQUE, MERCURY WIRE CAN MAKE NO WARRANTIES AS TO THE SUITABILITY OF ANY PRODUCT FOR A PARTICULAR USE.</p>	<p>ACCEPTED: _____                   COMPANY NAME</p> <p>NAME (PRINTED) _____ DATE _____</p> <p>NAME (SIGNATURE) _____</p>																												
<p>Mercury Wire Products, Inc. proprietary drawing. Not to be reproduced or disseminated without prior written permission.</p>																													

**Figure 67.** Spec. sheet for 13-conductor submersible wire

## Bibliography

*Arduino*. (n.d.). Retrieved from [arduino.cc](http://arduino.cc)

Brenner, D. (2002, 10 26). Retrieved from iStockphoto:

<http://www.istockphoto.com/photo/harbor-seal-face-57189>

Dehnhardt, G., Bjorn, M., Hanke, W., & Horst, B. (2001, July 6). Hydrodynamic Trail-Following in Harbor Seals (*Phoca vitulina*). *Science*, 102-104.

doi:10.1126

Kattell, J., & Merv, E. (1998). *Bridge Scour Evaluation: Screening, Analysis & Countermeasures*. United States Department of Agriculture, Forest Service.

maniacbug. (2011, November 27). *Arduino on ATmega1284P*. Retrieved from WordPress: <http://maniacbug.wordpress.com/2011/11/27/arduino-on-atmega1284p-4/>

Michael, A. M. (2012). *Development of a Bio-Inspired Magnetostrictive Flow and Tactile Sensor*. Retrieved from Digital Repository at the University of Maryland: <http://hdl.handle.net/1903/13003>

Sirio, G. D., & Greiman, B. (2013, May 20). *NilRTOS-Arduino*. Retrieved from GitHub: <https://github.com/greiman/NilRTOS-Arduino>

*SparkFun Electronics*. (n.d.). Retrieved from <https://www.sparkfun.com/>

Waren, L. (2013, August 16). *Scour at Bridges - What's it all about?* Retrieved from U.S. Geological Survey: <http://ma.water.usgs.gov/publications/ofr/scour.htm>

